SNR-INDEPENDENT VELOCITY ESTIMATION IN RAYLEIGH FADING CHANNELS

by

Wei Sheng

A thesis submitted to the
Department of Electrical and Computer Engineering
in conformity with the requirements
for the degree of Master of Science (Engineering)

Queen's University
Kingston, Ontario, Canada
October, 2002

Abstract

Knowledge of the velocity of a mobile terminal is useful for a variety of radio resource management functions being contemplated for future wireless communications systems. Currently, the radial component of the velocity of a mobile terminal can be inferred from estimating the maximum Doppler fading bandwidth. Unfortunately, the practicality of current methods is limited since they require an estimate of the signal-to-noise ratio (SNR) of the link. In this thesis, novel autocorrelation function (ACF) based velocity estimators are proposed. These estimation methods are then extended to estimate mobile velocity without requiring knowledge of the SNR of the link. Monte-Carlo simulations of the proposed estimators are provided and compared to several existing methods.

After deriving the novel algorithms, we focus on approximate Cramer-Rao lower bounds of envelope-based and IQ-based estimators, under the assumption that the fading process can be approximated by the first-order Markov process.

Finally, the new estimation algorithms are applied to track a fading channel using a Kalman filter, and a performance analysis is also included.

Acknowledgments

My foremost appreciation goes to Dr. Blostein, for his guidance, support and encouragement while doing this research.

I also would like to thank all my lab-mates in IPCL for their friendship and collegiality through the years. In particular, Yi, Neng, Costi, and Joseph made many helpful suggestions based on their experiences.

For my dear parents, I would like to thank them for their patience, understanding, and for being beside me when I needed most.

Finally, I am especially grateful to my husband Yang Lu, for every hard time he has helped me through, and for every day he has been in my life.

Contents

List of Tables

List of Figures

Symbols and Abbreviations

f_m	Normalized maximum Doppler frequency
F_m	Continuous-time maximum Doppler frequency
v	Mobile speed
L	Number of multi-paths
λ	Wavelength of transmitted signal
α_n	Amplitude of the n^{th} incoming wave
ψ_n	Phase of the n^{th} incoming wave
f_c	Carrier frequency
ω_n	Doppler frequency of the n^{th} incoming wave
θ_n	Incident angle of the n^{th} incoming wave
c	Speed of light
n	Number of samples
$CRLB_{env}$	CRLB for envelope-based estimators
$CRLB_{IQ}$	CRLB for IQ-based estimators
$v(n)$	Data sequence at time n

$\{A_i\}$	The i^{th} AR filter parameter
$u(n)$	Driving noise at time n
σ_u^2	Variance of driving noise
$K(n)$	Kalman gain at time n
ACF	Autocorrelation function
IQ	In-phase or quadrature components
AR	Autoregressive
ARMA	Autoregressive and moving average
CRLB	Cramer-Rao lower bound
MSE	Mean-square-error
MMSE	Minimum mean-square-error
WSS	Wide-sense stationary

Chapter 1

Introduction

1.1 Motivation

The relative velocity between a mobile and a base-station is a very important parameter for wireless communication systems. Improved wireless communication requires accurate estimation of the velocity. The velocity information can be used to track mobile location [6], and it is observed that if the velocity is high, accurate velocity information will help to improve tracking quality [6]. Hand-off commands may also utilize mobile velocity information. In [3], velocity-adaptive hand-off algorithms were proposed. It was also shown how information in signal strength measurements can be exploited to improve the quality of hand-off decisions.

There exist a variety of methods for the estimation of velocity. These methods need Signal-to-Noise Ratio (SNR) information, which is not always available at a receiver.

Also, despite the importance in assessing system performance in an algorithm-independent fashion, the CRLB for envelope-based Doppler estimation seems not to have appeared in the literature. In [20], the author derives the Cramer-Rao lower bound (CRLB) for in-phase/quadrature (IQ) based estimators, but fails to obtain the CRLB for envelope-based estimators.

The focus of this thesis is on the development of both IQ-based and envelope-based SNR-independent velocity estimates, in which additive noise is present. In addition, we also focus on the derivation of approximate CRLB for envelope-based velocity estimators. The velocity estimators are then applied to the problem of tracking a fading channel.

1.2 Contributions

The contributions of this thesis are listed as follows:

- New envelope-autocorrelation function (ACF)-based and squared-envelope-ACF-based velocity estimation algorithms are developed.
- New envelope-ACF-based and squared-envelope-ACF-based velocity estimation algorithms are presented, which do not require SNR estimation.
- A new IQ-ACF-based joint SNR and velocity estimation algorithm is proposed.

- New Cramer-Rao lower bounds are derived for IQ-based and envelope-based unbiased velocity estimators, under a first-order Markov fading process assumption; as a by-product, the Cramer-Rao lower bounds for all IQ-based and envelope-based unbiased signal-to-noise ratio estimators are also derived under the same assumption.

- An analysis showing that under a first-order Markovian fading process assumption, unbiased SNR-independent velocity (Doppler) estimators would have very poor performance.

- Evaluation of the improvement in channel estimation by incorporating mobile velocity as an input to a Kalman filter based channel tracker.

1.3 Thesis Organization

We start with a background review in Chapter 2, which includes a brief discussion of relevant previous work. Chapter 3 presents a novel algorithm for joint estimation of velocity (Doppler) and SNR, which requires coherent demodulation. Envelope-based and squared-envelope-based velocity (Doppler) estimation algorithms, which can be SNR-independent, are proposed in Chapter 4 for non-coherent demodulation. In Chapter 5, the proposed methods are compared to several existing methods by Monte-Carlo simulations. In Chapter 6, approximate CRLBs for velocity (Doppler) estimation are derived, under a first-order Markov fading process assumption. In

Chapter 7, the joint velocity and SNR estimation is applied to track the fading channel gain. We provide concluding remarks and suggestions for future work in Chapter 8.

Chapter 2

Background

2.1 Introduction

In this chapter, we briefly review some relevant literature and background for the problem of mobile velocity estimation.

We begin with a discussion of the signal model in Section 2.2, in which the Rayleigh fading multi-path channel for a pure carrier and/or modulated transmitted signal is introduced. The generation of a Rayleigh fading process using inverse discrete Fourier transform (IDFT), as well as autoregressive (AR) process methods are then presented in Section 2.3. In Section 2.4, we review several existing velocity estimation methods.

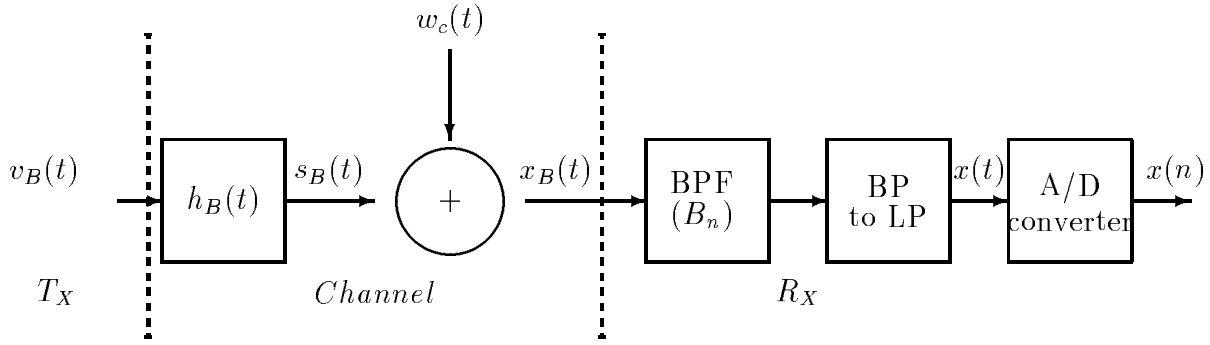

Figure 2.1: General signal model

2.2 Signal Model

Figure 2.1 shows the general signal model, where $v_B(t)$ is the transmitted sequence, $h_B(t)$ is the impulse response of a multi-path Rayleigh fading channel, modeled as a linear time-invariant system for narrow-band transmitted signal, and time-variant system for wide-band input system. $w_c(t)$ represents additive white noise. At the receiver, the received band-pass signal $x_B(t)$ can be written as

$$\begin{aligned} x_B(t) &= s_B(t) + w_c(t) \\ &= v_B(t) * h_B(t) + w_c(t) \end{aligned} \tag{2.1}$$

where $*$ denotes convolution.

In the following, we present signal models for a pure carrier and a modulated

sequence, respectively.

2.2.1 Clarke's Fading Signal Model for a Pure Carrier

Clarke [1] has proposed a statistical propagation model for the scattering of a received signal of a flat-fading channel. When the transmitted signal is a pure carrier, i.e., $v_B(t) = \cos(2\pi f_c t)$, where f_c is the carrier frequency, the received signal $s_B(t)$ can be written as the sum of L horizontally traveling plane waves [1]

$$s_B(t) = \sum_{n=1}^{L} \alpha_n \cos(2\pi f_c t + \omega_n t + \psi_n) \tag{2.2}$$

where α_n and ψ_n are the amplitude and phase of the n^{th} incoming wave, respectively, and $\omega_n = 2\pi F_m \cos\theta_n$ is the Doppler shift for the n^{th} path, in which F_m is the maximum Doppler frequency and θ_n is the incident angle of the n^{th} incoming wave.

Equation (2.2) can also be expressed in complex notation as

$$\begin{aligned} s_B(t) &= \Re[s(t)\exp(j2\pi f_c t)] \\ &= \Re[(s_I(t) + js_Q(t))\exp(j2\pi f_c t)] \end{aligned}$$

where $\Re[.]$ denotes real part, and $s(t)$ is the equivalent low-pass signal of $s_B(t)$, which can be written as

$$s(t) = \sum_{n=1}^{L} \alpha_n \exp\left(j(\omega_n t + \psi_n)\right) \tag{2.3}$$

$s_I(t)$ and $s_Q(t)$ are the in-phase (I) and quadrature (Q) components of s(t), i.e.,

$$\begin{aligned} s_I(t) &= \sum_{n=1}^{L} \alpha_n \cos(\omega_n t + \psi_n) \\ s_Q(t) &= \sum_{n=1}^{L} \alpha_n \sin(\omega_n t + \psi_n) \end{aligned}$$

If additive white Gaussian noise (AWGN) is present, which has a flat spectrum with constant spectral density $N_0/2$ over all frequencies, the received signal will be

$$x_B(t) = s_B(t) + w_c(t) \tag{2.4}$$

At the receiver portion of Figure 2.1, a band-pass filter (BPF) with bandwidth B_n is assumed at the front-end to model the receiver amplifier and limit out-of-band noise. Also, the A/D conversion yields the discrete-time signal used to estimate velocity. The output of the BPF in Figure 2.1 is a band-limited signal at carrier frequency f_c, which is always very high relative to the signal bandwidth. Therefore, before A/D conversion, the bandpass signal should be down-converted into a low-pass signal in order to reduce the sampling rate. We note that quantization effects from A/D conversion are ignored.

The signal model in Figure 2.1 can be shown to be equivalent to the low-pass signal model in Figure 2.2 [24], in which the received signal can be written as

$$\begin{aligned} x(t) &= s(t) + n(t) \\ &= v(t) * h(t) + n(t) \qquad (2.5) \\ &= \sum_{n=1}^{L} \alpha_n \exp\left(j(\omega_n t + \psi_n)\right) + n(t) \qquad (2.6) \end{aligned}$$

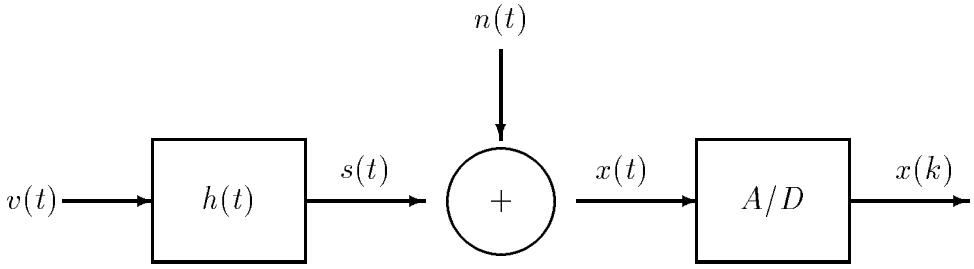

Figure 2.2: The equivalent low-pass signal model

where $x(t)$, $v(t)$ and $h(t)$ are the low-pass equivalent signals of $x_B(t)$, $v_B(t)$ and $h_B(t)$, respectively, and $n(t)$ represents narrow-band noise, which is obtained by filtering white noise $w_c(t)$ through BPF and band-pass to low-pass (BP-LP) conversion.

The discrete-time signal $x(k)$ can be expressed as

$$x(k) = s(k) + n(k) \tag{2.7}$$

$$= s_I(k) + n_I(k) + j(s_Q(k) + n_Q(k)) \tag{2.8}$$

where $x(k)$, $s(k)$ and $n(k)$ are the sampled versions of $x(t)$, $s(t)$ and $n(t)$, respectively, at sampling rate F_s. In (2.8), $n_I(k)$ and $n_Q(k)$ are the I and Q components of $n(k)$, respectively; $s_I(k)$ and $s_Q(k)$ are the I and Q components of $s(k)$, respectively, which

can be written as

$$\begin{aligned} s_I(k) &= \sum_{n=1}^{L} \alpha_n \cos(\omega_n T_s k + \psi_n) \\ &= \sum_{n=1}^{L} \alpha_n \cos(2\pi f_m \cos(\theta_n) k + \psi_n) \end{aligned} \tag{2.9}$$

$$\begin{aligned} s_Q(k) &= \sum_{n=1}^{L} \alpha_n \sin(\omega_n T_s k + \psi_n) \\ &= \sum_{n=1}^{L} \alpha_n \sin(2\pi f_m \cos(\theta_n) k + \psi_n) \end{aligned} \tag{2.10}$$

where $T_s = \frac{1}{F_s}$ is the sampling period, and normalized Doppler frequency f_m is defined as $\frac{F_m}{F_s}$, which is proportional to the radial component of the relative velocity between the transmitter and receiver [2]

$$f_m = \frac{v}{\lambda F_s} \tag{2.11}$$

where v, F_s and λ are the mobile velocity, the sampling rate and the wavelength of the transmitted wave, respectively.

By summing (2.9) and (2.10), Equation (2.8) can be written as

$$x(k) = \sum_{n=1}^{L} \alpha_n \exp\left(j(2\pi f_m \cos(\theta_n) k + \psi_n)\right) + n(k) \tag{2.12}$$

The discrete-time low-pass signal in (2.12) for a pure carrier is very widely used in practical systems, and will be adopted in this thesis.

2.2.2 Signal Model for a Data Modulated Carrier

Equation (2.12) presents the received low-pass signal for a pure carrier. In this section, the system model for modulated signals will be discussed.

For narrow-band transmitted signal, the received signal can be written as

$$x(t) = h_{nar}(t)v(t) + n(t) \tag{2.13}$$

where $h_{nar}(t)$ represents the channel gain of frequency non-selective Rayleigh fading channel. Above equation assumes that the inter-symbol interference (ISI) terms can be neglected.

Dividing Equation (2.13) by the known data, we obtain

$$x(t)/v(t) = h_{nar}(t) + n(t)/v(t) \tag{2.14}$$

as long as training data sequence $v(t)$ is nonzero for all t.

Equation (2.14) gives a signal with same form as in (2.6), except that the noise components may be non-identically distributed.

For wide-band transmitted signals, the received signal may be represented by [10]

$$x(t) = \sum_{i=1}^{l} h_i(t)v(t - \tau_i(t)) + n_w(t) \tag{2.15}$$

where l is the number of resolvable paths, $\tau_i(t)$ and $h_i(t)$ are the propagation delay and complex channel gain of the i^{th} resolvable multi-path, respectively, and $n_w(t)$ represents the wide-band noise. $h_i(t), i = 1, 2, .., l$ has the same form as in (2.3). It can be assumed that a RAKE receiver [2] can resolve each of the paths in (2.15), and

the channel gain for i^{th} path, $h_i(t)$ can be obtained via a pilot channel or other means [11].

2.2.3 Statistics of the Received Fading Process

In Equations (2.9) and (2.10), if the number of multi-paths, L, is large enough, according to the Central Limit Theorem [31], $s_I(t)$ and $s_Q(t)$ can be considered to be normally distributed [27]. Thus the received signals

$$x_I(t) = s_I(t) + n_I(t) \tag{2.16}$$

$$x_Q(t) = s_Q(t) + n_Q(t) \tag{2.17}$$

will be normally distributed and assumed to have zero-mean and variance $\sigma^2 + \sigma_n^2$, where $n_I(t)$, $n_Q(t)$, and $x_I(t)$, $x_Q(t)$ are the I/Q components of $n(t)$ and $x(t)$, respectively; σ^2 and σ_n^2 are the variance of either the I or Q components of the fading signal $s(t)$ and the narrow-band noise $n(t)$, respectively.

In [6], the autocorrelation function (ACF) of the I or Q components of $s(t)$ is shown to be a Bessel function in terms of Doppler frequency, the ACF of either $n_I(t)$ or $n_Q(t)$ is a sinc function, and the fading signal $s(t)$ is assumed to be independent of the noise $n(t)$, so the ACF of I or Q components of the received signal $x(t)$ can be derived as [6]

$$\begin{aligned} \phi_{II}(\tau) &= E[x_I(t)x_I(t-\tau)] \\ &= \sigma^2 J_0(2\pi F_m \tau) + \sigma_n^2 \mathrm{sinc}(B_n \tau) \end{aligned} \tag{2.18}$$

where B_n is the bandwidth of the band-pass filter as discussed earlier.

It is known that $x(t)$ is a wide-sense stationary (WSS) continuous-time process. With T_s an arbitrary constant, the ACFs of the process $x(n)$, which is formed via $x(n) = x(t)|_{t=nT_s}$, will equal the samples of the ACFs of the continuous-time process $x(t)$ [31], i.e.,

$$\begin{aligned} \phi_{II}(k) &= E[x_I(n)x_I(n-k)] \\ &= \sigma^2 J_0(2\pi f_m k) + \sigma_n^2 \text{sinc}(B_n T_s k) \end{aligned} \tag{2.19}$$

The in-phase components $x_I(k)$ and quadrature components $x_Q(k)$ are assumed to be independent. As a result, the envelope of the low-pass equivalent signal is Rayleigh distributed with probability density function (PDF) [27]

$$p(z(k)) = \frac{z(k)}{\sigma^2 + \sigma_n^2} \exp\left\{ -\frac{z^2(k)}{2(\sigma^2 + \sigma_n^2)} \right\} \quad (z(k) \geq 0) \tag{2.20}$$

where $z(k) = \sqrt{x_I^2(k) + x_Q^2(k)}$ is the envelope of the received sample at time instant k.

The joint PDF of two adjacent envelope samples can be derived by transformation of the joint normal PDF as done in [7], which is given by

$$p\left(z(k), z(k+1)\right) = \frac{z(k)z(k+1) \exp\left\{ -\frac{\phi_{II}(0)(z^2(k)+z^2(k+1))}{2(\phi_{II}^2(0)-\phi_{II}^2(1))} \right\}}{\phi_{II}^2(0) - \phi_{II}^2(1)} I_0(k, k+1) \tag{2.21}$$

where

$$I_0(k, k+1) \equiv I_0\left(\frac{\phi_{II}(1)z(k)z(k+1)}{\phi_{II}^2(0) - \phi_{II}^2(1)} \right) \tag{2.22}$$

$$\phi_{II}(0) = \sigma^2 + \sigma_n^2 \tag{2.23}$$

$$\phi_{II}(1) = \sigma^2 J_0(2\pi f_m) + \sigma_n^2 \text{sinc}(B_n T_s) \tag{2.24}$$

In (2.22), $I_0(\cdot)$ represents the zero-order modified Bessel function of the first kind; $\phi_{II}(0)$ and $\phi_{II}(1)$ are the autocorrelation function of IQ components of the received signal at lags 0 and 1, respectively, which are obtained from Equation (2.19).

2.3 Computer Simulation of a Fading Process

In recent years, the development of computationally efficient and accurate channel simulation of Rayleigh fading channels [27] has been of great interest in the area of wireless communications. As a result, there are a number of different algorithms which can generate a fading process.

One popular method to model the Rayleigh fading process is to sum the outputs of N complex sinusoidal generators. In practice, the generated sequence will closely approximate a Gaussian process if a sufficient number of sinusoids is used. Correlated Rayleigh variables can also be generated by filtering two zero-mean independent white Gaussian processes and then adding the outputs in quadrature [38].

In this thesis, Smith's IDFT algorithm [17] and an AR(p) generator [38] are both considered to generate the fading process. Next, we review these two methods briefly.

2.3.1 IDFT Algorithm

The IDFT operation for generation of Rayleigh random variables is applied to complex-valued sequences of independent, normally distributed coefficients. These variables

are then compatible with the low-pass equivalent signal model discussed in Section 2.2.

The basic idea of this popular method is to use the inverse discrete Fourier transform to generate Rayleigh correlated fading process. Young and Beaulieu [17] have modified this algorithm for greater computational efficiency and provided a statistical analysis of the method.

The procedure of generating the fading process using IDFT method is as follows: starting with two real Gaussian sequences $\{A[k]\}$ and $\{B[k]\}$, $k = 0, 1, ..., N-1$, where $\{A[k]\}$ and $\{B[k]\}$ each denote N independent real normal random variates with zero mean and variance σ^2, the complex Gaussian sequence $\{A[k]\} + j\{B[k]\}$ is then formed. This complex sequence is then filtered by frequency domain multiplication, and we obtain

$$X[k] = A[k]F[k] - jB[k]F[k] \tag{2.25}$$

where $\{F[k]\}, k = 0, 1, ..., N-1$ are filter coefficients. An inverse DFT is then taken to form a complex-valued time domain signal [32], which can be written as

$$x(n) = \frac{1}{N}\sum_{k=0}^{N-1} X[k]\exp(j\frac{2\pi kn}{N}) \qquad n = 0, 1, ..., N-1 \tag{2.26}$$

The real and imaginary parts of $x(n)$ have identical statistics, and each approximates the real or imaginary part of the baseband fading signal. The real and imaginary parts at the output of Smith's IDFT algorithm [5] are correlated, so they cannot be

used to form a sequence of Rayleigh variates. Instead, the real part at the output of the IDFT is taken and the imaginary part is discarded. This real sequence is added in quadrature with the real part from a second identical and independent branch. Young and Beaulieu modified the IDFT fading simulator by using different coefficients $\{F[k]\}$, which is chosen to make the real and imaginary parts at the output uncorrelated, thus reducing the computation time of the simulator by using only one sequence $x(n)$.

2.3.2 AR(p) Generator

The IDFT algorithm is widely accepted as a generator of realistic Rayleigh fading processes. However, the computational efficiency of the IDFT approach comes at a cost in storage requirements as all variates are generated using a single inverse fast Fourier transform, while the AR filtering method can generate fading variates as they are required [38]. The AR generator has fewer parameters, and lower complexity, compared with the IDFT algorithm, and can also provide easy analysis of algorithm performance in processing fading signals [38].

For the AR(p) generator, the fading process $h(n)$ is generated via the time domain recursion

$$h(n) = \sum_{i=1}^{p} A_i h(n-i) + u(n) \tag{2.27}$$

where p is the order of the AR model and driving noise $u(n)$ is an independent and identical distributed (i.i.d.) normal process with zero mean and variance σ_u^2. To create

an approximate model for the Jakes' fading channel, we use the first p correlation lags of the autocorrelation function of the Rayleigh fading process to specify a $p-th$ order autoregressive AR(p) model. We calculate the AR model parameters $A_1, ..., A_p$ and σ_u^2 according to the autocorrelation function of the desired statistics of correlated Rayleigh variables using the Levinson algorithm [32] (see Appendix B for details).

Obtaining all the parameters of $AR(p)$ model, we use the model in (2.27) to generate the fading process recursively. The initial p samples of $h(n)$ can be set according to Baddour and Beaulieu's start-up procedure [38].

2.4 Review of Previous Work on Mobile Velocity Estimation

In the following, we briefly review several mobile velocity estimation methods.

2.4.1 Level Crossing Rate (LCR) Method

A discrete-time LCR-based Doppler frequency method was developed in [6], in which the discrete-time level-crossing-rate was defined as the ratio of the expected number of level crossings a signal makes for a given predetermined voltage level A_{LCR}, to the number of given samples n.

A special case is where $A_{LCR} = 0$, which is denoted as the zero-crossing-rate (ZCR). The ZCR is defined as the average number of positive going zero crossings

of the IQ components of a signal. From here on, IQ denotes either the in-phase or quadrature signal components.

The discrete-LCR is defined as

$$\text{LCR} = \frac{E\{X\}}{n} \tag{2.28}$$

where X is the number of level crossings defined as

$$X = \sum_{k=i}^{i+n-1} X_k \tag{2.29}$$

where X_k is the level crossing state between two samples. If there is no level crossing, $X_k = 0$, otherwise, $X_k = 1$. Sampling rate F_s should be chosen to ensure that multiple crossings do not occur between two adjacent samples.

From Equation (2.28), it is observed that if n is large enough, the discrete-LCR can be considered as the probability of a positive crossing between two samples.

The LCR may be calculated from the joint PDF of two envelope samples via

$$\begin{aligned} \text{LCR} &= P\{z(k) \leq A_{LCR}, z(k+1) > A_{LCR}\} \\ &= \int_0^{A_{LCR}} \int_{A_{LCR}}^{\infty} p(z(k), z(k+1)) dz(k) dz(k+1) \end{aligned} \tag{2.30}$$

where $p(z(k), z(k+1))$ is the joint PDF of two adjacent envelope samples, which is given in (2.21).

By substituting Equation (2.21) into (2.30),

$$LCR = (1 - R^2) \exp\left(\frac{-2\rho^2}{1 - R^2}\right) \sum_{n=0}^{\infty} \sum_{k=1}^{\infty} R^{n-k} I_{n+k}\left(\frac{2R\rho^2}{1 - R^2}\right) \tag{2.31}$$

in which $\rho = \frac{A_{LCR}}{\sqrt{2\phi_{II}(0)}}$ is the power level ratio, $R = \frac{J_0(2\pi f_m)+\text{sinc}(B_n T_s)/snr}{1+1/snr}$, $snr = \frac{\sigma^2}{\sigma_n^2}$ is the signal-to-noise ratio, and I_{n+k} is the $(n+k)^{th}$ order modified Bessel function of the first kind[1].

By counting the LCR using (2.28), the Doppler frequency can be solved numerically via Equation (2.31).

2.4.2 Recursive Maximum Likelihood Method (MLE)

In [7], a recursive maximum likelihood approach was proposed to estimate the Doppler frequency from the received discrete-time fading samples by modeling the fading process as a first-order discrete-time Markov process.

Since the joint PDF of envelope samples is a function of f_m, the goal of this method is to estimate f_m as a non-random parameter based on maximum likelihood estimation.

The joint PDF of n observed envelope samples can be written as follows under the assumption of first-order Markov process

$$p_n(z(1), z(2), ..., z(n)) = p(z(1)) \prod_{k=1}^{n-1} \frac{p(z(k), z(k+1))}{p(z(k))}$$

We maximize the log-likelihood function

$$L(z(1), z(2), ..., z(n); f_m) = \ln[p_n(z(1), z(2), ..., z(n))] \tag{2.32}$$

[1] We acknowledge Lin Zhao for pointing out this correction to Eqn.(8) in [6]

Setting $\frac{\partial \ln L(z(1),z(2),\ldots,z(n);f_m)}{\partial f_m}$ to zero, we obtain the likelihood equation

$$\sum_{k=1}^{n-1}[-(z^2(k)+z^2(k+1))\phi_{II}(0)\phi_{II}(1)+2\phi_{II}(1)(\phi_{II}^2(0)-\phi_{II}^2(1)) \\ +z(k)z(k+1)(\phi_{II}^2(0)+\phi_{II}^2(1))\frac{I_1(k,k+1)}{I_0(k,k+1)}]=0 \tag{2.33}$$

where $I_0(k,k+1)$ and $I_1(k,k+1)$, each with arguments of $\frac{\phi_{II}(1)z(k)z(k+1)}{\phi_{II}^2(0)-\phi_{II}^2(1)}$, are zero-order and first-order modified Bessel function of the first kind, respectively.

Unfortunately, the Doppler frequency f_m cannot be solved in a closed-form. Instead, the following recursive stochastic approximation method to estimate parameter f_m is employed [29].

Equation (2.33) can be written as

$$\sum_{k=1}^{n}\psi(Z_k;\hat{f_m})=0 \tag{2.34}$$

where $\psi(Z_k;\hat{f_m})=\frac{\partial}{\partial f_m}p(z(k),z(k+1))$.

Under mild conditions, the difference, $\hat{f}_{m_n}-\hat{f}_{m_{n-1}}$ converges to zero as n goes to infinity.

We obtain the following recursive solution of $\hat{f_m}$

$$\hat{f}_{m_n}\approx\hat{f}_{m_{n-1}}-\frac{\sum_{k=1}^{n}\psi(z(k);\hat{f}_{m_{n-1}})}{\sum_{k=1}^{n}\psi'(z(k);\hat{f}_{m_{n-1}})} \tag{2.35}$$

where $\psi(z(k);\hat{f_m})$ and $\psi'(z(k);\hat{f_m})$ can be derived as follows [7]

$$\begin{aligned}
\psi(z(k);\hat{f_m}) &= -(z^2(k)+z^2(k+1))\phi_{II}(0)\phi_{II}(1)+2\phi_{II}(1)(\phi_{II}^2(0)-\phi_{II}^2(1)) \\
&\quad +z(k)z(k+1)(\phi_{II}^2(0)+\phi_{II}^2(1))\frac{I_1(k,k+1)}{I_0(k,k+1)} \\
\psi'(z(k);\hat{f_m}) &= -2\pi\sigma^2 J_1(2\pi f_m)[-(z^2(k)+z^2(k+1))\phi_{II}(0)+2\phi_{II}^2(0)-6\phi_{II}^2(1) \\
&\quad +2z(k)z(k+1)\phi_{II}(1)\frac{I_1(k,k+1)}{I_0(k,k+1)}+z^2(k)z^2(k+1) \\
&\quad \times\frac{(\phi_{II}^2(0)+\phi_{II}^2(1))^2}{(\phi_{II}^2(0)-\phi_{II}^2(1))^2}\left(1-\frac{(\phi_{II}^2(0)-\phi_{II}^2(1))I_1(k,k+1)}{\phi_{II}(1)z(k)z(k+1)I_0(k,k+1)}-\frac{I_1^2(k,k+1)}{I_0^2(k,k+1)}\right)]
\end{aligned}$$

where

$$I_1(k,k+1) \equiv I_1\left(\frac{\phi_{II}(1)z(k)z(k+1)}{\phi_{II}^2(0)-\phi_{II}^2(1)}\right) \tag{2.36}$$

and $I_0(k,k+1)$ is defined in (2.22). Thus, f_m can be estimated from Equation (2.35) recursively by choosing an initial guess for f_m appropriately.

2.4.3 ACF-Based Method

In [6], an IQ-based ACF method is derived to estimate the velocity. This approach is very simple but effective.

It is well known that the autocorrelation function of the in-phase or quadrature components is a Bessel function as presented in Equation (2.19).

Define the ratios

$$snr = \frac{\sigma^2}{\sigma_n^2} \tag{2.37}$$

$$c_1 = \frac{\phi_{II}(1)}{\phi_{II}(0)} \tag{2.38}$$

Substituting Equations (2.37) and (2.19) into (2.38), we obtain that

$$c_1 = \frac{snr J_0(2\pi f_m) + \mathrm{sinc}(B_n T_s)}{1 + snr} \tag{2.39}$$

Normalized Doppler f_m can be solved from this nonlinear function [6]

$$f_m = \frac{1}{2\pi} J_0^{-1}[\frac{c_1(1 + snr) - \mathrm{sinc}(B_n T_s)}{snr}] \tag{2.40}$$

by estimating ACF lags $\phi_{II}(1)$ and $\phi_{II}(0)$ via sample averages. We note that B_n and T_s should be chosen appropriately to ensure that the above equation has a unique root.

2.4.4 Covariance-Based Method

In [3], Sampath and Holtzman developed a covariance-based method to estimate the Doppler frequency, which also can be extended to a Rician fading environment. Austin and Stuber then modified this method in [15], and studied the estimator sensitivity and the effect of the scattering distribution.

In [3], V_{cov} is defined as a measure of the squared deviations

$$V_{cov} = \frac{1}{n} \sum_{i=0}^{n-1} (z^2(i+1) - z^2(i))^2 \tag{2.41}$$

where $z(i)$'s are samples of the envelope and n is the number of samples. If n is large and the signal experiences isotropic-scattering frequency non-selective Rayleigh

fading, V_{cov} can be replaced by the ensemble average [3]

$$\begin{aligned} E[V_{cov}] &= 2[var(z^2(i)) - cov(z^2(i+1), z^2(i))] \\ &= 8\sigma^4(1 - J_0^2(2\pi f_m)) + 8\sigma_n^4(1 - \mathrm{sinc}^2(B_n T_s)) \\ &\quad +8\sigma_n^2\sigma^2(1 - J_0(2\pi f_m)\mathrm{sinc}(B_n T_s)) \end{aligned} \tag{2.42}$$

Assuming that σ^2 and σ_n^2 are available, and V_{cov} can be estimated from (2.41), f_m can be solved numerically from Equation (2.42).

2.4.5 Spectral-Moments-Based Method

Recently, a novel velocity estimator is proposed in [19], which uses the spectral moments of the in-phase and the quadrature phase components or the envelope of the received signal to estimate velocity. The very important advantage of this method is that it characterizes the joint effects of the Ricean K factor, the directivity, the angle of non-isotropic scattering, and the effects of additive white noise on the proposed estimator and other covariance-based velocity estimators analytically.

It is well known that f_m is directly proportional to the second spectral moments of the in-phase and quadrature components, which is a measure of the Doppler bandwidth and a decreasing function of $r_h''(0)$, the curvature of the ACF $r_h(\tau)$ at lag zero. From [19],

$$f_m = \frac{1}{2\pi F_s}\sqrt{\frac{-2r_h''(0)}{r_h(0)}} \tag{2.43}$$

where $r_h(k) = \sigma^2 J_0(2\pi f_m k)$ is the autocorrelation function at lag k. To estimate f_m from Equation (2.43), a parabola is fit to m points $\hat{r}_h(iT_s), i = 0, 1, ..., m$, where T_s is the sampling period.

The steps for estimating f_m from the IQ components of the received signal are as follows:

1. Estimate the autocorrelation function $r_h(iT_s)$, $i = 0, ..., m$ by taking a sample average estimate.
2. Find $\hat{a}_k = argmin_{a_k} \sum_{i=0}^{m} |\hat{r}_h(iT_s) - \sum_{k=0}^{2} a_k i^k|^2$.
3. Obtain $\hat{r}_h^{(n)}(0) = \frac{n!\hat{a_n}}{T_s^n}$, $n = 0, 2$.
4. Substitute $\hat{r}_h^{(n)}(0), n = 0, 2$, in Equation (2.43).

If we only observe the signal envelope, we can use squared-envelope samples to estimate f_m. We would still use the steps 1-4 except that in step one, the autocorrelation of squared-envelope components would be estimated instead of the autocorrelation of IQ components.

The above algorithm does not consider the effect of uncorrelated additive noise. To circumvent the effect of white noise on the proposed scheme, the algorithm is modified as follows [19]. Given noisy channel estimates $x(nT_s) = h(nT_s) + w(nT_s)$, we first obtain the estimates of

$$\begin{aligned} r_x(iT_s) &= r_h(iT_s) + r_w(iT_s) \\ &= r_h(iT_s) + \sigma_w^2 \delta(i) \end{aligned} \tag{2.44}$$

via sample average, where σ_w^2 is the variance of white noise $w(i)$. We then fit a polynomial to $\hat{r}_x(iT_s) = \hat{a}_2 i^2 + \hat{a}_0$ for $i = 1, 2, .., m-1$, discarding the $i = 0$ lag to obtain estimates $\hat{r}_h''(0) = \frac{2\hat{a}_2}{T_s^2}$, $\hat{r}_h(0) = \hat{a}_0$. As a result, this method is unaffected by noise asymptotically in the number of samples.

In [19], this method is shown to outperform existing covariance-based and LCR-based estimators in the sense of speed of convergence and robustness to white noise.

2.4.6 Other Methods

An eigen-matrix pencil method is proposed in [14], which assumes that the received signal can be modeled as the sum of a finite number of complex exponentials.

An instantaneous frequency-based velocity estimation was proposed for micro-cellular systems in [12]. The performance of this method was shown to be superior to that of the continuous-time level crossing rate method [27].

Kofi uses the higher order statistics of the fading channel to estimate mobile velocity in [16], which is a generalization of the covariance method. In [16], the effect of additive noise is not considered, and no simulation results are provided to assess the performance of the velocity estimation technique in real situations.

2.5 Summary

The Rayleigh fading channel for a pure carrier is very widely used in practical cellular systems, and will be adopted in this thesis. Both the IDFT algorithm and AR(p) process can be employed to generate realistic Rayleigh fading process and perform efficiently. Several existing velocity estimation methods are briefly reviewed. We observe that these existing estimators require SNR information as input. In the following chapter, we remove this restriction.

Chapter 3

IQ-ACF-Based Joint Velocity and SNR Estimation

3.1 Introduction

In Section 2.4.3, we discussed an existing IQ-ACF based velocity estimation method, which has been shown to attain high accuracy. However, this method requires knowledge of the signal noise ratio (SNR) at the receiver. In this section, we develop a SNR-independent velocity (Doppler) estimation algorithm, which still maintains high accuracy, though not as high as that of the SNR-dependent estimators in Section 2.4.3 at high velocities. The SNR information can also be estimated jointly with mobile velocity and is shown to perform with reasonable accuracy.

This chapter is organized as follows: in Section 3.2, a novel algorithm, which

estimates velocity and SNR jointly, is proposed. In Sections 3.3 and 3.4, the estimation procedure and simulation results are presented to compare the performance of our proposed estimators with the SNR-dependent ACF-based method described in Chapter 2.

3.2 IQ-ACF-Based Estimation method

For Rayleigh fading channels, the ACF of the IQ components of the received signal can be expressed as a Bessel function in terms of f_m, as presented in (2.19).

Letting $k = 0, 1, 2$ in Equation (2.19), we obtain

$$\begin{aligned} \phi_{II}(0) &= \sigma^2 + \sigma_n^2 \\ \phi_{II}(1) &= \sigma^2 J_0(2\pi f_m) + \sigma_n^2 \mathrm{sinc}(B_n T_s) \\ \phi_{II}(2) &= \sigma^2 J_0(4\pi f_m) + \sigma_n^2 \mathrm{sinc}(2B_n T_s) \end{aligned} \tag{3.1}$$

The normalized ACFs are defined as

$$c_1 \equiv \frac{\phi_{II}(1)}{\phi_{II}(0)} \tag{3.2}$$

$$c_2 \equiv \frac{\phi_{II}(2)}{\phi_{II}(0)} \tag{3.3}$$

By inserting (3.1) into (3.2) and (3.3), the normalized ACFs will be

$$\begin{aligned} c_1 &= \frac{snr\,J_0(2\pi f_m) + \mathrm{sinc}(B_n T_s)}{1 + snr} \\ c_2 &= \frac{snr\,J_0(4\pi f_m) + \mathrm{sinc}(2B_n T_s)}{1 + snr} \end{aligned} \tag{3.4}$$

where $snr \equiv \frac{\sigma^2}{\sigma_n^2}$.

If snr is known, f_m can be estimated from c_1 directly [6]

$$\hat{f_m} = \frac{1}{2\pi} J_0^{-1}[\frac{c_1(1 + snr) - \mathrm{sinc}(B_n T_s)}{snr}] \tag{3.5}$$

If snr is not available, the two equations in (3.4) are both required to obtain $\hat{f_m}$ by combining into

$$c_3 J_0(4\pi \hat{f_m}) - c_4 J_0(2\pi \hat{f_m}) = c_5 \tag{3.6}$$

where

$$c_3 = \mathrm{sinc}(B_n T_s) - c_1 \tag{3.7}$$

$$c_4 = \mathrm{sinc}(2B_n T_s) - c_2 \tag{3.8}$$

$$c_5 = c_2 \mathrm{sinc}(B_n T_s) - c_1 \mathrm{sinc}(2B_n T_s) \tag{3.9}$$

If $\hat{c_1} = \frac{\hat{\phi}_{II}(1)}{\hat{\phi}_{II}(0)}$ and $\hat{c_2} = \frac{\hat{\phi}_{II}(2)}{\hat{\phi}_{II}(0)}$ are the estimates of c_1 and c_2, respectively, based on n received signal samples, $\hat{\phi}_{II}(0)$, $\hat{\phi}_{II}(1)$, and $\hat{\phi}_{II}(2)$ can be obtained via the averages of n samples

$$\begin{aligned} \hat{\phi}_{II}(0) &= \frac{1}{n} \sum_{i=1}^{n} x_I(i) x_I(i) \\ \hat{\phi}_{II}(1) &= \frac{1}{n-1} \sum_{i=1}^{n-1} x_I(i) x_I(i+1) \\ \hat{\phi}_{II}(2) &= \frac{1}{n-2} \sum_{i=1}^{n-2} x_I(i) x_I(i+2) \end{aligned} \tag{3.10}$$

where $x_I(i)$ is the in-phase component of the received complex signal at time i.

SNR Independent Property

To ensure that there is only one root in Equation (3.6), the following function should have a unique zero:

$$g(x) = c_3 J_0(4\pi x) - c_4 J_0(2\pi x) - c_5 \tag{3.11}$$

where c_3, c_4, and c_5 are defined in Equations (3.7) to (3.9), which are functions in terms of the estimated IQ ACFs. If the number of samples is very large, the estimated ACFs will be very close to the true ACFs. By inserting Equations (3.4), (3.7) to (3.9) into (3.11), Equation (3.11) can be written as

$$g(x) = \frac{snr}{1 + snr}\left(c_3^{'} J_0(4\pi x) - c_4^{'} J_0(2\pi x) - c_5^{'}\right) \tag{3.12}$$

where

$$\begin{aligned} c_3^{'} &= \mathrm{sinc}(B_n T_s) - J_0(2\pi f_m) \\ c_4^{'} &= \mathrm{sinc}(2B_n T_s) - J_0(4\pi f_m) \\ c_5^{'} &= J_0(4\pi f_m)\mathrm{sinc}(B_n T_s) - J_0(2\pi f_m)\mathrm{sinc}(2B_n T_s) \end{aligned} \tag{3.13}$$

From (3.12), it is observed that the root of Equation (3.6) becomes independent of SNR.

Root-Finding Procedure

Doppler frequency f_m can be obtained by solving non-linear Equation (3.6). Here a brute force method is used, which is presented briefly as follows:

1. Limit f_m within a certain range $0 \leq f_m \leq R_{upp}$, where R_{upp} is chosen to ensure a unique root of Eqn. (3.6). Appendix A discusses the choice of R_{upp} in detail.

2. Divide the range $[0, R_{upp}]$ into N equal intervals: f_{m1}, f_{m2}, .., and f_{mN}, where N is the total number of the intervals, and $f_{mi}, i = 1, 2, .., N$ is the mid-point of the i^{th} interval.

3. Calculate $g(f_{mi}) = c_3 J_0(4\pi f_{mi}) - c_4 J_0(2\pi f_{mi}) - c_5$ for $i = 1, 2, .., N$.

4. Find $argmin_{i=1,..,N}|g(f_{mi})|$.

5. If $|g(f_{mk})|$ attains the minimum value, the k^{th} interval will contain the solution to Equation (3.6).

6. For large enough N, the solution of f_m can be approximated by the mid-point of the k^{th} interval, i.e., $\hat{f}_m \approx f_{mk}$.

This method is guaranteed to find the unique root of Equation (3.6) if R_{upp} is chosen appropriately.

Once f_m is estimated, the velocity may be estimated via [2]

$$\hat{v} = \hat{F}_m \lambda \tag{3.14}$$

Substituting $F_m = f_m F_s$ and $\lambda = \frac{c}{f_c}$ into (3.14),

$$v = \frac{\hat{f}_m F_s c}{f_c} \tag{3.15}$$

where c is the speed of light.

The accuracy of the f_m estimate in (3.6) depends on the accuracy of autocorrelation function estimates $\hat{\phi_{II}}(0)$, $\hat{\phi_{II}}(1)$ and $\hat{\phi_{II}}(2)$, which can be shown to be asymptotically unbiased and consistent [32].

It is well known that for the zeroth order Bessel function, if $x \ll 1$, the following approximation holds

$$J_0(x) \approx 1 - \frac{x^2}{4} \tag{3.16}$$

Therefore, for small f_m, an approximate closed-form solution to Equation (3.6) can be obtained as

$$\hat{f_m} \approx \sqrt{\frac{c_3 - c_4 - c_5}{4c_3\pi^2 - c_4\pi^2}} \tag{3.17}$$

After obtaining f_m from (3.6) or (3.17), snr can also be estimated in closed-form via

$$\hat{snr} = \frac{\mathrm{sinc}(2B_n T_s) - c_2}{c_2 - J_0(4\pi \hat{f_m})} \tag{3.18}$$

which is derived from Equation (3.4).

We remark that if we replace the IQ components by the complex low-pass equivalent signal, f_m can be estimated from the autocorrelation function of the complex

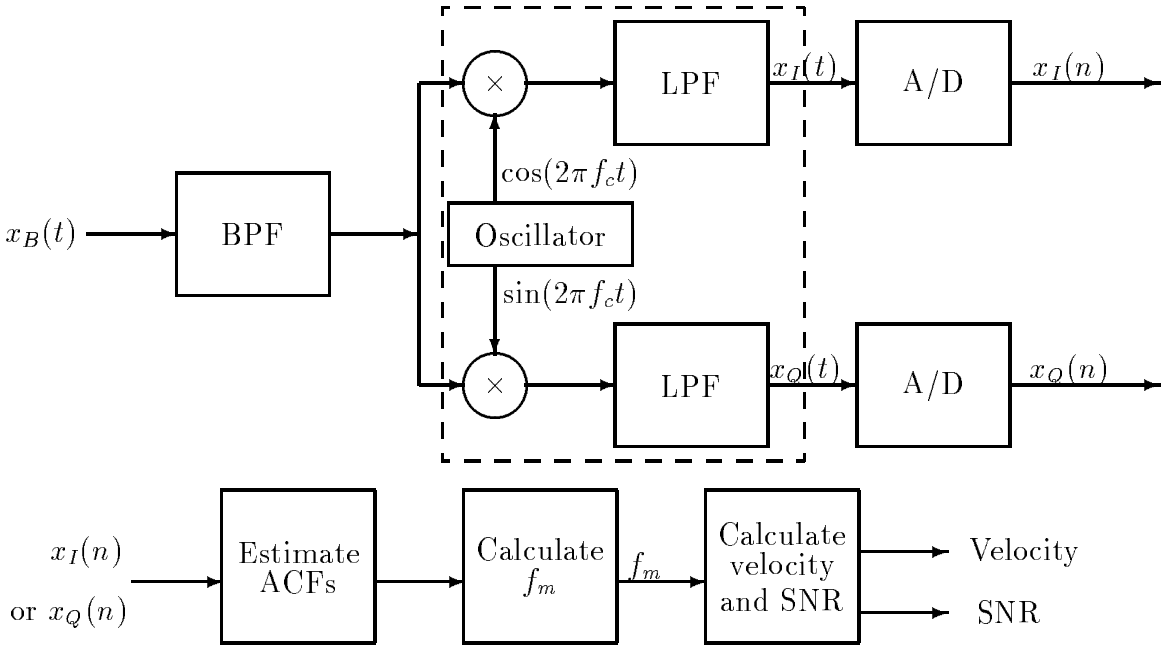

Figure 3.1: Procedures for IQ-ACF-based joint velocity and SNR estimation

signal, which is also a Bessel function and should have better performance than the above method, since more information (both I and Q) is employed to estimate the velocity.

3.3 Estimation Procedures

At the mobile station, the steps for velocity (Doppler) estimation are shown in Figure 3.1. As we discussed in previous sections, the first step is to band-pass filter the received signal to reduce the out-of-band noise components. After that, the bandpass signal is down-converted into a low-pass signal. The function inside the dashed box is the band-pass to low-pass signal conversion: an oscillator is employed to generate

the quadrature carriers $\cos(2\pi f_c t)$ and $\sin(2\pi f_c t)$, and low-pass filters are added to filter out the out-of-band noise. Above converter assumes that perfect carrier recovery is available at the receiver. After conversion, $x_I(t)$ and $x_Q(t)$ are the in-phase and quadrature components of the low-pass equivalent signal, which is then sampled at sampling rate F_s to obtain discrete-time signals $x_I(n)$ and $x_Q(n)$. Obtaining the discrete signal $x_I(n)$ or $x_Q(n)$, we can estimate ACFs of IQ components at lags 0, 1, and 2, respectively, by computing sample averages. The Doppler frequency f_m, the velocity and SNR can then be estimated according to Equations (3.6), (3.15) and (3.18).

Next we discuss how to choose bandwidth B_n and sampling rate F_s.

In our signal model, the spectrum of the received fading signal is within the range $(f_c - F_m,\ f_c + F_m)$. Therefore, the bandwidth of the bandpass filter B_n should be larger than $2F_m$. It is known that F_m is a linear function of mobile [2] velocity,

$$F_m = \frac{v f_c}{c} \tag{3.19}$$

where f_c is usually fixed in a specific communication system. Therefore, the maximum F_m is only affected by the maximum velocity.

It has been shown in Appendix A that if $0 \leq f_m \leq R_{upp}$, i.e., $0 \leq \frac{F_m}{F_s} \leq R_{upp}$, unique solution to (3.6) exists.

Therefore, F_s should satisfy the following inequality

$$F_s \geq \frac{F_{m,max}}{R_{upp}} \tag{3.20}$$

The sampling rate should be large enough to ensure a unique root of Eqn. (3.6). However, a very high sampling rate will result in a very small f_m, which will degrade estimation performance, since if f_m approaches to 0, Bessel function $J_0(2\pi f_m)$ is in the non-linear region, and even slight ACF estimation error will result in a large deviation from the true f_m. Thus, an optimum sampling rate exists for the ACF-based velocity estimation problem.

Algorithm summary

The algorithm for joint f_m and SNR estimation using IQ ACF can be summarized as below:

- Design an analog band-pass filter with bandwidth B_n, which might be a Butterworth filter with upper cutoff frequency $F_{cu} = f_c + \frac{B_n}{2}$, lower cutoff frequency $F_{cl} = f_c - \frac{B_n}{2}$, upper stopband frequency $F_{su} = F_{cu} + \frac{B_n}{4}$, lower stopband frequency $F_{sl} = F_{cl} - \frac{B_n}{4}$, and 60 dB stopband attenuation [6].
- Use the above filter to bandpass filter the received signal.
- Convert the received band-pass signal into its equivalent low-pass signal.
- Sample the low-pass signal at sampling rate F_s.
- Estimate ACFs by computing $\hat{\phi}_0$, $\hat{\phi}_1$ and $\hat{\phi}_2$ over n samples
- Solve $\hat{f_m}$ based on Equation (3.6).

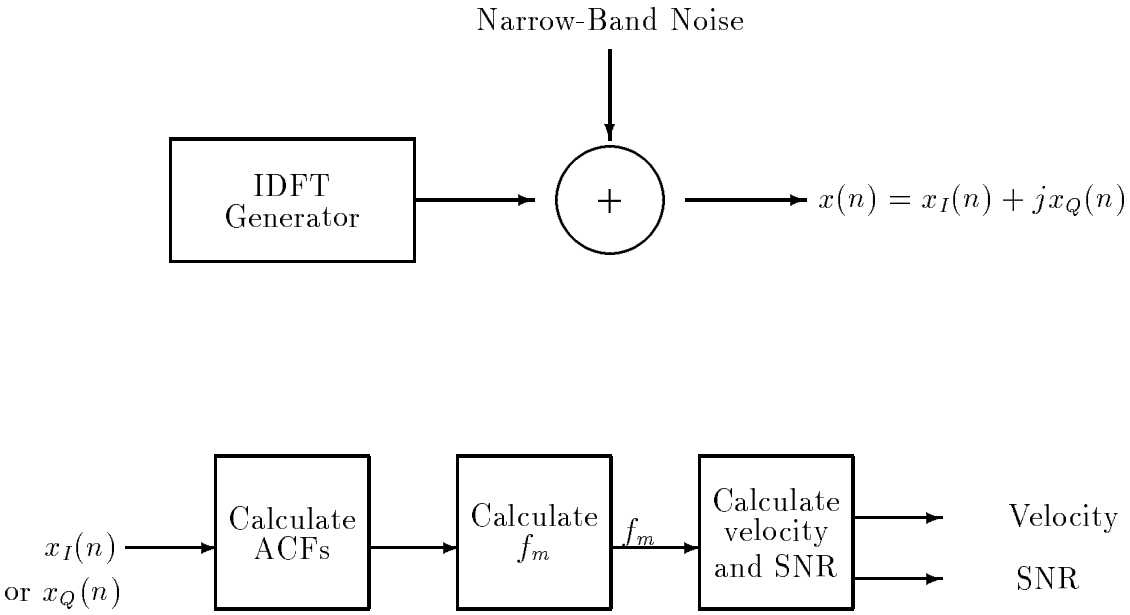

Figure 3.2: The implementation procedure for joint IQ-based velocity and SNR estimation

- Calculate velocity and SNR based on the estimated f_m using Equations (3.15) and (3.18).

3.4 Implementation Issues and Simulation Results

3.4.1 Implementation Issues

In this section, we evaluate the performance of our proposed SNR-independent estimation algorithms by computer simulation.

Assuming that the velocity is in the range ($10km/h$, $185km/h$), and the carrier frequency is $2GHz$, we can obtain the the maximum $F_m = 342.4Hz$ via Equation

(3.19). The sampling rate F_s should be chosen to be at least $\frac{F_{m,max}}{R_{upp}}$. From Appendix A, we know that $R_{upp} = 0.214$ for $B_n T_s = \frac{1}{2}$. Therefore, $F_s \geq 1600Hz$. We choose $F_s = 1600Hz$, and $B_n = 800Hz$, which is also greater than twice $F_{m,max}$. The parameters are shown in Table 3.1.

f_c	Maximum velocity	$F_{m,max}$	B_n	F_s	$f_{m,max}$	Number of samples
$2GHz$	$185km/h$	342.4 Hz	$800Hz$	$1600Hz$	0.2140	1000

Table 3.1: The parameters for IQ-ACF-based velocity estimation

After obtaining all the required parameters, we next present the summary of the implementation procedure.

Summary of the Implementation Procedure

The procedure is shown in Figure 3.2 and summarized as follows

- Generate the fading process using Young and Beaulieu's IDFT algorithm [17].
- Generate the narrow-band Gaussian noise via filtering an identical and independent distributed (i.i.d.) Gaussian sequence through a digital Butterworth filter with bandwidth B_n and order 5 [6].
- Add the additive Gaussian noise to the fading process.

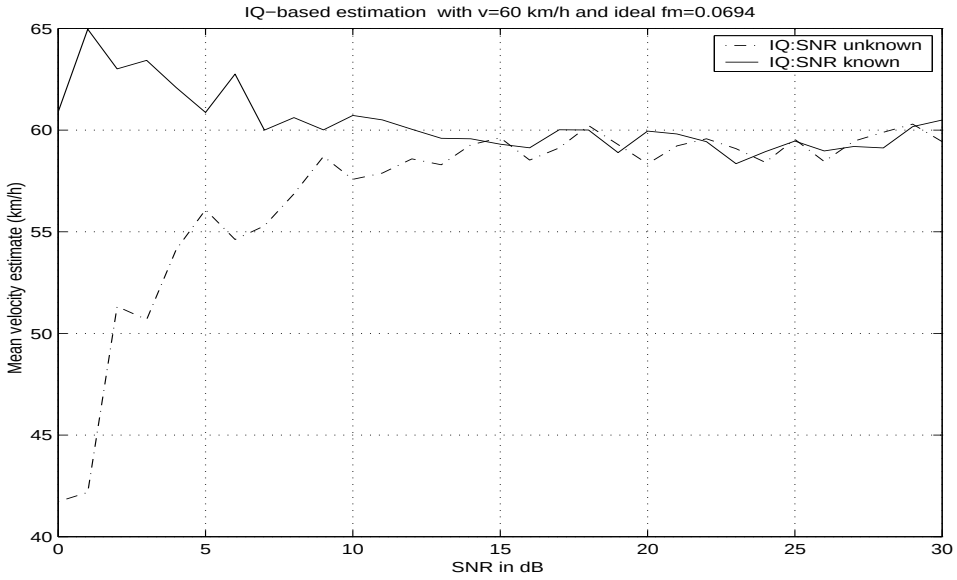

Figure 3.3: Velocity estimate for IQ-ACF-based estimation with true velocity $60km/h$.

- Estimate the autocorrelation function of the received IQ components over n samples according to Equation (3.10).
- Estimate f_m according to Equation (3.6).
- Compute the velocity using $v = \frac{cf_m F_s}{f_c}$.
- Estimate SNR according to Equation (3.18) based on estimated f_m.
- Repeat the above steps until the total number of Monte-Carlo trials is reached, and calculate the average value of estimated velocity and SNR.

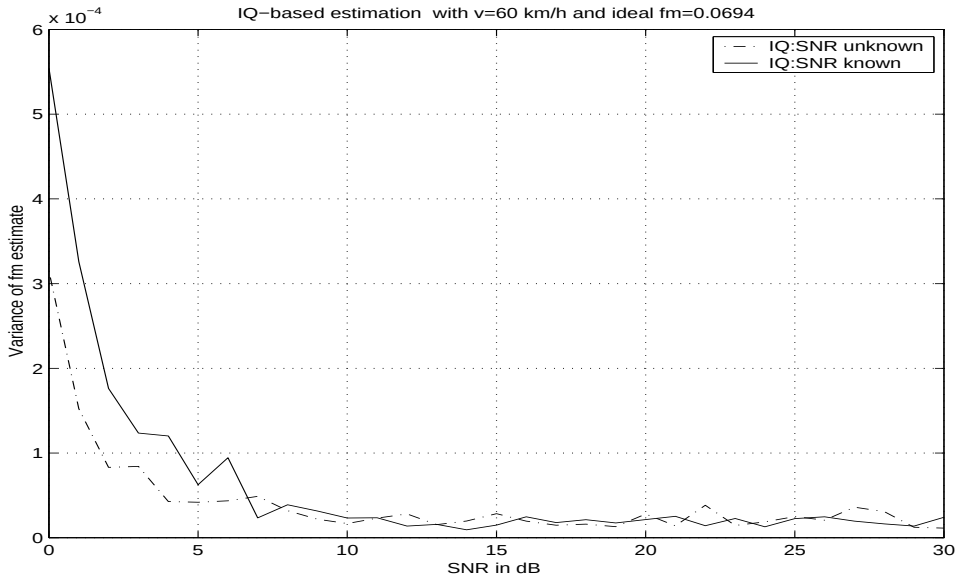

Figure 3.4: Variance of Doppler estimate for IQ-ACF-based estimation with true velocity $60km/h$.

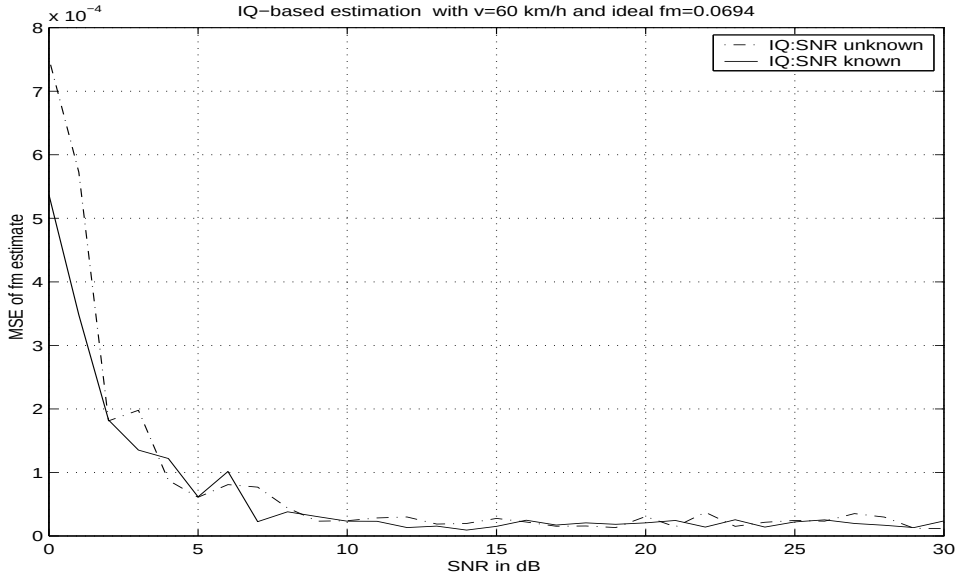

Figure 3.5: MSE of Doppler estimate for IQ-ACF-based estimation with true velocity $60km/h$.

True velocity	$10km/h$	$20km/h$	$40km/h$	$60km/h$
velocity estimate (proposed)	8.136	20.0592	39.3811	59.5699
velocity estimate in [6]	9.5443	20.2723	40.0896	59.4605
True velocity	$80km/h$	$100km/h$	$120km/h$	$140km/h$
velocity estimate (proposed)	78.5232	96.9293	122.7859	143.2253
velocity estimate in [6]	80.1274	99.7747	119.0045	142.0099
True velocity	$160km/h$	$180km/h$	$200km/h$	
velocity estimate (proposed)	157.4986	178.0906	95.2877	
velocity estimate in [6]	158.3885	176.9155	181.4400	

Table 3.2: IQ-ACF-based velocity estimation over 30 Monte-Carlo trials for SNR=20 dB

3.4.2 Simulation Results

Velocity estimation

We now compare the performance of our proposed SNR-independent velocity estimator to that of the SNR-dependent method proposed in [6]. By following the estimation procedure described in Section 3.4.1, we obtain the simulation results for different velocities shown in Table 3.2. The simulation results for the SNR-dependent method [6] are also presented in this table.

It is observed that when the velocity is not very high (less than $160km/h$), our

proposed method is quite accurate, and the bias is small. For larger velocities, the fading becomes fast, and the bias in velocity estimation is increased. For velocities within the range [$160km/h$, $185km/h$], our proposed method seems inferior to that of [6], but only moderately. In general, our proposed IQ-ACF-based method can obtain very accurate velocity estimates within the range [$10km/h$, $185km/h$]. We note that in our simulations, $185km/h$ is the upper bound velocity to ensure a unique root of Equation (3.6). We remark that SNR-dependent algorithms can obtain good quality estimates within the range [$180km/h$, $200km/h$] with lower bias, since the corresponding upper bound velocity for the SNR-dependent case is over $200km/h$.

Figures 3.3 and 3.6 present simulation results of mean velocity as a function of SNRs with fixed velocities $60km/h$ and $100km/h$, respectively. Figures 3.4-3.5 and 3.7-3.8 show the corresponding variance and mean-square-errors (MSE). Unless otherwise indicated, 30 independent Monte-Carlo trials are used. We mention that the curves in these figures are jagged due to the insufficient Monte-Carlo trials.

It can be seen that, as the SNR increases, the velocity estimates have lower bias, and the Doppler frequency estimate has lower variance and mean-square-error (MSE). However, we note that the MSE does not approach zero for very high SNR.

From above figures, it is also observed that under low SNR, our proposed SNR-independent method is not as accurate as the SNR-dependent method. This may be explained by the fact that more ACF samples are needed in the SNR-independent method. However, when SNR is larger than 10 dB, the performance of SNR-independent

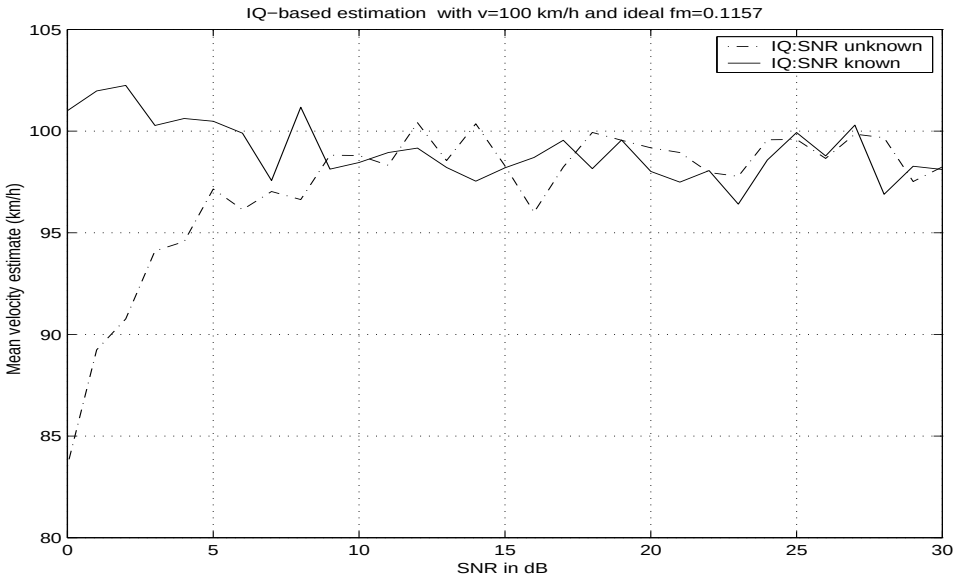

Figure 3.6: Velocity estimate for IQ-ACF-based estimation with true velocity $100km/h$.

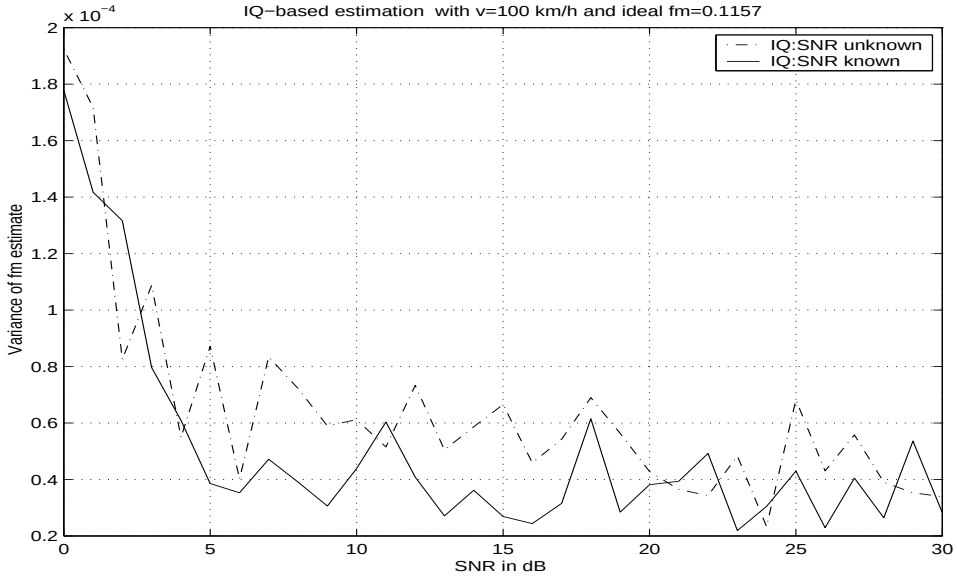

Figure 3.7: Variance of Doppler estimate for IQ-ACF-based estimation with true velocity $100km/h$.

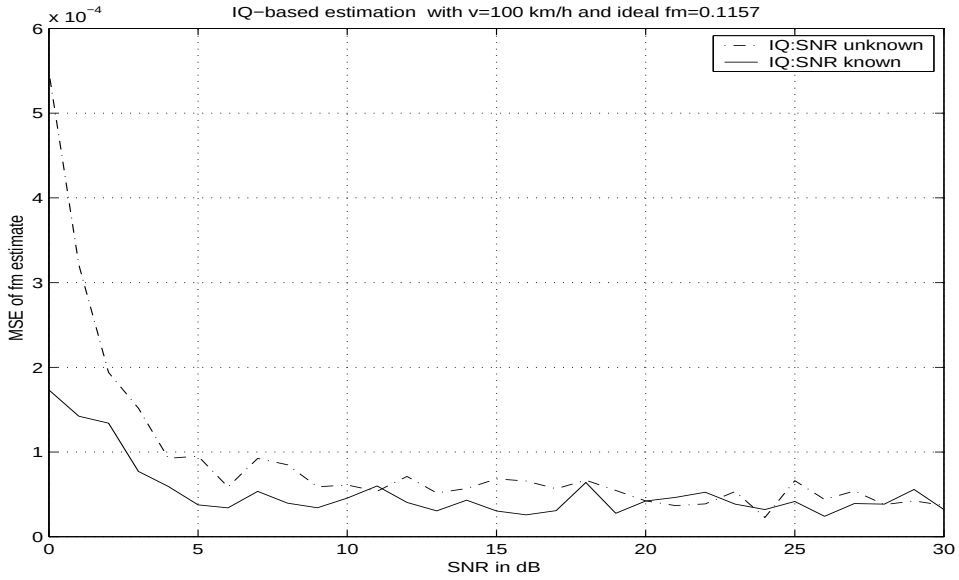

Figure 3.8: MSE of Doppler estimate for IQ-ACF-based estimation with true velocity $100km/h$.

estimation becomes very close to that of SNR-dependent estimation.

SNR estimate

An important by-product of our proposed algorithm is SNR estimation, which is obtained from Equation (3.18) once f_m is estimated.

Figures (3.9) to (3.10) show that IQ-based ACF estimation can obtain accurate SNR estimates if the true SNR is not high. In general, performance of SNR estimation gets poor for true SNRs that exceed 20 dB.

Comparison of Figures (3.9) to (3.10), and tests at other velocities also show that both the values of the true SNR and velocity affect the performance of SNR

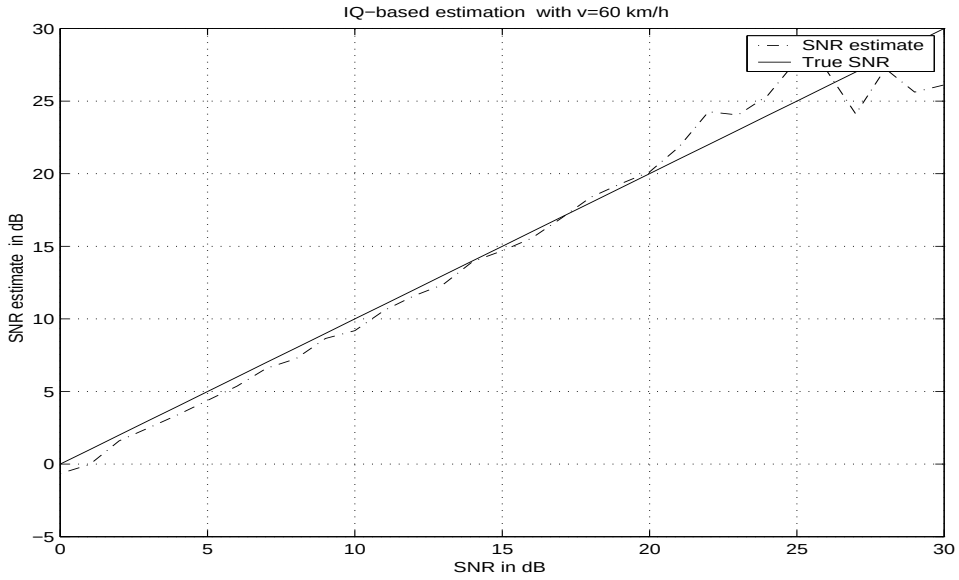

Figure 3.9: SNR estimate for the case of velocity $60km/h$.

estimation. It is clear that SNR estimation at high mobile velocities is worse than that for low velocities.

3.5 Summary

We have derived a joint velocity and SNR estimation algorithm, which needs coherent demodulation. The simulation results show that SNR-independent velocity estimates are very accurate while only slightly inferior to the SNR-dependent estimates at low SNR. Also, the SNR itself can be estimated and is shown to perform well where the SNR is not very high.

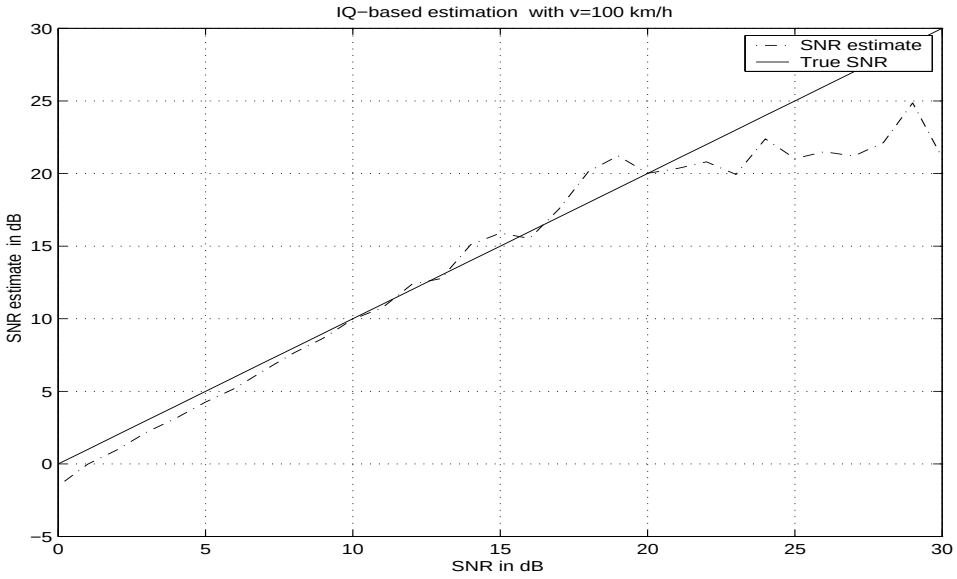

Figure 3.10: SNR estimate for the case of velocity $100km/h$.

Chapter 4

Envelope-ACF-Based Joint Velocity and SNR Estimation

4.1 Introduction

In the previous chapter, it was shown that IQ-ACF based velocity estimators can be made SNR-independent, and still maintain their accuracy. However, IQ-ACF-based velocity estimation requires coherent demodulation. In this section, we propose envelope-based and squared-envelope-based estimation methods, in which coherent demodulation is not required. Similar to the IQ-ACF based method, these estimators can be extended to estimate mobile velocity without a priori knowledge of the link SNR.

This chapter begins by presenting a new velocity estimation algorithm in Section 4.2, which is based on the envelope autocorrelation function derived in [27], and Monte-Carlo simulations have shown good performance under low velocities. In Section 4.3, a squared-envelope-ACF based velocity estimation method is then proposed, which can achieve accurate estimates for both low and high velocities.

4.2 Envelope-ACF-Based Estimation Method

4.2.1 Envelope-ACF-Based Algorithm

In [27], the autocorrelation function of the envelope of a fading signal is derived as

$$\begin{aligned} \phi_{zz}(k) &= E[z(i+k)z(i)] \\ &= \frac{\pi}{4}\Omega_p F[-0.5,-0.5;1,\rho^2(k)] \end{aligned} \tag{4.1}$$

in which $z(k)$ is the envelope at the k^{th} sampling instant, Ω_p is the averaged received power, $F[-0.5,-0.5;1,\rho^2(k)]$ is the hyper-geometric function, which can be expanded in the series

$$F[-0.5,-0.5;1,\rho^2(k)] = 1 + \frac{1}{4}\rho^2(k) + \frac{1}{64}\rho^4(k) + ... \tag{4.2}$$

where $\rho^2(k) = \frac{4}{\Omega_p^2}\phi_{II}^2(k)$, and the ACF of IQ components $\phi_{II}(k)$ is given in Equation (2.19).

By considering the effect of AWGN, and approximating the hyper-geometric function by the first two terms [9], the expression in (4.1) becomes

$$\phi_{zz}(k) \approx \frac{\pi}{4}\Omega_p \left(1 + \frac{1}{4}\left[\frac{\sigma^2 J_0(2\pi f_m k) + \sigma_n^2 \mathrm{sinc}(B_n T_s k)}{\sigma^2 + \sigma_n^2}\right]^2\right) \tag{4.3}$$

Letting $k = 0, 1, 2$ in (4.3), we get the system of equations

$$\begin{aligned}
\phi_{zz}(0) &= \frac{5\pi}{16}\Omega_p & (4.4)\\
\phi_{zz}(1) &= \frac{\pi}{4}\Omega_p(1 + \frac{1}{4}[\frac{\sigma^2 J_0(2\pi f_m) + \sigma_n^2 \mathrm{sinc}(B_n T_s)}{\sigma^2 + \sigma_n^2}]^2) & (4.5)\\
\phi_{zz}(2) &= \frac{\pi}{4}\Omega_p(1 + \frac{1}{4}[\frac{\sigma^2 J_0(4\pi f_m) + \sigma_n^2 \mathrm{sinc}(2B_n T_s)}{\sigma^2 + \sigma_n^2}]^2) & (4.6)
\end{aligned}$$

where σ^2, σ_n^2 and snr have the same definitions as in Chapter 2.

The normalized envelope ACFs are defined as

$$\begin{aligned}
e_1 &= \frac{\phi_{zz}(1)}{\phi_{zz}(0)}\\
&= \frac{4}{5}[1 + \frac{1}{4}\frac{(snr J_0(2\pi f_m) + \mathrm{sinc}(B_n T_s))^2}{(1 + snr)^2}]\\
e_2 &= \frac{\phi_{zz}(2)}{\phi_{zz}(0)}\\
&= \frac{4}{5}[1 + \frac{1}{4}\frac{(snr J_0(4\pi f_m) + \mathrm{sinc}(2B_n T_s))^2}{(1 + snr)^2}]
\end{aligned} \tag{4.7}$$

If the SNR is known, f_m can be estimated from e_1 directly as

$$f_m = \frac{1}{2\pi} J_0^{-1}[\frac{\sqrt{5e_1 - 4}(1 + snr) - \mathrm{sinc}(B_n T_s)}{snr}] \tag{4.8}$$

which can again be obtained by inverting a Bessel function.

If the SNR is unknown, two equations in (4.7) are both needed to estimate f_m. Combining the two equations in (4.7) into one equation in terms of f_m, we obtain the

same form as (3.6) with e_3, e_4, and e_5 replacing c_3, c_4, and c_5, respectively,

$$e_3 J_0(4\pi f_m) - e_4 J_0(2\pi f_m) = e_5 \tag{4.9}$$

where

$$\begin{aligned} e_3 &= \text{sinc}(B_n T_s) - \sqrt{5e_1 - 4} \\ e_4 &= \text{sinc}(2B_n T_s) - \sqrt{5e_2 - 4} \\ e_5 &= \sqrt{5e_2 - 4}\text{sinc}(B_n T_s) - \sqrt{5e_1 - 4}\text{sinc}(2B_n T_s) \end{aligned} \tag{4.10}$$

e_1 and e_2 can be estimated by

$$\hat{e}_1 = \frac{\hat{\phi}_{zz}(1)}{\hat{\phi}_{zz}(0)} \tag{4.11}$$

$$\hat{e}_2 = \frac{\hat{\phi}_{zz}(2)}{\hat{\phi}_{zz}(0)} \tag{4.12}$$

where $\hat{\phi}_{zz}(0)$, $\hat{\phi}_{zz}(1)$ and $\hat{\phi}_{zz}(2)$ can be estimated similarly using (3.10) with envelope samples replacing the IQ components of samples.

Similar to IQ-based method, the f_m estimate can be obtained from solving (4.9) via brute-force method.

When $x \ll 1$, the Bessel function $J_0(x) \approx 1 - \frac{x^2}{4}$. Using this approximation, a closed-form expression for $\hat{f_m}$ can be obtained from (4.9) as

$$\hat{f_m} \approx \sqrt{\frac{e_3 - e_4 - e_5}{4e_3\pi^2 - e_4\pi^2}} \tag{4.13}$$

We can also obtain the snr estimate from Equation (4.7) as

$$snr = \frac{\text{sinc}(B_n T_s) - \sqrt{5e_1 - 4}}{\sqrt{5e_1 - 4} - J_0(2\pi f_m)} \tag{4.14}$$

4.2.2 Implementation Issues and Simulation Results for Envelope-Based Estimation

Implementation issues

At the mobile station, the procedure for envelope-based velocity (Doppler) estimation is similar to that for IQ-based method with envelope samples replacing IQ components of samples. Figure 4.1 shows the estimation procedure.

The bandwidth B_n and sampling rate F_s are chosen based on the same considerations as in Section 3.4 and are presented in Table 3.1.

The algorithm for SNR-independent f_m estimation using envelope ACF can be summarized as follows:

- Use a bandpass filter as designed in Section 3.4.
- Convert the band-pass signal into its equivalent low-pass signal.
- Sample the low-pass equivalent signal at sampling rate F_s.
- Estimate envelope-ACFs by sample averaging.
- Calculate $\hat{f_m}$ numerically from (4.9).
- Calculate the velocity using $v = \frac{c f_m F_s}{f_c}$.

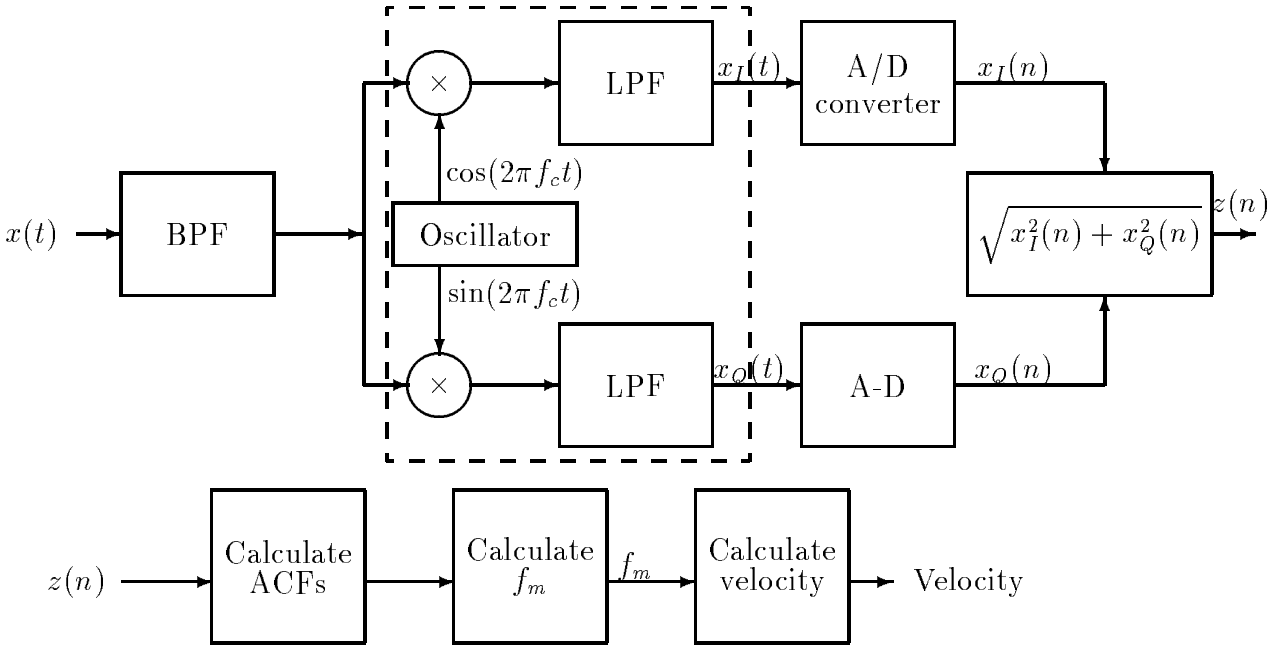

Figure 4.1: Estimation procedure for envelope-ACF-based method

Simulation Results

The generation of the simulated fading signal is shown in Figure 4.2, and the simulation results for different velocities are shown in Table 4.1.

It is observed that when the velocity is not high (under $100km/h$), both estimators perform well. Comparison between the two envelope-based methods shows that as the velocity increases, the SNR-independent estimates are not as accurate as the SNR-dependent ones. When the velocity is higher than $140km/h$, the estimation errors for both algorithms are large, and the performance degrades greatly. Therefore, the envelope-ACF-based method can only be used under low-velocity (below $100km/h$) conditions.

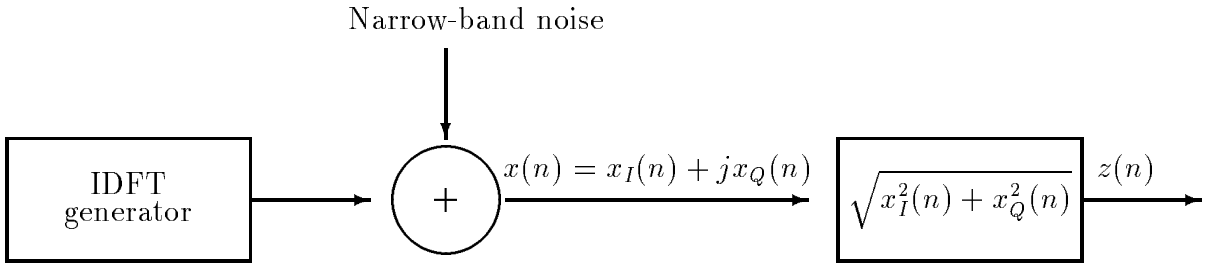

Figure 4.2: Implementation procedure of the envelope of samples of the received signal

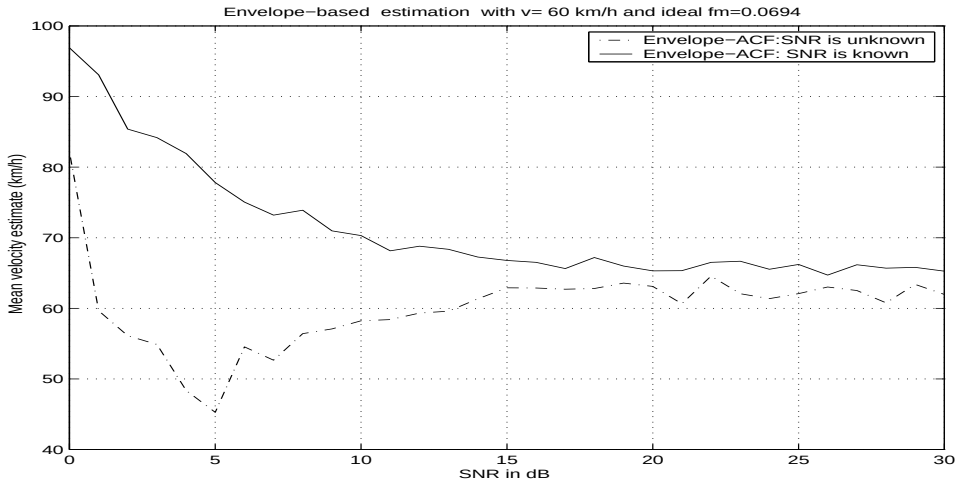

Figure 4.3: Velocity estimate for envelope-ACF-based estimation with true velocity $60km/h$.

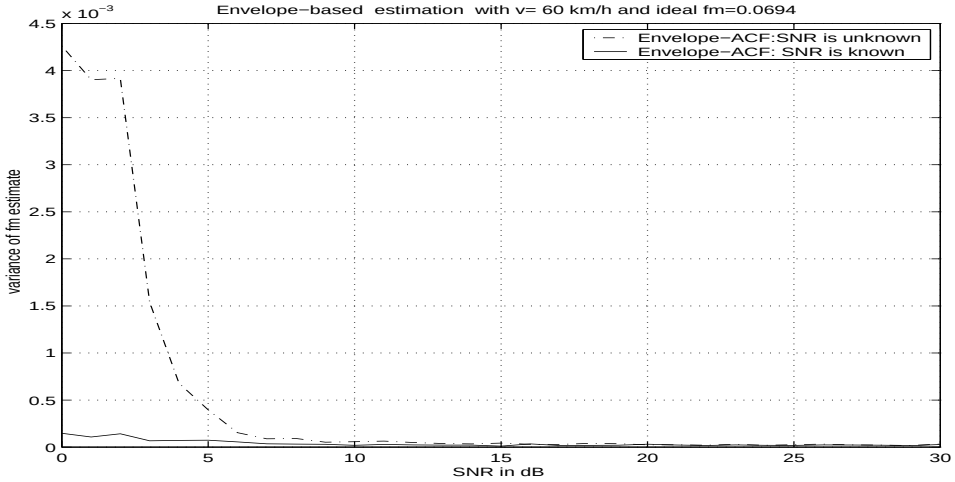

Figure 4.4: Variance of Doppler estimate for envelope-ACF-based estimation with true velocity $60km/h$.

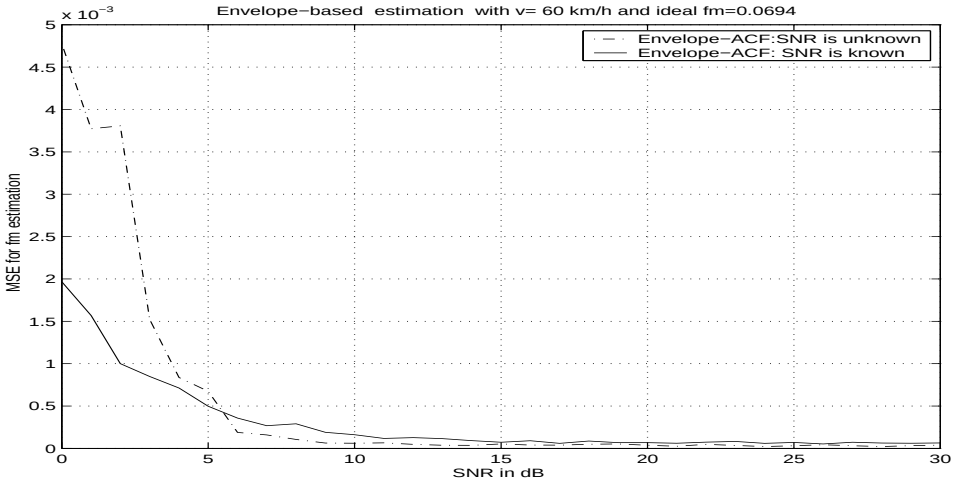

Figure 4.5: MSE of Doppler estimate for envelope-ACF-based estimation with true velocity $60km/h$.

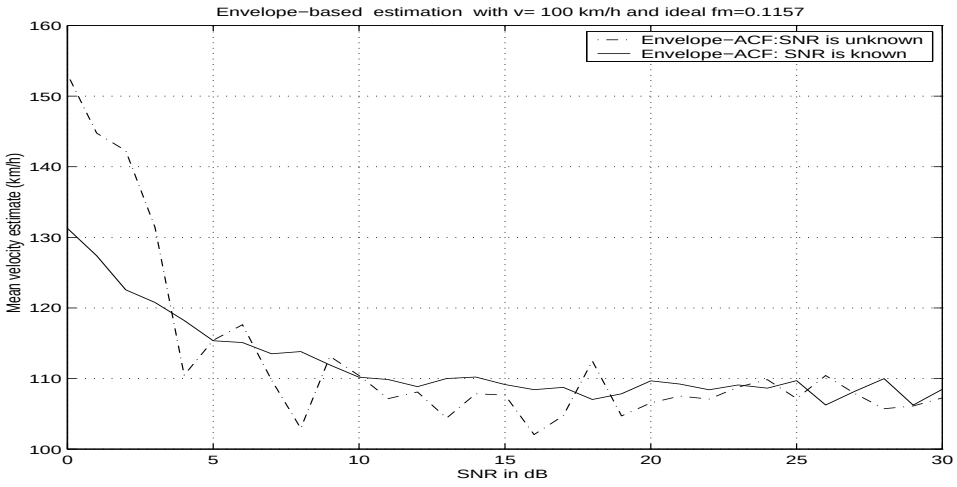

Figure 4.6: Velocity estimate for envelope-ACF-based estimation with true velocity $100km/h$.

Figures 4.3 and 4.6 depict the bias of the envelope-ACF-based velocity estimation for velocities $60km/h$ and $100km/h$, respectively, in which estimators for known SNR and unknown SNR are compared. Figures 4.4-4.5 and 4.7-4.8 present the mean-square-error for the envelope based method when velocity is $60km/h$ and $100km/h$, respectively. It is observed that the performance of velocity estimation is improved as the SNR increases. It can also be seen from these figures that under low SNR, the SNR-independent method is inferior to the SNR-dependent method, since more ACF lags need to be estimated if SNR is not available. When the SNR is larger than 10 dB, the performance of the SNR-independent method is very close to that of SNR-dependent one.

True velocity	$10km/h$	$20km/h$	$40km/h$	$60km/h$
SNR-independent algorithm	8.8790	20.1686	41.8781	63.9878
SNR-dependent algorithm	12.2142	23.8464	46.5235	66.9571
True velocity	$80km/h$	$100km/h$	$120km/h$	$140km/h$
SNR-independent algorithm	82.9181	104.5008	141.2726	159.4282
SNR-dependent algorithm	88.0848	108.4205	130.5101	152.0093
True velocity	$160km/h$	$180km/h$	$200km/h$	
SNR-independent algorithm	173.7504	171.5587	168.0134	
SNR-dependent algorithm	174.9024	189.7430	211.3949	

Table 4.1: Envelope-ACF-based velocity estimation over 30 Monte-Carlo trials for SNR=20 dB.

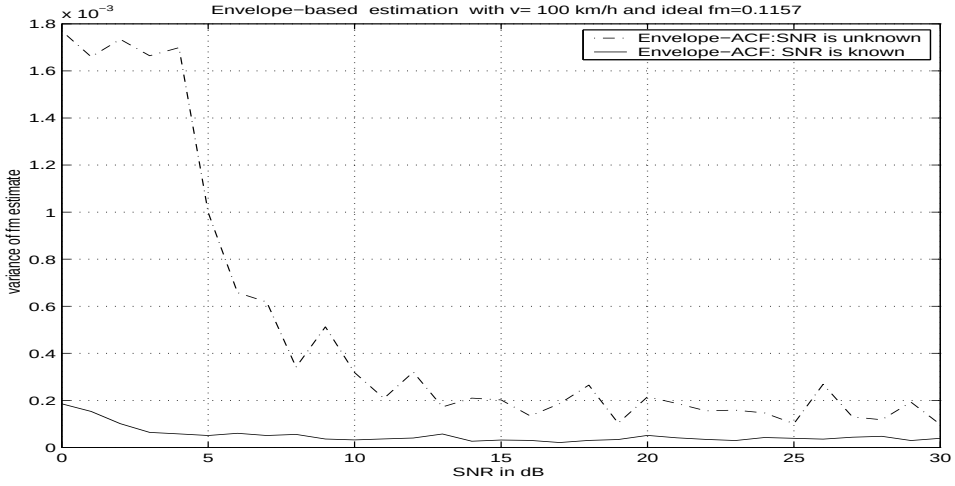

Figure 4.7: Variance of Doppler estimate for envelope-ACF-based estimation with true velocity $100km/h$.

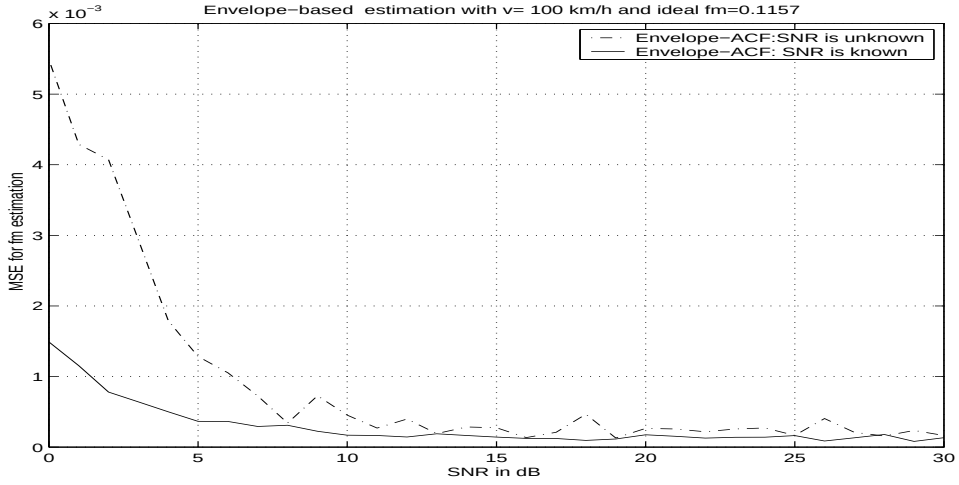

Figure 4.8: MSE of Doppler estimate for envelope-ACF-based estimation with true velocity $100km/h$.

4.3 Squared-Envelope-ACF-Based Estimation Method

4.3.1 Squared-Envelope-ACF-Based Algorithm

It is observed that envelope-ACF-based methods cannot provide accurate estimates at high velocities. An alternative algorithm is proposed in this section, which employs the squared-envelope ACF of the received signal, and can be shown to obtain accurate performance at both low and high velocities.

According to [9], the covariance of the squared-envelope samples can be written as

$$cov\left(r(i), r(i+k)\right) = 4\phi_{II}^2(k) \tag{4.15}$$

where $r(i)$ is the squared-envelope sample at time i.

From (4.15), we derive the autocorrelation function of squared-envelope samples as

$$\begin{aligned}\phi_{rr}(k) &= E[r(i)r(i+k)] \\ &= cov(r(i), r(i+k)) + (E[r(i)])^2 \\ &= 4\phi_{II}^2(k) + 4\phi_{II}^2(0) \end{aligned} \tag{4.16}$$

Letting $k = 0, 1, 2$, (4.16) generates the equations

$$\phi_{rr}(0) = 8(\sigma^2 + \sigma_n^2)^2 \tag{4.17}$$

$$\phi_{rr}(1) = 4(\sigma^2 J_0(2\pi f_m) + \sigma_n^2 \mathrm{sinc}(B_n T_s))^2 + 4(\sigma^2 + \sigma_n^2)^2 \tag{4.18}$$

$$\phi_{rr}(2) = 4(\sigma^2 J_0(4\pi f_m) + \sigma_n^2 \mathrm{sinc}(2B_n T_s))^2 + 4(\sigma^2 + \sigma_n^2)^2 \tag{4.19}$$

The normalized ACFs are defined as

$$\begin{aligned} g_1 &= \frac{\phi_{rr}(1)}{\phi_{rr}(0)} \\ &= \frac{1}{2} + \frac{1}{2}[\frac{snr J_0(2\pi f_m) + \mathrm{sinc}(B_n T_s)}{1 + snr}]^2 \\ g_2 &= \frac{\phi_{rr}(2)}{\phi_{rr}(0)} \\ &= \frac{1}{2} + \frac{1}{2}[\frac{snr J_0(4\pi f_m) + \mathrm{sinc}(2B_n T_s)}{1 + snr}]^2 \end{aligned} \tag{4.20}$$

If SNR is known, f_m can be estimated from g_1 directly as

$$f_m = \frac{1}{2\pi} J_0^{-1}[\frac{\sqrt{2g_1 - 1}(1 + snr) - \mathrm{sinc}(B_n T_s)}{snr}] \tag{4.21}$$

If SNR is unknown, the two equations for g_1 and g_2 in (4.20) are both required to obtain an identical form to (3.6) with c_3, c_4 and c_5 replaced by g_3, g_4 and g_5, respectively, e.g., where

$$\begin{aligned} g_3 &= \text{sinc}(B_n T_s) - \sqrt{2g_1 - 1} \\ g_4 &= \text{sinc}(2B_n T_s) - \sqrt{2g_2 - 1} \\ g_5 &= -\sqrt{2g_1 - 1}\text{sinc}(2B_n T_s) + \sqrt{2g_2 - 1}\text{sinc}(B_n T_s) \end{aligned} \tag{4.22}$$

In (4.20), g_1 and g_2 can be estimated by $\hat{g_1} = \frac{\hat{\phi}_{rr}(1)}{\hat{\phi}_{rr}(0)}$ and $\hat{g_2} = \frac{\hat{\phi}_{rr}(2)}{\hat{\phi}_{rr}(0)}$, where $\hat{\phi}_{rr}(0)$, $\hat{\phi}_{rr}(1)$ and $\hat{\phi}_{rr}(2)$ can be estimated using (3.10) with squared-envelope samples replacing the IQ components. Doppler frequency f_m can be estimated via brute force method, which is presented in Section 3.2.

For small f_m, a closed-form approximation analogous to (3.17) can be obtained as

$$\hat{f_m} \approx \sqrt{\frac{g_3 - g_4 - g_5}{4g_3\pi^2 - g_4\pi^2}} \tag{4.23}$$

The snr can be estimated from Equations (4.20)

$$snr = \frac{\text{sinc}(B_n T_s) - \sqrt{2g_1 - 1}}{\sqrt{2g_1 - 1} - J_0(2\pi f_m)} \tag{4.24}$$

4.3.2 Implementation Issues and Simulation Results for Squared-Envelope-Based Estimation

The implementation procedure for squared-envelope-ACF-based method is similar to that for envelope-ACF-based method, except that squared-envelope samples are used

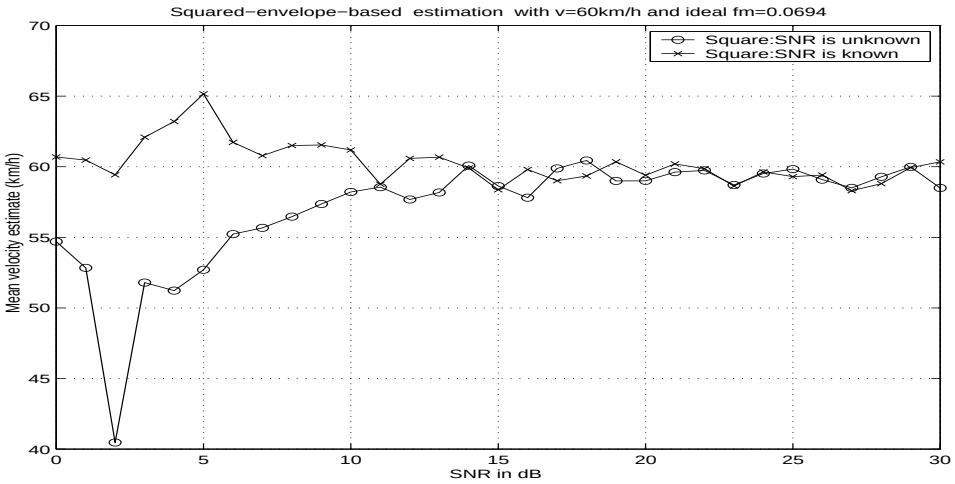

Figure 4.9: Velocity estimate for squared-envelope-ACF-based estimation with true velocity $60km/h$.

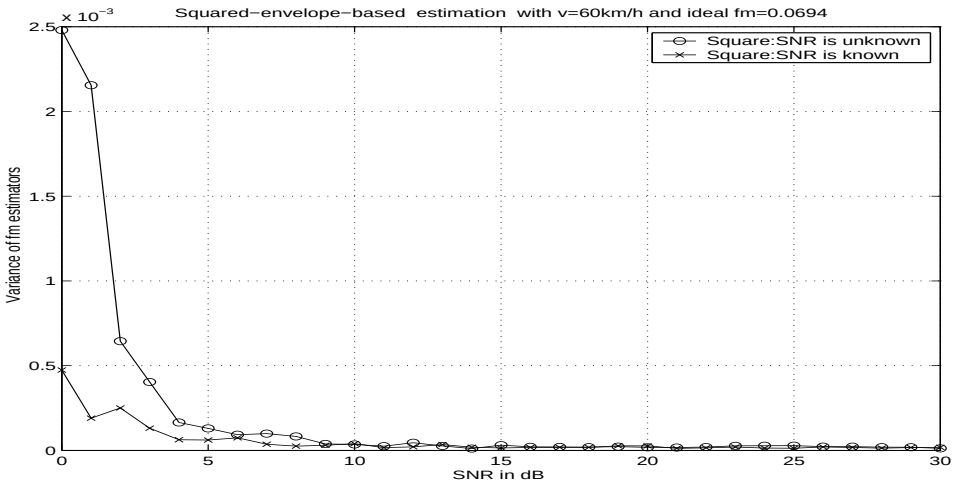

Figure 4.10: Variance of Doppler estimate for squared-envelope-ACF-based estimation with true velocity $60km/h$.

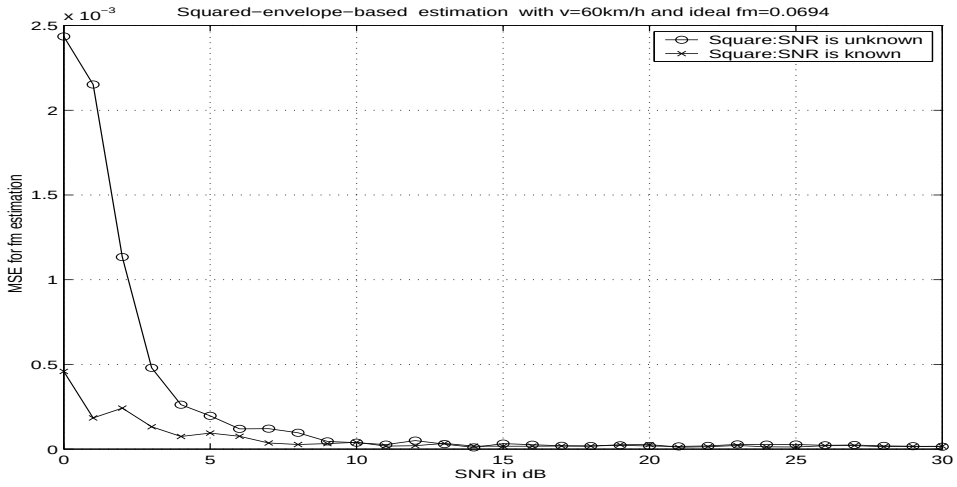

Figure 4.11: MSE of f_m estimate for squared-envelope-ACF-based estimation with true velocity $60km/h$.

instead of envelope samples. The bandwidth B_n and sampling rate F_s are chosen based on the same considerations as in Section 3.4 and are presented in Table 3.1.

The simulation results for SNR-dependent and SNR-independent squared-envelope methods at different velocities are shown in Table 4.2. It is observed that both methods can obtain accurate velocity estimates. Comparison of these two methods shows that the SNR-dependent method has much better performance than the SNR-independent one under high velocities, especially when the velocity is larger than $140km/h$.

Figures 4.9 and 4.12 show the mean velocity estimate based on the squared-envelope-ACF when velocity is $60km/h$ and $100km/h$, respectively; Figures 4.10-4.11 and 4.13-4.14 present the MSEs encountered in velocity estimates for velocity

True velocity	$10km/h$	$20km/h$	$40km/h$	$60km/h$
SNR-independent algorithm	9.5069	19.8806	38.5315	59.8982
SNR-dependent algorithm	9.1094	21.3322	40.1443	60.1056
True velocity	$80km/h$	$100km/h$	$120km/h$	$140km/h$
SNR-independent algorithm	80.0294	99.0029	123.4800	133.5689
SNR-dependent algorithm	78.5059	99.4147	120.0442	141.8141
True velocity	$160km/h$	$180km/h$	$200km/h$	
SNR-independent algorithm	141.9264	172.4544	170.1734	
SNR-dependent algorithm	158.2589	177.6845	181.4400	

Table 4.2: Squared-envelope-ACF-based velocity estimation over 30 Monte-Carlo trials for SNR=20 dB.

$60km/h$ and $100km/h$. Under low SNR, the SNR-dependent method has better performance than the SNR-independent one. As the SNR increases, the performance of the SNR-independent method improves since more accurate ACFs estimates are obtained. It is also shown that when the SNR is large, the two methods have very similar performance.

Comparison between the envelope-based and squared-envelope-based methods shows that the squared-envelope algorithm can obtain more accurate velocity estimates than envelope-based method, especially at high velocities.

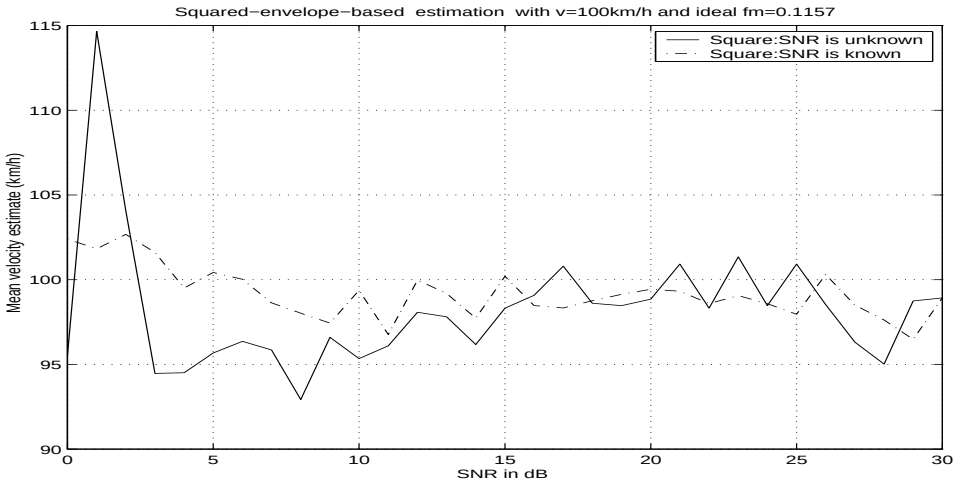

Figure 4.12: Velocity estimate for squared-envelope-ACF-based estimation with true velocity $100km/h$.

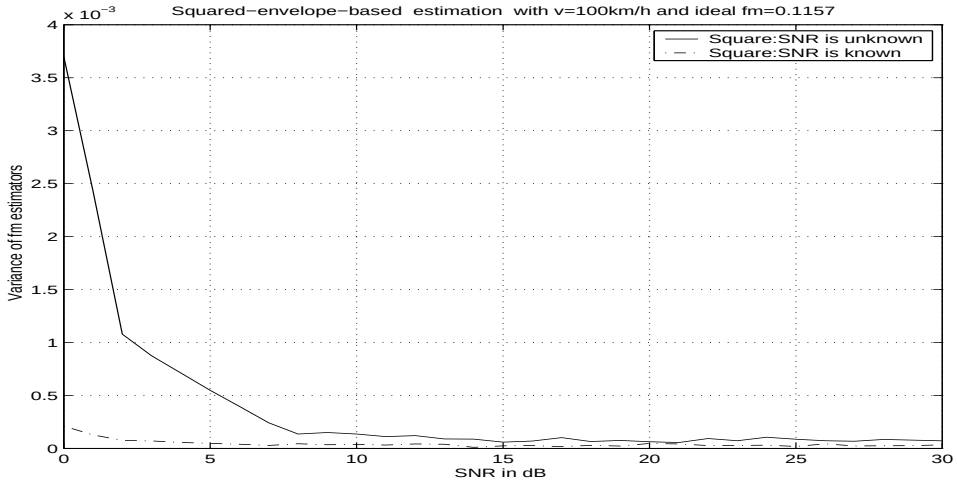

Figure 4.13: Variance of Doppler estimate for squared-envelope-ACF-based estimation with true velocity $100km/h$.

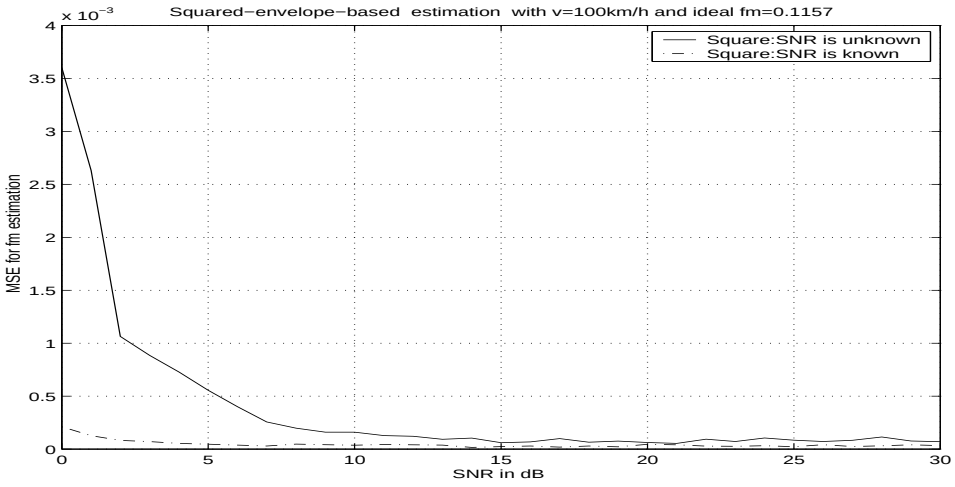

Figure 4.14: MSE of Doppler estimate for squared-envelope-ACF-based estimation with true velocity $100km/h$.

The SNR can be estimated using Equation (4.24) for squared-envelope based estimation. Figures 4.15 to 4.17 show SNR estimates for different velocities. From extensive simulation studies, it is observed that SNR estimates degrade with an increase of both SNR and velocity. We remark that while squared-envelope-based SNR estimation is not as accurate as IQ-based estimation, it avoids coherent demodulation and perfect carrier recovery, required by IQ-based method.

4.4 ACF-Based Velocity Estimation for Narrow-Band Modulated Signals

In Section 2.2.2, we presented the system model for a modulated transmitted signal, where a training sequence or pilot symbols are used. In this section, we focus on the

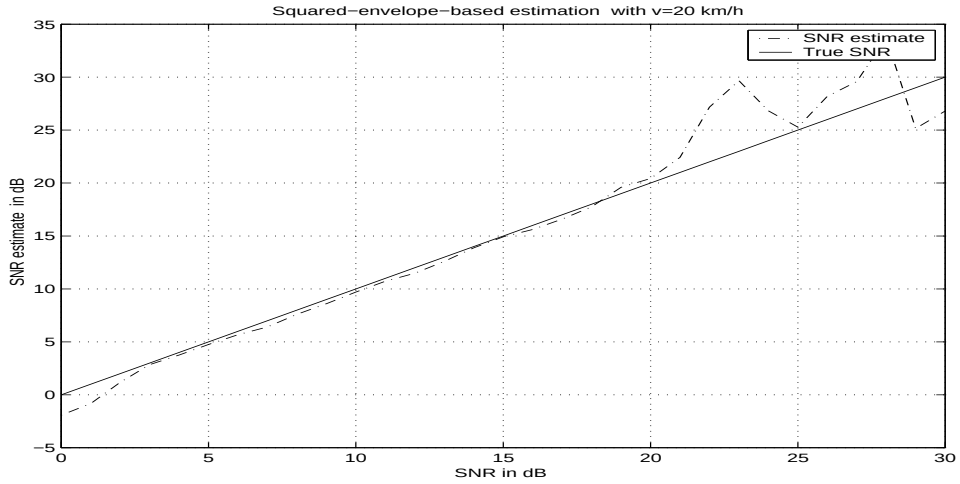

Figure 4.15: SNR estimate versus SNR with mobile velocity $20km/h$ for squared-envelope-based ACF estimation

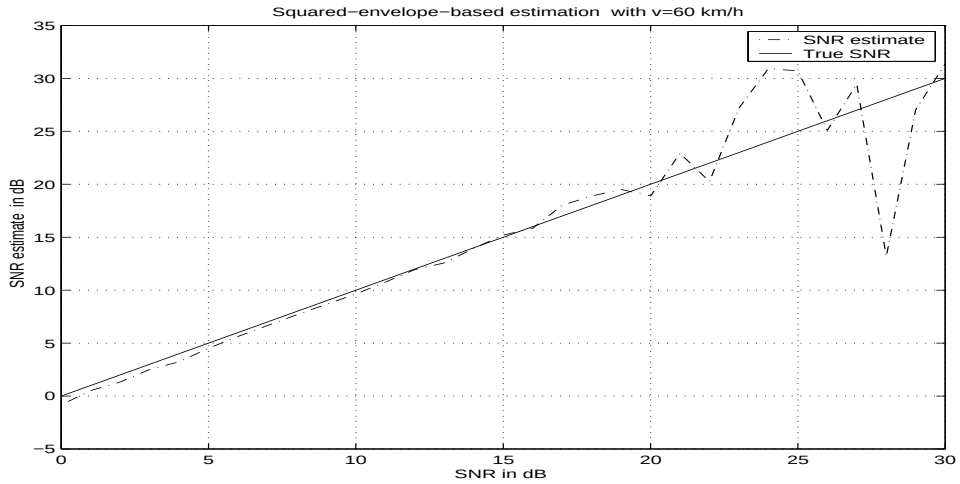

Figure 4.16: SNR estimate versus SNR with mobile velocity $60km/h$ for squared-envelope-based ACF estimation

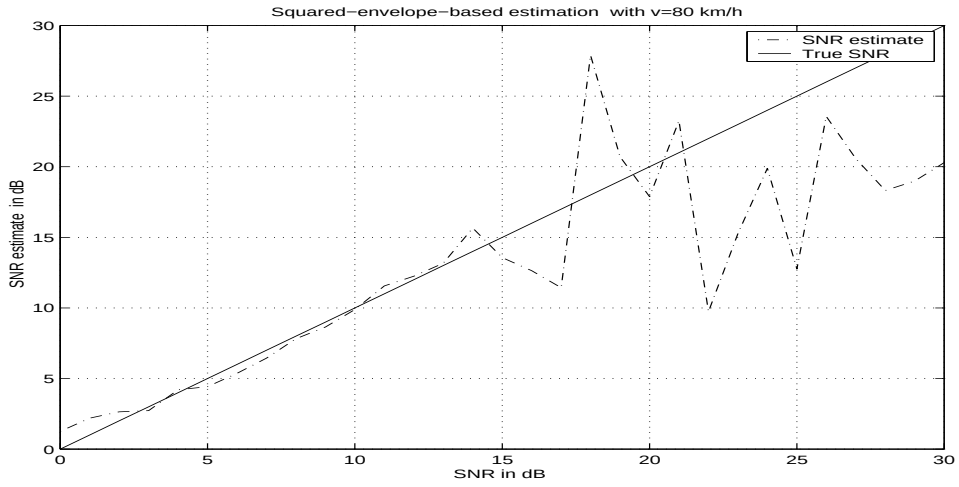

Figure 4.17: SNR estimate versus SNR with mobile velocity $80km/h$ for squared-envelope-based ACF estimation

velocity estimation problem for narrow-band transmitted sequences when training or pilot symbols are not available.

4.4.1 IQ-Based Estimation

The discrete-time received signal can be obtained via Equation (2.13),

$$\begin{aligned} x(k) &= v(k)h(k) + n(k) \\ &= (v_I(k) + jv_Q(k))(h_I(k) + jh_Q(k)) + (n_I(k) + jn_Q(k)) \end{aligned} \tag{4.25}$$

where $v(k), k = 1, 2, ..,$ is the data sequence, which is assumed to be independent of $h(k)$; $h(k)$ and $n(k)$ are the fading channel gain and narrow-band Gaussian noise, respectively; $v_I(k)$, $v_Q(k)$, $h_I(k)$ and $h_Q(k)$ denote the I/Q components of the data sequence, and the fading channel gains, respectively.

The autocorrelation function of the received IQ components can be written as

$$E[x_I(m)x_I(m-k)] =$$

$$E[v_I(m)v_I(m-k)+v_Q(m)v_Q(m-k)]E[h_I(m)h_I(m-k)]+E[n_I(m)n_I(m-k)] \tag{4.26}$$

According to [6], the IQ ACFs of the fading channel and the additive noise can be written as

$$E[h_I(m)h_I(m-k)] = \sigma^2 J_0(2\pi f_m k) \tag{4.27}$$

$$E[n_I(m)n_I(m-k)] = \sigma_n^2 \mathrm{sinc}(B_n T_s k) \tag{4.28}$$

Inserting (4.27) and (4.28) into Equation (4.26),

$$\begin{aligned} \phi_{II}(k) &= E[x_I(m)x_I(m-k)] \\ &= [\phi_{v_I}(k)+\phi_{v_Q}(k)]\sigma^2 J_0(2\pi f_m k)+\sigma_n^2 \mathrm{sinc}(B_n T_s k) \end{aligned} \tag{4.29}$$

where $\phi_{v_I}(m)$ and $\phi_{v_Q}(m)$ are the I/Q-based ACFs of the sample sequence of $v(t)$, respectively.

By defining $snr = \frac{\sigma^2}{\sigma_n^2}$, and following the similar procedures to the pure carrier case, we obtain

$$\frac{\phi_{v_I}(2)+\phi_{v_Q}(2)}{\phi_{v_I}(0)+\phi_{v_Q}(0)} c_3 J_0(4\pi \hat{f}_m) - \frac{\phi_{v_I}(1)+\phi_{v_Q}(1)}{\phi_{v_I}(0)+\phi_{v_Q}(0)} c_4 J_0(2\pi \hat{f}_m) = c_5 \tag{4.30}$$

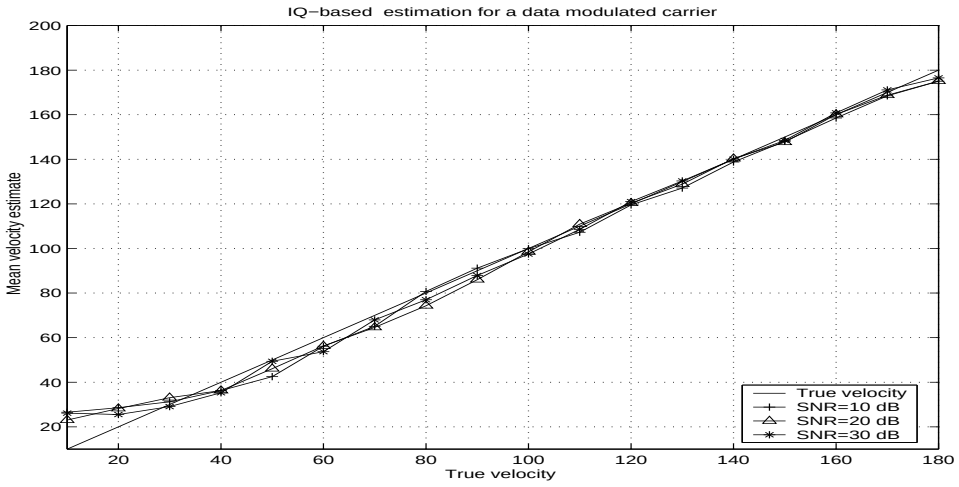

Figure 4.18: IQ-based velocity estimation for a data modulated carrier

where c_3, c_4, and c_5 have the same definitions as in Equations (3.7) to (3.9), in which c_1 and c_2 are defined as

$$c_1 \equiv \frac{\phi_{II}(1)}{\phi_{II}(0)} \tag{4.31}$$

$$c_2 \equiv \frac{\phi_{II}(2)}{\phi_{II}(0)} \tag{4.32}$$

Similar to a pure carrier case, f_m can be estimated via (4.30).

Figure 4.18 shows simulation results of IQ-based estimation for a data modulated carrier. The transmitted data $v(k)$ is assumed to be either zero or one with equal probability. Velocities from 20 km/h to 180 km/h are tested for SNR=10 dB, 20 dB, and 30 dB, and 100 Monte-Carlo trials are used. It is observed that this algorithm can obtain accurate velocity estimates, even at lower SNR. If the SNR is increased, the performance of velocity estimators improves.

4.4.2 Envelope-Based Estimation

In Equation (4.25), $v(k)$ is a random process, which in general makes $x(k)$ a non-Gaussian random process. As a result, the squared-envelope of the received signal may not have a chi-square distribution, and the squared-envelope-based ACF in Eqn. (4.16) cannot be applied directly. However, if the AWGN is not present, or can be neglected (high SNR case), the autocorrelation function of the amplitude of the received signal can be derived easily, e.g.,

$$\begin{aligned} \phi_{rr}(k) &= E\left[|x(m)|^2|x(m-k)|^2\right] \\ &= E[|v(m)h(m)|^2|v(m-k)h(m-k)|^2] \\ &= \phi_{|v|^2}(k)\phi_{|h|^2}(k) \end{aligned} \tag{4.33}$$

where $\phi_{|v|^2}(k)$ is the squared-envelope ACF of the modulated signal, and $\phi_{|h|^2}(k)$ is the squared-envelope ACF of the fading channel, which is given by (4.16).

For a constant-amplitude modulated signal $v(k)$, Equation (4.33) becomes

$$\phi_{rr}(k) = 4\sigma^4\alpha^4[1 + J_0^2(2\pi f_m k)] \tag{4.34}$$

where α is the constant amplitude of the modulated signal.

Using (4.34) and applying the method in Section 4.3, Doppler frequency f_m can be estimated as

$$f_m = \frac{1}{2\pi} J_0^{-1}\left(\sqrt{\frac{2\hat{\phi}_{rr}(1)}{\hat{\phi}_{rr}(0)} - 1}\right) \tag{4.35}$$

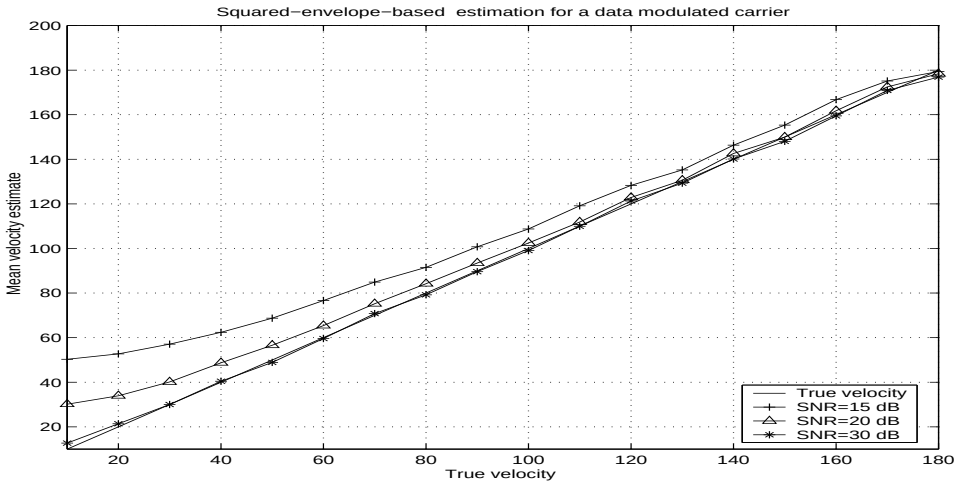

Figure 4.19: Squared-envelope-based velocity estimation for a data modulated carrier

Figure 4.19 presents the simulation results of squared-envelope-based estimation for a data modulated carrier, in which 100 Monte-Carlo trials and a constant-amplitude modulated signal $v(k)$ are assumed. Figure 4.19 shows that this algorithm can obtain accurate velocity estimates only for SNRs higher than about 15 dB. This is due to the fact that we ignore the additive noise in Equation (4.35).

4.5 Summary

In this chapter, we propose envelope-ACF-based and squared-envelope-ACF-based velocity estimators, which do not require coherent demodulation nor SNR information.

For $60km/h$ and $100km/h$, as well as other velocities tested, we observe that

the squared-envelope-ACF-based estimator outperforms the envelope-ACF-based estimator, especially at high velocities. Comparisons between the SNR-independent and SNR-dependent methods show that the SNR-independent method is always less accurate, especially at low SNR.

Chapter 5

Comparison of Velocity Estimators

5.1 Introduction

Existing algorithms can be classified into envelope-based and in-phase/quadrature component-based methods according to the available signal at the receiver; as well as classified into SNR-dependent and SNR-independent methods according to whether the SNR information is known a priori.

This chapter presents a comparison between our proposed estimators and several existing methods, including the covariance-based [3] and LCR-based methods [6].

All comparisons are performed by Monte-Carlo simulation. Bias and mean-square-error are used as criteria to evaluate the performance of these estimators. We compare the estimation results of different estimators under the same conditions. Since the received low-pass signal is a random process, the estimation of velocity depends on

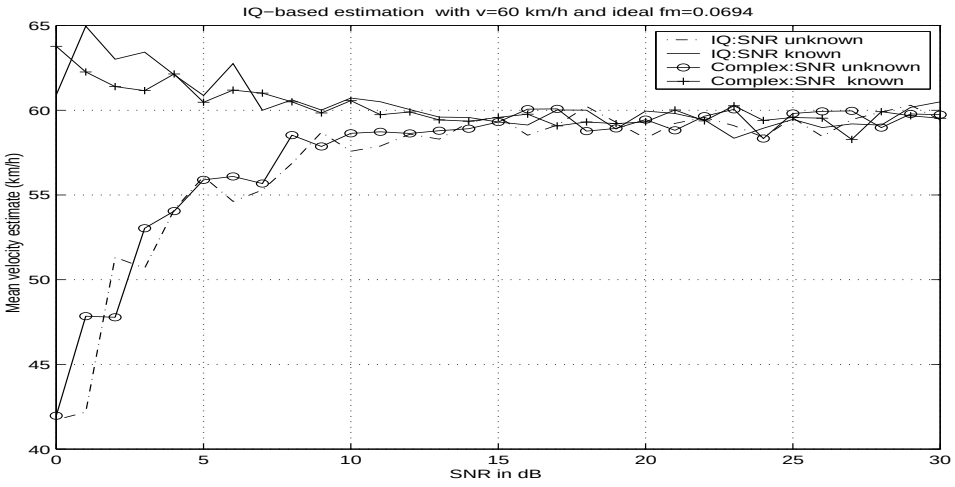

Figure 5.1: Mean velocity estimate for IQ-based methods with true velocity $60km/h$.

the specific realization of the fading channel. In our simulation, unless otherwise indicated, 30 independent Monte-Carlo trials are used to obtain mean velocity estimates.

5.2 Comparison of IQ-Based Velocity Estimators

In this section, IQ-ACF-based methods in Chapter 3 are compared to complex-ACF-based methods.

The ACF of a complex low-pass signal can be written as

$$\begin{aligned} \phi_{xx}(k) &= E[x(i)x^*(i-k)] \\ &= E[x_I(i)x_I(i-k) + x_Q(i)x_Q(i-k)] \\ &= 2\phi_{II}(k) \end{aligned} \tag{5.1}$$

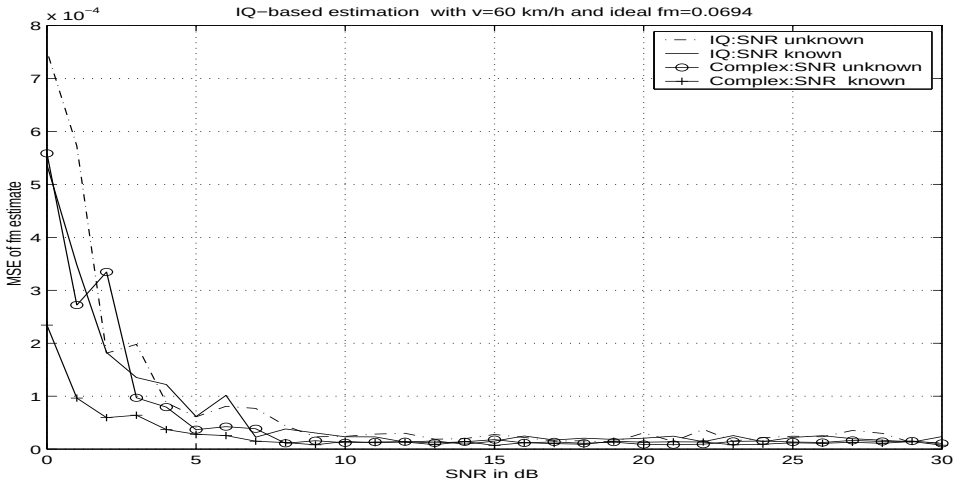

Figure 5.2: MSE of Doppler estimate for IQ-based methods with true velocity $60km/h$.

which is twice the IQ-based ACF. The above equation uses the assumption that the in-phase components are independent of the quadrature components, i.e., $E[x_I(m)x_Q(n)] = 0$ for any m and n.

Figures 5.1 and 5.3 show the mean velocity estimate when the true velocity is $60km/h$ and $100km/h$, respectively; Figures 5.2 and 5.4 present the mean-square-error (MSE) of Doppler estimators for velocities $60km/h$ and $100km/h$, respectively.

Some observations from Figures 5.1 to 5.4 are presented below:

- Complex-ACF-based methods can attain better performance, since more information (both I and Q) is employed to estimate the velocity.
- Generally speaking, the performance of SNR-dependent IQ estimators surpasses that of SNR-independent ones, especially for low SNRs, as we discussed in

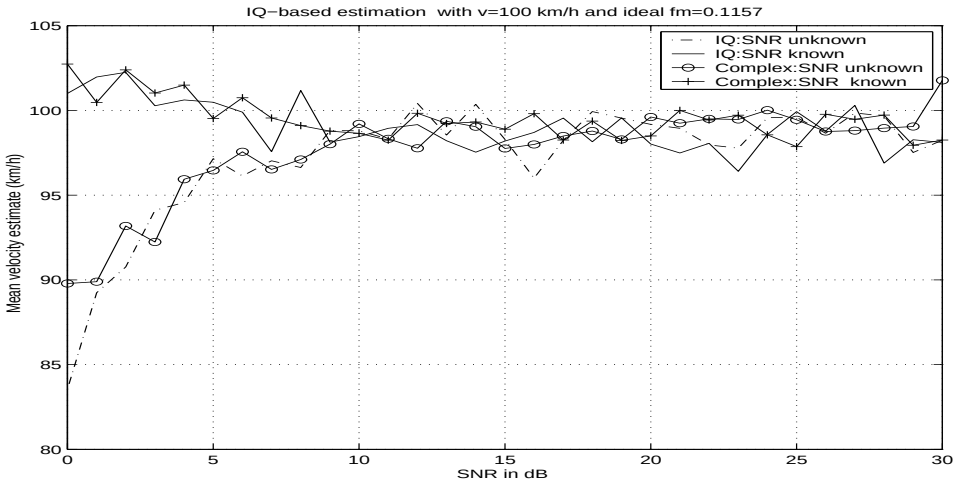

Figure 5.3: Mean velocity estimate for IQ-based methods with true velocity $100km/h$.

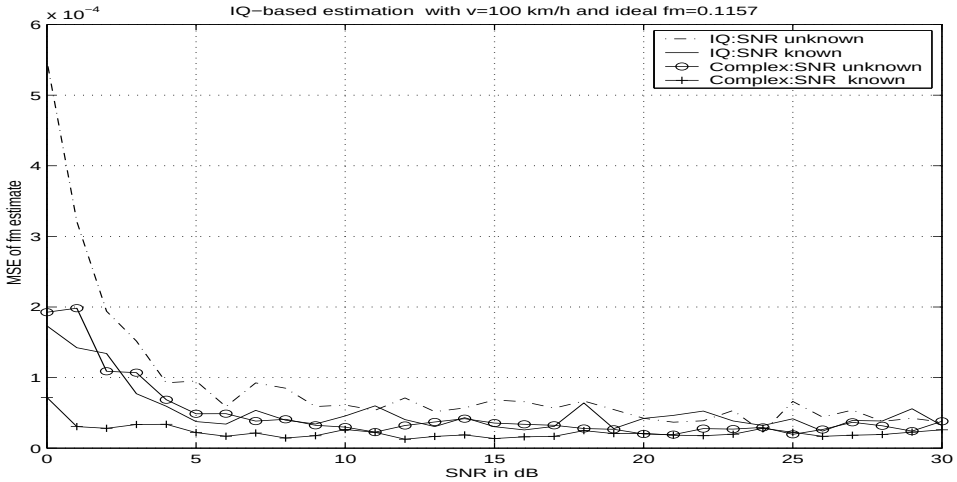

Figure 5.4: MSE of Doppler estimate for IQ-based methods with true velocity $100km/h$.

Chapter 3.

We remark that the spectral-moment-based method for IQ components [19] is not compared to our proposed IQ-based method, since for the spectral-moment-based method, the sampling rate should be very large to ensure accurate velocity estimation, and the additive noise is required to be white; while, our proposed IQ and complex ACF-based methods do not face such limitations. As a result, the performance of the spectral-moment-based method will be very poor under the simulation conditions presented in Table 3.1.

5.3 Comparison of Envelope-Based Velocity Estimators

Up to now, we have discussed six envelope-based velocity (Doppler) estimators: LCR method (Section 2.4.1), covariance method (Section 2.4.4), SNR-dependent and SNR-independent envelope-ACF methods (Section 4.2.1) and squared-envelope-ACF-based methods (Section 4.3.1).

Figures 5.5 and 5.7 show the comparison of the mean-velocity estimate when the true velocity is $60km/h$ and $100km/h$, respectively. Figures 5.6 and 5.8 present the mean-square-error of Doppler estimators for true velocity $60km/h$ and $100km/h$, respectively. Some observations from these figures are now listed as follows

- The SNR-dependent squared-envelope-based and covariance-based methods can

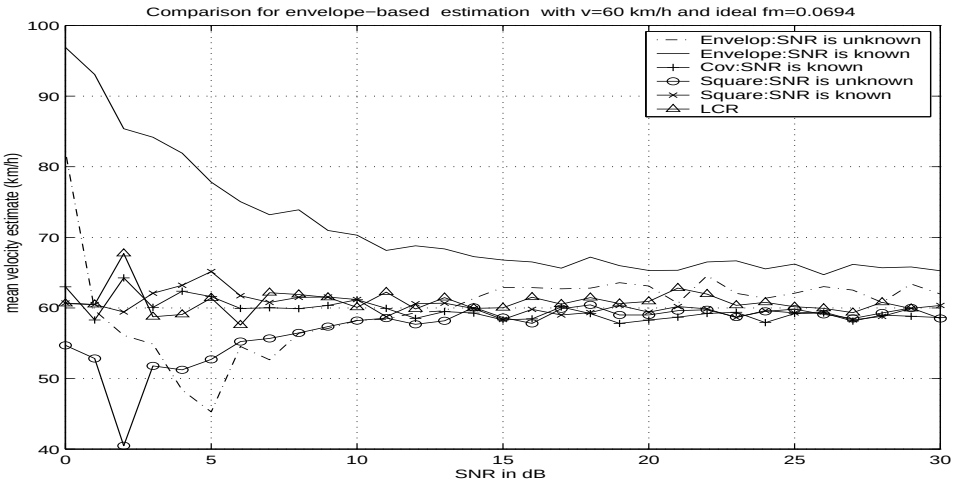

Figure 5.5: Mean velocity estimate for envelope-based methods with true velocity $60km/h$.

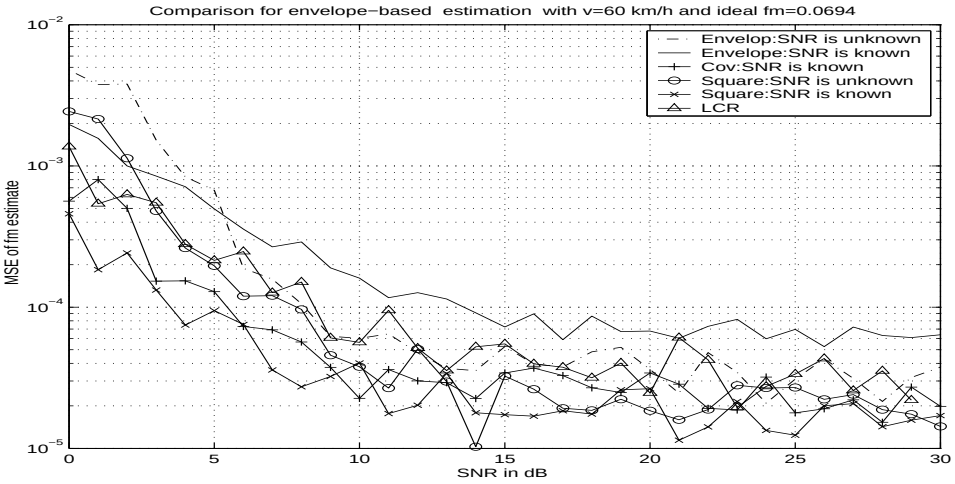

Figure 5.6: MSE of Doppler estimate for envelope-based methods with true velocity $60km/h$.

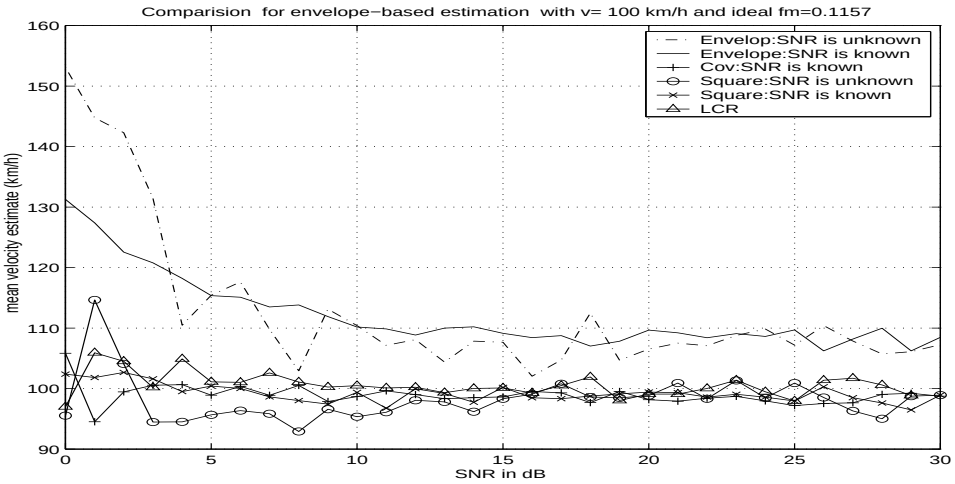

Figure 5.7: Mean velocity estimate for envelope-based methods with true velocity $100km/h$.

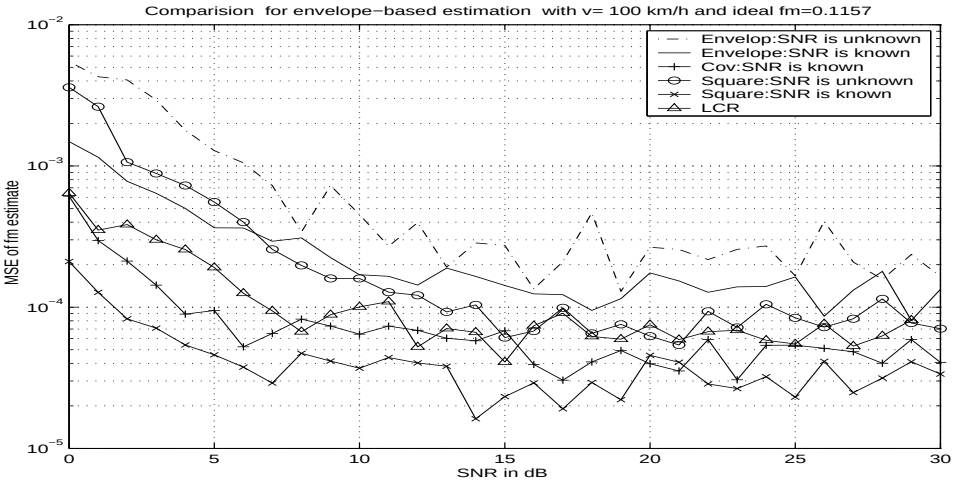

Figure 5.8: MSE of Doppler estimate for envelope-based methods with true velocity $100km/h$.

attain very similar performance and they out-perform other methods, especially at low SNR.

- An advantage of the squared-envelope-based method is that it can be made SNR-independent, with performance close to that of the SNR-dependent method.

- The performance of the LCR method is inferior to the squared-envelope ACF and covariance methods, which can be explained by a lack of samples for accurate LCR estimation. In our simulations, 1000 samples are used, which is not large enough to obtain accurate LCR estimates [6].

- The performance of the envelope-ACF method is the worst among all six methods. It is observed that as the velocity increases, especially to over $100km/h$, the performance of the envelope-ACF method degrades greatly, while the squared-envelope-ACF-based and covariance-based methods still maintain accuracy, even at very high velocities.

- In general, SNR-dependent algorithms attain better performance than SNR-independent ones, especially at low SNRs, since for the case of unknown SNR, additional autocorrelation functions need to be estimated to provide the missing SNR information, and these ACF estimates at low SNRs are inaccurate.

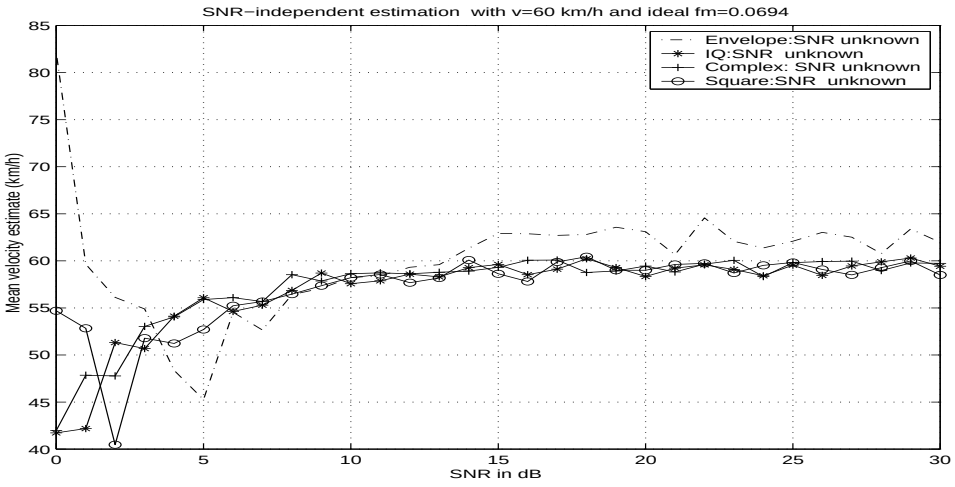

Figure 5.9: Mean velocity estimate for SNR-independent methods with true velocity $60km/h$.

5.4 Comparison of SNR-Independent Velocity Estimators

Next, we wish to evaluate the performance of velocity estimation when SNR is unknown. The proposed SNR-independent algorithms based on IQ-ACF, envelope-ACF and squared-envelope-ACF, which are described in Chapter 3 and 4, are compared in this section.

Figures 5.9 and 5.11 show the comparison of the mean-velocity estimate when the true velocities are $60km/h$ and $100km/h$, respectively. Figures 5.10 and 5.12 present the mean-square-error of Doppler estimators for true velocities $60km/h$ and $100km/h$, respectively.

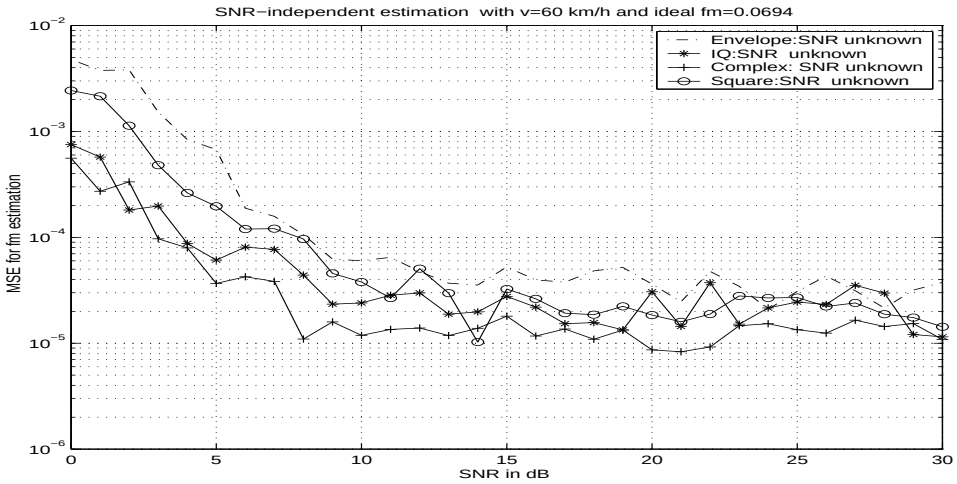

Figure 5.10: MSE of Doppler estimates for SNR-independent methods with true velocity $60km/h$.

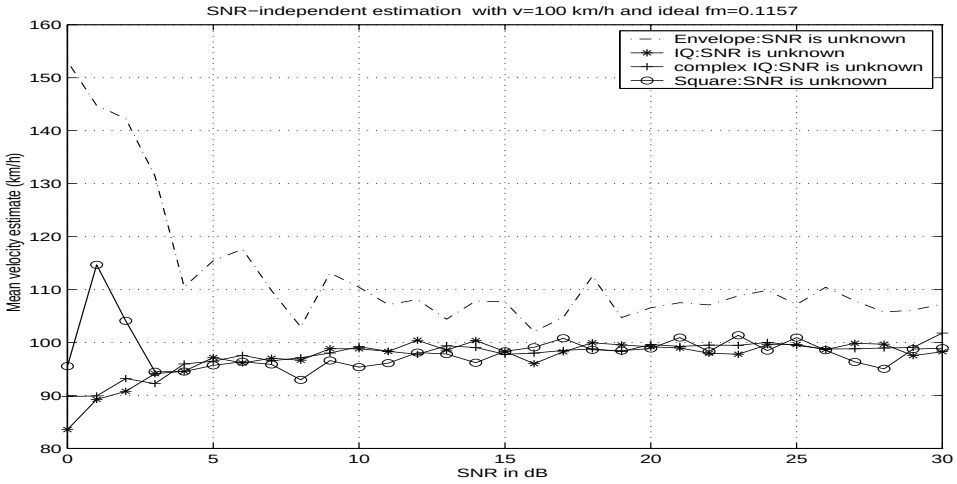

Figure 5.11: Mean velocity estimate for SNR-independent methods with true velocity $100km/h$.

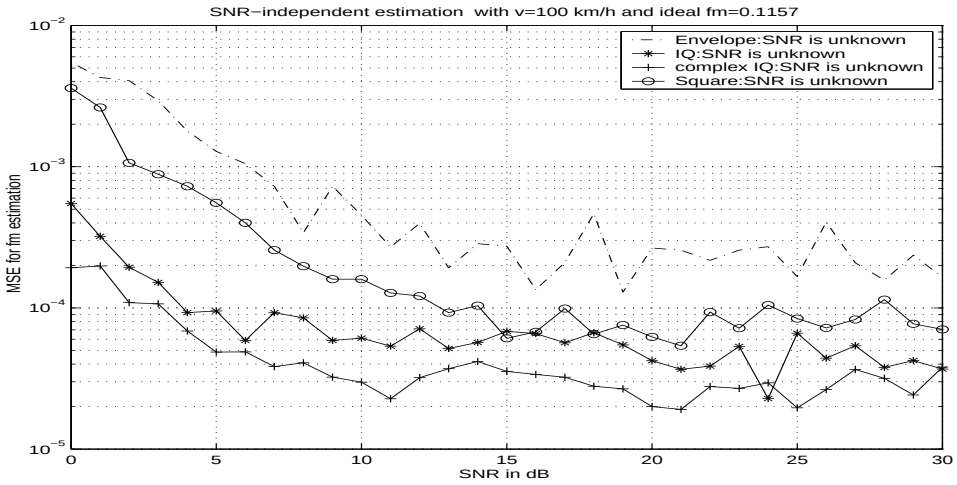

Figure 5.12: MSE of Doppler estimates for SNR-independent estimates with true velocity $100km/h$.

Some observations from Figures 5.9 to 5.12 are described as follows:

- When the SNR is over 10 dB, SNR-independent estimators based on squared-envelope ACF and IQ ACF are very accurate.
- The envelope-ACF method has relatively large estimation bias and mean-square-error, especially at low SNRs, and high velocities.
- Comparison between squared-envelope-ACF and IQ-ACF methods shows that the IQ-ACF-based method, which requires coherent demodulation, outperforms the squared-envelope method.

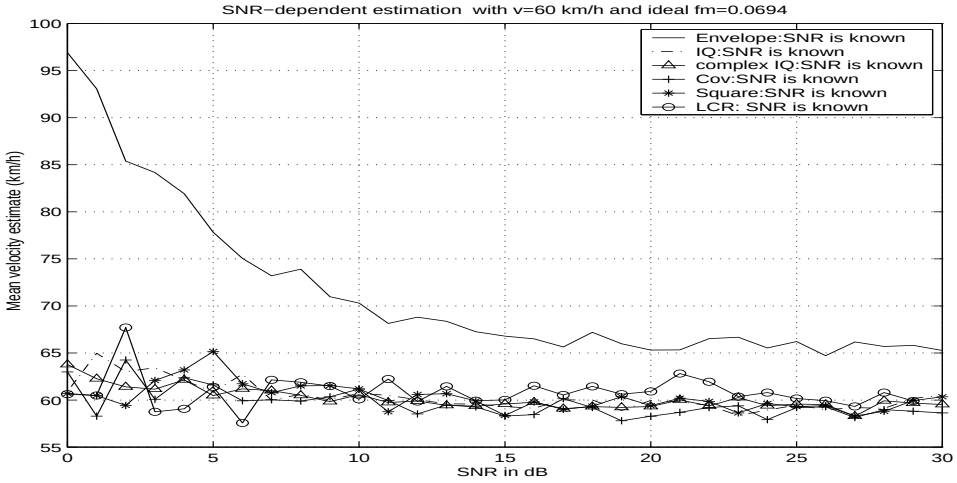

Figure 5.13: Mean velocity estimate for SNR-dependent methods with true velocity $60km/h$.

5.5 Comparison of SNR-Dependent Velocity Estimators

We have discussed several Doppler estimators, which require knowledge of the link's SNR. Figures (5.13) and (5.15) show a comparison of the mean-velocity estimate when the true velocities are $60km/h$ and $100km/h$, respectively. Figures (5.14) and (5.16) present the mean-square-error of Doppler estimators for true velocity $60km/h$ and $100km/h$, respectively.

Some observations are as follows:

- The IQ-ACF-based method outperforms other estimators, followed by squared-envelope-ACF-based and covariance-based methods.

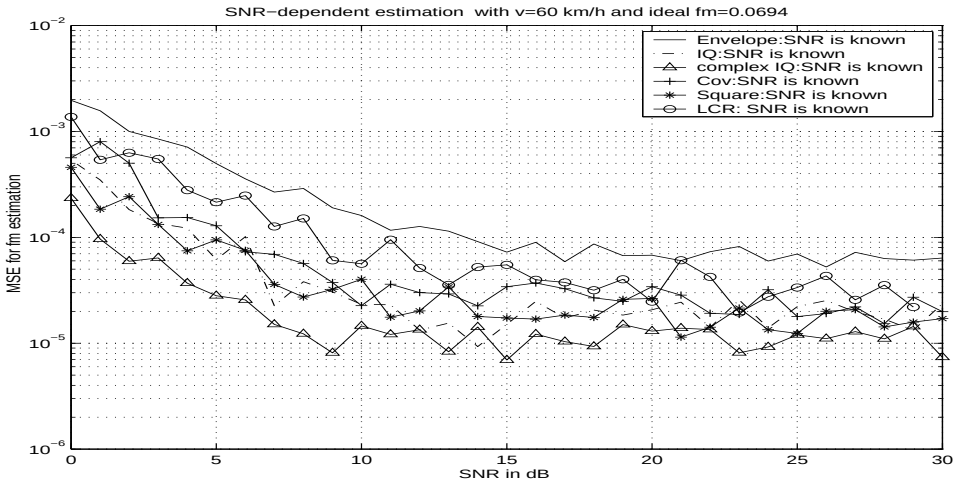

Figure 5.14: MSE of Doppler estimates for SNR-dependent methods with true velocity $60km/h$.

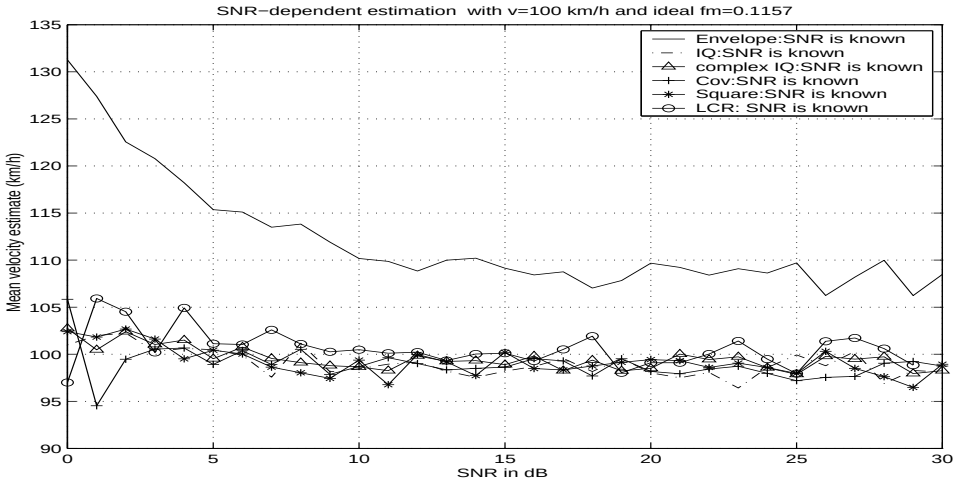

Figure 5.15: Mean velocity estimate for SNR-dependent methods with true velocity $100km/h$.

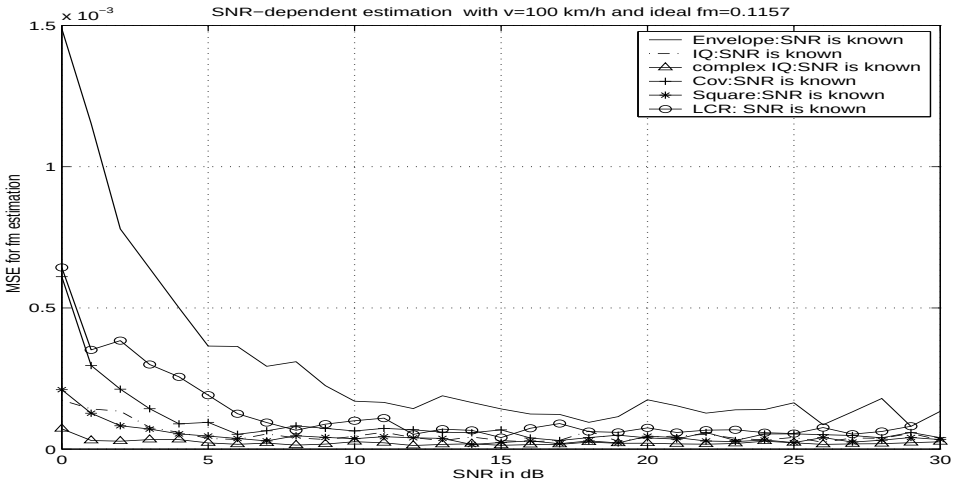

Figure 5.16: MSE of Doppler estimates for SNR-dependent methods with true velocity $100km/h$.

- The drawback of the IQ-ACF method is that it requires coherent demodulation as we discussed before.

- Squared-envelope-ACF-based and covariance-based methods have performance very close to that of the IQ-ACF, as the SNR becomes large.

- The LCR method is superior to envelope-ACF-based method, but inferior to the rest of the SNR-dependent methods, since the number of samples employed in our simulation is not large enough to obtain accurate LCR estimates.

- The envelope-ACF method is inferior to other methods, especially at high velocities. In our simulations, it is seen that when velocity is increased to $100km/h$, the estimation bias of the envelope-ACF-based method increases greatly.

5.6 Summary

This chapter compares different velocity estimation methods. The best estimators in their respective categories are summarized in Table 5.1.

Available information	Known SNR	Unknown SNR
Coherent demodulation	IQ-ACF-based SNR-dependent method [6]	IQ-ACF-based SNR-independent method (Section 3.2)
Non-coherent demodulation	Covariance-based [3] or SNR-dependent squared-envelope-based method (Section 4.3)	SNR-independent squared-envelope-based method (Section 4.3)

Table 5.1: The preferred estimation methods for different available information

Chapter 6

Cramer-Rao Lower Bounds for Velocity (Doppler) Estimators

6.1 Introduction

As discussed in Chapter 5, existing velocity estimation algorithms can be classified into IQ and envelope-based methods, as well as classified into SNR-independent and SNR-dependent methods according to the available measurements and information at the receiver.

Recently, a lower variance bound for velocity (Doppler) estimation has appeared in [20], in which (coherent) IQ-based Doppler estimation is considered using a general Gaussian CRLB framework [21]. Although this would also serve as lower bound for (non-coherent) envelope-based estimation, a tighter bound may be obtained by considering a bound specifically for signal envelope-based estimation. In fact, a CRLB

specifically for envelope-based estimators seems not to have appeared in the literature. In this chapter, we derive approximate CRLBs for envelope-based estimators under the assumption that the fading process can be approximated by a first-order Markovian process. Unlike [20] this bound does not require the symbolic inversion of matrices. Under this assumption, an approximate closed-form CRLB for IQ-based estimators is also presented. This chapter also concludes with an insight into joint velocity and SNR estimation.

In Section 6.2, the CRLBs for Doppler estimators are derived assuming that SNR information is available. The CRLBs for *snr* estimators are then derived in Section 6.3 by following similar procedures assuming that Doppler information is known. In Section 6.4, the CRLB for joint Doppler and SNR estimation is discussed. Analysis and simulation results are given at the end of this chapter.

6.2 Approximate CRLBs for SNR-Dependent Velocity (Doppler) Estimators

6.2.1 Approximate CRLB for Envelope-Based Velocity Estimators

In order to calculate the CRLB for envelope-based estimators, we first derive closed-form expression of the joint probability density function (PDF) for n observed envelope samples.

The joint PDF of the observed envelope samples, under the assumption that the Rayleigh fading channel can be approximated by a first-order Markovian process, as proposed and verified by Chang and Wang in [4], can be obtained as

$$p_n\left(z(1), z(2), ..., z(n)\right) = p\left(z(1)\right) \prod_{k=1}^{n-1} \frac{p(z(k), z(k+1))}{p\left(z(k)\right)} \tag{6.1}$$

where $z(i)$, $i = 1, ..., n$, is the envelope of the samples at time instant i.

The signal envelope $z(k)$ is known to be Rayleigh distributed [27] as shown in Equation (2.20).

The joint PDF of two adjacent envelope samples $z(k)$ and $z(k+1)$ can be derived by transformation of the joint normal PDF as done in [7], which is presented in Equation (2.21).

Inserting (2.20) and (2.21) into (6.1), the closed-form of the joint PDF can be achieved as

$$\begin{aligned} p_n\left(z(1), z(2), ..., z(n)\right) &= \frac{z(1)}{\phi_{II}(0)} \exp\left\{-\frac{z^2(1)}{2\phi_{II}(0)}\right\} \\ &\prod_{k=1}^{n-1} \frac{z(k)z(k+1) \exp\left\{-\frac{\phi_{II}(0)(z^2(k)+z^2(k+1))}{2(\phi_{II}^2(0)-\phi_{II}^2(1))} + \frac{z^2(k)}{2\phi_{II}(0)}\right\} \phi_{II}(0)}{(\phi_{II}^2(0) - \phi_{II}^2(1))z(k)} I_0(k, k+1) \end{aligned} \tag{6.2}$$

Within the first-order Markov approximation, the CRLB for envelope-based Doppler estimation assuming known SNR can be written as follows [28]

$$CRLB_{env}(\hat{f_m}) = \frac{1}{-E(\frac{\partial^2 \Psi_{env}}{\partial f_m^2})} \tag{6.3}$$

where Ψ_{env} is the log-likelihood function of joint PDF $p_n(z(1), ..., z(n))$.

According to the chain rule, the expectation term in (6.3) will be

$$E[\frac{\partial^2 \Psi_{env}}{\partial f_m^2}] = (\frac{\partial \phi_{II}(1)}{\partial f_m})^2 E(\frac{\partial^2 \Psi_{env}}{\partial \phi_{II}^2(1)}) + \frac{\partial^2 \phi_{II}(1)}{\partial f_m^2} E(\frac{\partial \Psi_{env}}{\partial \phi_{II}(1)}) \tag{6.4}$$

Inserting (6.4) into Equation (6.3), we obtain

$$CRLB_{env}(\hat{f_m}) = \frac{-1}{(\frac{\partial \phi_{II}(1)}{\partial f_m})^2 E(\frac{\partial^2 \Psi_{env}}{\partial \phi_{II}^2(1)}) + \frac{\partial^2 \phi_{II}(1)}{\partial f_m^2} E(\frac{\partial \Psi_{env}}{\partial \phi_{II}(1)})} \tag{6.5}$$

The expectation terms in (6.5), after manipulation (see Appendix C for details), can be solved as

$$E[\frac{\partial \Psi_{env}}{\partial \phi_{II}(1)}] = 0 \tag{6.6}$$

$$E[\frac{\partial^2 \Psi_{env}}{\partial \phi_{II}^2(1)}] = (n-1)\frac{(\phi_{II}^2(0) + \phi_{II}^2(1))(8\phi_{II}^2(0)\phi_{II}^2(1) - \sigma_y^2(\phi_{II}^2(0) + \phi_{II}^2(1)))}{(\phi_{II}^2(0) - \phi_{II}^2(1))^4} \tag{6.7}$$

where

$$\sigma_y^2 = variance\left(z(k)z(k+1)\frac{I_1(k,k+1)}{I_0(k,k+1)}\right) \tag{6.8}$$

$$I_1(k,k+1) = I_1\left(\frac{\phi_{II}(1)z(k)z(k+1)}{\phi_{II}^2(0) - \phi_{II}^2(1)}\right) \tag{6.9}$$

in which $I_1(.)$ is the first-order modified Bessel function of the first kind, and σ_y^2 can be obtained numerically or by Monte-Carlo means. We note that Equation (6.6) is also the regularity condition for CRLB [28]. By substituting Equations (6.6) and (6.7) into (6.5), and using the fact that

$$\frac{\partial \phi_{II}(1)}{\partial f_m} = -\frac{2\pi \phi_{II}(0) J_1(2\pi f_m) snr}{1+snr} \tag{6.10}$$

approximate CRLB for envelope-based Doppler estimators is given as

$$CRLB_{env}(\hat{f_m}) = \frac{(1+snr)^2(\phi_{II}^2(0)-\phi_{II}^2(1))^4}{(1-n)4\pi^2\phi_{II}^2(0)J_1^2(2\pi f_m)snr^2(\phi_{II}^2(0)+\phi_{II}^2(1))[8\phi_{II}^2(0)\phi_{II}^2(1)-\sigma_y^2(\phi_{II}^2(0)+\phi_{II}^2(1))]} \tag{6.11}$$

The CRLB for velocity estimators can be obtained via transformation of parameter [28],

$$\begin{aligned} CRLB_{env}(\hat{v}) &= (\frac{\partial v}{\partial f_m})^2 CRLB_{env}(\hat{f_m}) \\ &= (\frac{cF_s}{f_c})^2 CRLB_{env}(\hat{f_m}) \end{aligned} \tag{6.12}$$

Next we show that squared-envelope-based Doppler estimators will have the same CRLB as envelope-based ones. This can be explained by the fact that for the two estimation methods, the same information is employed.

It is well known that the joint PDF of samples' squared-envelope can be derived by the transformation of the joint PDF of samples' envelope [31]

$$p_n\left(r(1), r(2), .., r(n)\right) = \frac{p_n\left(z(1), z(2), .., z(n)\right)}{\left|J\left(z(1), z(2), .., z(n)\right)\right|} \tag{6.13}$$

where $p_n\left(r(1), r(2), .., r(n)\right)$ is the joint PDFs of samples of the received squared-envelope.

In (6.13), $J\left(z(1), z(2), .., z(n)\right)$ is the Jacobian of the transformation, which can be written as

$$J\left(z(1), z(2), .., z(n)\right) = \begin{bmatrix} \frac{\partial r(1)}{\partial z(1)} & \frac{\partial r(1)}{\partial z(2)} & .. & \frac{\partial r(1)}{\partial z(n)} \\ \frac{\partial r(2)}{\partial z(1)} & \frac{\partial r(2)}{\partial z(2)} & .. & \frac{\partial r(2)}{\partial z(n)} \\ .. & .. & .. & .. \\ \frac{\partial r(n)}{\partial z(1)} & \frac{\partial r(n)}{\partial z(2)} & .. & \frac{\partial r(n)}{\partial z(n)} \end{bmatrix} \tag{6.14}$$

The determinant of above matrix can be derived as

$$\left|J\left(z(1), z(2), .., z(n)\right)\right| = 2^n z(1)z(2)...z(n) \tag{6.15}$$

Therefore, Equation (6.13) will be

$$p_n\left(r(1), r(2), .., r(n)\right) = \frac{p_n\left(z(1), z(2), .., z(n)\right)}{2^n z(1)z(2)...z(n)} \tag{6.16}$$

Defining the log-likelihood function for samples' squared-envelope as

$$\Psi_{square} \equiv \ln p_n\left(r(1), r(2), .., r(n)\right) \tag{6.17}$$

Inserting (6.16) into (6.17), we obtain

$$\begin{aligned} \Psi_{square} &= \ln p_n\left(z(1), z(2), .., z(n)\right) - \ln(2^n z(1)z(2)...z(n)) \\ &= \Psi_{env} - \ln(2^n z(1)z(2)...z(n)) \end{aligned} \tag{6.18}$$

Since the last term in (6.18) is independent of f_m, it is straightforward to obtain

$$\frac{\partial^2 \Psi_{square}}{\partial f_m^2} = \frac{\partial^2 \Psi_{env}}{\partial f_m^2} \tag{6.19}$$

Therefore, the following equation holds

$$CRLB_{env}(\hat{f_m}) \;=\; CRLB_{square}(\hat{f_m}) \tag{6.20}$$

6.2.2 Approximate CRLB for IQ-Based Velocity Estimators

Based on the assumption that the received signal is a first-order Markovian process, the joint PDF of $x_I(1),..,x_I(n)$, can be written in the same form as Equation (6.1),

$$p_n\left(x_I(1),x_I(2),...,x_I(n)\right) \;=\; p\left(x_I(1)\right)\prod_{k=1}^{n-1}\frac{p\left(x_I(k),x_I(k+1)\right)}{p\left(x_I(k)\right)} \tag{6.21}$$

where the joint PDF of $x_I(k)$ and $x_I(k+1)$ can be derived as [31]

$$\begin{aligned} p\left(x_I(k),x_I(k+1)\right) \;=\; & \frac{1}{2\pi\sqrt{\phi_{II}^2(0)-\phi_{II}^2(1)}} \\ & \exp\left(-\frac{\phi_{II}(0)x_I^2(k)+\phi_{II}(0)x_I^2(k+1)-2\phi_{II}(1)x_I(k)x_I(k+1)}{2(\phi_{II}^2(0)-\phi_{II}^2(1))}\right) \end{aligned} \tag{6.22}$$

and the sample at time k of IQ components has a normal distribution [27]

$$p\left(x_I(k)\right)=\frac{1}{\sqrt{2\pi\phi_{II}(0)}}\exp\left(-\frac{x_I^2(k)}{2\phi_{II}(0)}\right) \tag{6.23}$$

Inserting (6.22) and (6.23) into (6.21), we obtain the joint PDF as

$$\begin{aligned} p_n(x_I(1),x_I(2),...,x_I(n)) \;=\; & \frac{1}{\sqrt{2\pi\phi_{II}(0)}}\exp\left(-\frac{x_I^2(1)}{2\phi_{II}(0)}\right)\prod_{k=1}^{n-1}\frac{\sqrt{2\pi\phi_{II}(0)}}{2\pi\sqrt{\phi_{II}^2(0)-\phi_{II}^2(1)}} \\ & \exp\left(-\frac{\phi_{II}(0)x_I^2(k)+\phi_{II}(0)x_I^2(k+1)-2\phi_{II}(1)x_I(k)x_I(k+1)}{2(\phi_{II}^2(0)-\phi_{II}^2(1))}+\frac{x_I^2(k)}{2\phi_{II}(0)}\right) \end{aligned} \tag{6.24}$$

The Cramer Rao Lower Bound for IQ-based $\hat{f_m}$ is given by

$$\begin{aligned} CRLB_{IQ}(\hat{f_m}) &= \frac{1}{-E[\frac{\partial^2 \Psi_{IQ}}{\partial f_m^2}]} \\ &= \frac{-1}{(\frac{\partial \phi_{II}(1)}{\partial f_m})^2 E(\frac{\partial^2 \Psi_{IQ}}{\partial \phi_{II}^2(1)}) + \frac{\partial^2 \phi_{II}(1)}{\partial f_m^2} E(\frac{\partial \Psi_{IQ}}{\partial \phi_{II}(1)})} \end{aligned} \tag{6.25}$$

where Ψ_{IQ} is the logarithm of joint PDF $p_n\left(x_I(1), x_I(2), ..., x_I(n)\right)$, which is given in (6.25).

The expectation terms in (6.25) can be derived as

$$E[\frac{\partial \Psi_{IQ}}{\partial \phi_1}] = \frac{(n-1)\phi_1}{\phi_0^2 - \phi_1^2} \\ \frac{(1-n)[(-\phi_{II}^2(0) - \phi_{II}^2(1))E[x_I(i)x_I(i+1)] + \phi_{II}(0)\phi_{II}(1)E[x_I^2(i) + x_I^2(i+1)]]}{(\phi_{II}^2(0) - \phi_{II}^2(1))^2} \tag{6.26}$$

$$E[\frac{\partial^2 \Psi_{IQ}}{\partial \phi_{II}^2(1)}] = \\ \frac{(1-n)\left(\phi_{II}^3(0) + 3\phi_{II}(0)\phi_{II}^2(1)\right)E[x_I^2(i) + x_I^2(i+1)]}{(\phi_{II}^2(0) - \phi_{II}^2(1))^3} \\ + \frac{(1-n)(-6\phi_{II}^2(0)\phi_{II}(1) - 2\phi_{II}^2)E[x_I(i)x_I(i+1)]}{(\phi_{II}^2(0) - \phi_{II}^2(1))^3} + \frac{(n-1)(\phi_{II}^2(0) + \phi_{II}^2(1))}{(\phi_{II}^2(0) - \phi_{II}^2(1))^2} \tag{6.27}$$

which can be simplified as

$$E[\frac{\partial \Psi_{IQ}}{\partial \phi_1}] = 0 \tag{6.28}$$

$$E[\frac{\partial^2 \Psi_{IQ}}{\partial \phi_{II}^2(1)}] = \frac{(1-n)(\phi_{II}^2(0) + \phi_{II}^2(1))}{(\phi_{II}^2(0) - \phi_{II}^2(1))^2} \tag{6.29}$$

By inserting (6.28) and (6.29) into (6.25), a closed-form of approximate CRLB for

IQ-based $\hat{f_m}$ with available SNR information can be derived as

$$CRLB_{IQ}(\hat{f_m}) = \frac{(\phi_{II}^2(0)-\phi_{II}^2(1))^2(1+snr)^2}{(n-1)(\phi_{II}^2(0)+\phi_{II}^2(1))4\pi^2\phi_{II}^2(0)J_1^2(2\pi f_m)snr^2} \tag{6.30}$$

So far, we obtain the closed-form approximate CRLB for IQ-based Doppler estimators. Compared to the result in [20], which is not closed-form, our CRLB result has very simple expression and does not require the symbolic inversion of matrix, but requires the first-order Markov assumption.

6.3 Approximate CRLB for Doppler-Dependent *snr* Estimators

As a by-product, approximate CRLB for *snr* estimates when f_m is known can also be derived by following similar procedures.

6.3.1 Approximate CRLB for Envelope-Based *snr* Estimators

The CRLB for envelope-based *snr* estimators can be written as

$$CRLB_{env}(\hat{snr}) = \frac{1}{-E(\frac{\partial^2\Psi_{env}}{\partial snr^2})} \tag{6.31}$$

According to the chain rule, the expectation term in (6.31) will be

$$E[\frac{\partial^2 \Psi_{env}}{\partial snr^2}] = (\frac{\partial \phi_{II}(1)}{\partial snr})^2 E(\frac{\partial^2 \Psi_{env}}{\partial \phi_{II}^2(1)}) + \frac{\partial^2 \phi_{II}(1)}{\partial snr^2} E(\frac{\partial \Psi_{env}}{\partial \phi_{II}(1)}) \tag{6.32}$$

Inserting (6.32) into Equation (6.31), we obtain

$$CRLB_{env}(\hat{snr}) = \frac{-1}{(\frac{\partial \phi_{II}(1)}{\partial snr})^2 E(\frac{\partial^2 \Psi_{env}}{\partial \phi_{II}^2(1)}) + \frac{\partial^2 \phi_{II}(1)}{\partial snr^2} E(\frac{\partial \Psi_{env}}{\partial \phi_{II}(1)})} \tag{6.33}$$

By substituting the expectation terms, which are given in Equations (6.6) and (6.7), into (6.33), and using the fact that

$$\frac{\partial \phi_{II}(1)}{\partial snr} = \frac{\phi_{II}(0)\,(J_0(2\pi f_m) - \mathrm{sinc}(B_n T_s))}{(1+snr)^2} \tag{6.34}$$

approximate CRLB for envelope-based Doppler estimators is given by

$$CRLB_{env}(\hat{snr}) = \frac{(1+snr)^4}{-\phi_{II}^2(0)(J_0(2\pi f_m) - \mathrm{sinc}(B_n T_s))^2 E(\frac{\partial^2 \Psi_{env}}{\partial \phi_{II}^2(1)})} \tag{6.35}$$

where $E(\frac{\partial^2 \Psi_{env}}{\partial \phi_{II}^2(1)})$ is shown in (6.7).

We remark that the CRLB for squared-envelope-based *snr* estimators is same as that for envelope-based *snr* estimators as expected.

6.3.2 Approximate CRLB for IQ-Based *snr* Estimators

The CRLB for IQ-based *snr* estimators is given by

$$\begin{aligned} CRLB_{IQ}(\hat{snr}) &= \frac{1}{-E(\frac{\partial^2 \Psi_{IQ}}{\partial snr^2})} \\ &= \frac{-1}{(\frac{\partial \phi_{II}(1)}{\partial snr})^2 E(\frac{\partial^2 \Psi_{IQ}}{\partial \phi_{II}^2(1)}) + \frac{\partial^2 \phi_{II}(1)}{\partial snr^2} E(\frac{\partial \Psi_{IQ}}{\partial \phi_{II}(1)})} \end{aligned} \tag{6.36}$$

Inserting the expectation terms, presented in (6.28) and (6.29), into (6.36), the CRLB for IQ-based $\hat{snr}$ estimators with available f_m information can be derived as

$$\begin{aligned} CRLB_{IQ}(\hat{snr}) &= \frac{1}{-E[\frac{\partial^2 \Psi_{IQ}}{\partial snr^2}]} \\ &= \frac{\left(\phi_{II}^2(0) - \phi_{II}^2(1)\right)^2 (1+snr)^4}{(n-1)\left(\phi_{II}^2(0) + \phi_{II}^2(1)\right)\phi_{II}^2(0)[J_0(2\pi f_m) - \mathrm{sinc}(B_n T_s)]^2} \end{aligned} \tag{6.37}$$

As the snr is increased, the CRLB for IQ-based snr estimators increases exponentially as snr^4, and thus degrades the performance greatly.

6.4 Approximate CRLB for Joint Doppler and snr Estimators

If snr and f_m information are both unavailable, we have two unknown parameters. The Fisher's information matrix (FIM) for this case can be written as:

$$FIM = \begin{bmatrix} -E[\frac{\partial^2 \Psi}{\partial f_m^2}] & -E[\frac{\partial^2 \Psi}{\partial f_m \partial snr}] \\ -E(\frac{\partial^2 \Psi}{\partial snr \partial f_m}) & -E(\frac{\partial^2 \Psi}{\partial snr^2}) \end{bmatrix} \tag{6.38}$$

Using chain rule again, we obtain

$$
\begin{aligned}
[FIM]_{1,1} &= -E[\frac{\partial^2 \Psi}{\partial f_m^2}] \\
&= -(\frac{\partial \phi_{II}(1)}{\partial f_m})^2 E(\frac{\partial^2 \Psi}{\partial \phi_{II}^2(1)}) - \frac{\partial^2 \phi_{II}(1)}{\partial f_m^2} E(\frac{\partial \Psi}{\partial \phi_{II}(1)}) \\
[FIM]_{1,2} &= -E[\frac{\partial^2 \Psi}{\partial f_m \partial snr}] \\
&= -(\frac{\partial \phi_{II}(1)}{\partial f_m})(\frac{\partial \phi_{II}(1)}{\partial snr}) E(\frac{\partial^2 \Psi}{\partial \phi_{II}^2(1)}) - \frac{\partial^2 \phi_{II}(1)}{\partial f_m \partial snr} E(\frac{\partial \Psi}{\partial \phi_{II}(1)}) \\
[FIM]_{2,1} &= -E[\frac{\partial^2 \Psi}{\partial snr \partial f_m}] \\
&= -(\frac{\partial \phi_{II}(1)}{\partial snr})(\frac{\partial \phi_{II}(1)}{\partial f_m}) E(\frac{\partial^2 \Psi}{\partial \phi_{II}^2(1)}) - \frac{\partial^2 \phi_{II}(1)}{\partial snr \partial f_m} E(\frac{\partial \Psi}{\partial \phi_{II}(1)}) \\
[FIM]_{2,2} &= -E[\frac{\partial^2 \Psi}{\partial snr^2}] \\
&= -(\frac{\partial \phi_{II}(1)}{\partial snr})^2 E(\frac{\partial^2 \Psi}{\partial \phi_{II}^2(1)}) - \frac{\partial^2 \phi_{II}(1)}{\partial snr^2} E(\frac{\partial \Psi}{\partial \phi_{II}(1)})
\end{aligned}
$$

where Ψ is the log-likelihood function of joint PDF of observed n IQ or envelope samples.

Since the last expectation terms of $[FIM]_{1,1}$, $[FIM]_{1,2}$, $[FIM]_{2,1}$, and $[FIM]_{2,2}$ are all zero (regularity condition), it is straightforward to show that the determinant of FIM is zero. As a result, the Fisher's information matrix is singular, and for unbiased estimation, the variance is unbounded. Therefore, a reasonable estimator should be biased.

The above analysis applies to any estimator for velocity (Doppler) , which uses IQ or envelope information and assumes that the samples sequence of the received signal can be written in terms of a first order Markov random process.

6.5 Discussion and Simulation Results

6.5.1 General CRLB for Doppler frequency Estimators

In this chapter, the CRLBs are derived under the first-order Markovian fading process assumption. This is due to the fact that a first-order Markov model is analytically tractable, and may generate closed-form results easily. In [33], [34], and [35], the authors confirm the usefulness of the first-order Markovian assumption by the experimental measurements and simulation results. However, as indicated in [30], first-order Markov processes may not always be suitable for fading channels, including flat-fading channels.

If the first-order Markov assumption does not hold, it can be shown easily that the joint PDF of n envelope or IQ components should be a function in terms of $\phi_{II}(0)$, $\phi_{II}(1)$, $\phi_{II}(2)$, .., and $\phi_{II}(n-1)$, while for a first-order Markovian process, it is only a function of $\phi_{II}(0)$ and $\phi_{II}(1)$.

General CRLB for SNR-dependent Doppler frequency estimators

The general CRLB for f_m estimators can be written as

$$\begin{aligned} CRLB(\hat{f}_m) &= \frac{1}{-E[\frac{\partial^2 \Psi}{\partial f_m^2}]} \\ &= \frac{1}{-\sum_{i=1}^{n-1}\sum_{j=1}^{n-1} E[\frac{\partial^2 \Psi}{\partial \phi_{II}(j)\partial \phi_{II}(i)}]\frac{\partial \phi_{II}(i)}{\partial f_m}\frac{\partial \phi_{II}(j)}{\partial f_m}} \end{aligned} \tag{6.39}$$

where Ψ is the log-likelihood function of joint PDF of observed n IQ or envelope samples, and (6.39) is obtained directly by the chain rule.

The general CRLB for IQ-based estimators has been discussed in [20]. However, a general CRLB for envelope-based estimators without any simplifying assumptions on the fading process does not appear in the literature.

General CRLB for Doppler-dependent snr estimators

Similarly, the general CRLB for snr estimators will be

$$\begin{aligned} CRLB(\hat{snr}) &= \frac{1}{-E[\frac{\partial^2\Psi}{\partial snr^2}]} \\ &= \frac{1}{-\sum_{i=1}^{n-1}\sum_{j=1}^{n-1} E[\frac{\partial^2\Psi}{\partial\phi_{II}(j)\partial\phi_{II}(i)}]\frac{\partial\phi_{II}(i)}{\partial snr}\frac{\partial\phi_{II}(j)}{\partial snr}} \end{aligned}$$

General CRLB for joint Doppler frequency and snr estimators

The general Fisher's information matrix for joint f_m and snr estimators is shown in Equations (6.38). The element in matrix (6.38) can be written as

$$\begin{aligned} [FIM]_{1,1} &= -\sum_{i=1}^{n}\sum_{j=1}^{n} E[\frac{\partial^2\Psi}{\partial\phi_{II}(j)\partial\phi_{II}(i)}]\frac{\partial\phi_{II}(i)}{\partial f_m}\frac{\partial\phi_{II}(j)}{\partial f_m} \\ [FIM]_{1,2} &= -\sum_{i=1}^{n}\sum_{j=1}^{n} E[\frac{\partial^2\Psi}{\partial\phi_{II}(j)\partial\phi_{II}(i)}]\frac{\partial\phi_{II}(j)}{\partial f_m}\frac{\partial\phi_{II}(i)}{\partial snr} \\ [FIM]_{2,1} &= -\sum_{i=1}^{n}\sum_{j=1}^{n} E[\frac{\partial^2\Psi}{\partial\phi_{II}(j)\partial\phi_{II}(i)}]\frac{\partial\phi_{II}(j)}{\partial snr}\frac{\partial\phi_{II}(i)}{\partial f_m} \\ [FIM]_{2,2} &= -\sum_{i=1}^{n}\sum_{j=1}^{n} E[\frac{\partial^2\Psi}{\partial\phi_{II}(j)\partial\phi_{II}(i)}]\frac{\partial\phi_{II}(i)}{\partial snr}\frac{\partial\phi_{II}(j)}{\partial snr} \end{aligned}$$

where Ψ is the log-likelihood function of joint PDF of observed n IQ or envelope samples.

The CRLB for joint f_m and snr estimators can be obtained as the (1,1) and (2,2) elements of the inverse of Fisher's information matrix, respectively,

$$CRLB(\hat{f_m}) = [FIM^{-1}]_{1,1} \tag{6.40}$$

$$CRLB(\hat{snr}) = [FIM^{-1}]_{2,2} \tag{6.41}$$

We remark that for general case, the following equation is the sufficient condition for a singular FIM,

$$\frac{\partial \phi_{II}(i)}{\partial f_m}\frac{\partial \phi_{II}(j)}{\partial snr} = \frac{\partial \phi_{II}(i)}{\partial snr}\frac{\partial \phi_{II}(j)}{\partial f_m} \tag{6.42}$$

for any $i, j = 1, .., n-1$.

6.5.2 Comparison Between Optimum Unbiased IQ and Envelope Based Estimation

Obviously, the information contained in both in-phase and quadrature components of the received signal is equivalent to the information contained in both envelope and phase of the received signal, so

$$CRLB_{I||Q}(\hat{f_m}) = CRLB_{env||phase}(\hat{f_m}) \tag{6.43}$$

where $CRLB_{I||Q}(.)$ and $CRLB_{env||phase}(.)$ are the CRLB when in-phase and quadrature components are observed, and CRLB when envelope and phase information are available, respectively.

Since the I and Q components are assumed to be independent, and envelope and phase are also considered as independent, we can obtain the following equations

$$E[\frac{\partial^2 \Psi_{I||Q}}{\partial f_m^2}] = E[\frac{\partial^2 \Psi_I}{\partial f_m^2}] + E[\frac{\partial^2 \Psi_Q}{\partial f_m^2}] \quad (6.44)$$

$$E[\frac{\partial^2 \Psi_{env||phase}}{\partial f_m^2}] = E[\frac{\partial^2 \Psi_{env}}{\partial f_m^2}] + E[\frac{\partial^2 \Psi_{phase}}{\partial f_m^2}] \quad (6.45)$$

where $\Psi_{I||Q}$, Ψ_I, Ψ_Q, $\Psi_{env||phase}$, Ψ_{env}, and Ψ_{phase} are the logarithm of the n samples' joint IQ PDF, joint I PDF, joint Q PDF, joint envelope and phase PDF, joint envelope PDF, and joint phase PDF, respectively.

It is known that [28]

$$\frac{1}{-CRLB_I(\hat{f_m})} = E[\frac{\partial^2 \Psi_I}{\partial f_m^2}] \quad (6.46)$$

$$\frac{1}{-CRLB_Q(\hat{f_m})} = E[\frac{\partial^2 \Psi_Q}{\partial f_m^2}] \quad (6.47)$$

$$\frac{1}{-CRLB_{env}(\hat{f_m})} = E[\frac{\partial^2 \Psi_{env}}{\partial f_m^2}] \quad (6.48)$$

$$\frac{1}{-CRLB_{phase}(\hat{f_m})} = E[\frac{\partial^2 \Psi_{phase}}{\partial f_m^2}] \quad (6.49)$$

Inserting above equations into (6.44) and (6.45), we obtain

$$\frac{1}{CRLB_I(\hat{f_m})} + \frac{1}{CRLB_Q(\hat{f_m})} = \frac{1}{CRLB_{env}(\hat{f_m})} + \frac{1}{CRLB_{phase}(\hat{f_m})} \quad (6.50)$$

The above equation uses the fact that

$$E[\frac{\partial^2 \Psi_{I||Q}}{\partial f_m^2}] = E[\frac{\partial^2 \Psi_{env||phase}}{\partial f_m^2}] \quad (6.51)$$

which is straightforwardly obtained from Equation (6.43).

The in-phase and quadrature components have the same stochastic properties. As a result, $CRLB_I(\hat{f_m})$ should be equal to $CRLB_Q(\hat{f_m})$. Therefore, Equation (6.50)

can be written as

$$\frac{1}{CRLB_{env}(\hat{f_m})} + \frac{1}{CRLB_{phase}(\hat{f_m})} = \frac{2}{CRLB_{IQ}(\hat{f_m})} \tag{6.52}$$

where $CRLB_{IQ}(\hat{f_m})$ is the CRLB for f_m estimators when either I or Q components of the received signal is available.

Since $\frac{1}{CRLB_{phase}(\hat{f_m})}$ is positive, we obtain the relation

$$\frac{1}{CRLB_{env}(\hat{f_m})} \leq \frac{2}{CRLB_{IQ}(\hat{f_m})} \tag{6.53}$$

Thus

$$CRLB_{env}(\hat{f_m}) \geq \frac{1}{2} CRLB_{IQ}(\hat{f_m}) \tag{6.54}$$

From (6.30), we observe that $CRLB_{IQ}(\hat{f_m})$ converges to a positive constant instead of zero as the SNR gets large. It is easy to show from (6.54) that the CRLB for envelope-based Doppler estimators does not approach to zero for high SNR either.

We note that the above analysis can also be applied to the CRLBs for *snr* estimators. It is known from (6.36) that since the CRLB for IQ-based *snr* estimators increases exponentially as snr^4, we conclude that the CRLB for envelope-based *snr* estimators also increases exponentially as at least snr^4.

6.5.3 Simulation Results

For known SNR, we compare the approximate CRLBs for envelope and IQ-based f_m estimates to several existing estimators. The true mobile velocity is set to $100km/h$,

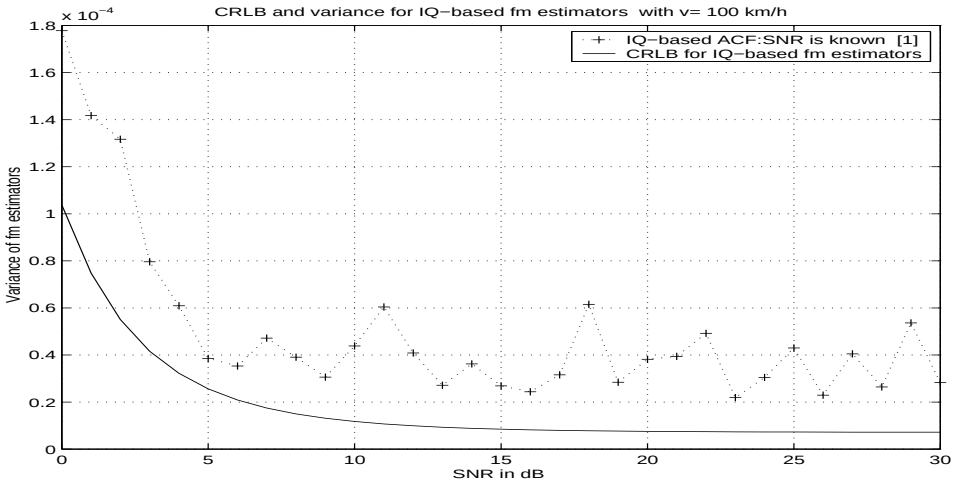

Figure 6.1: Variance comparison between a IQ-based ACF estimator and its CRLB, for the case of a $2GHz$ carrier, $1600Hz$ sampling rate, $800Hz$ band-pass filter bandwidth, mobile velocity of 100 km/h ($f_m = 0.1157$) and 30 Monte-Carlo trials.

and 1000 samples are used to estimate the velocity (normalized Doppler frequency f_m).

From previous sections, we know that IQ-ACF-based, LCR-based and covariance-based algorithms can obtain very accurate Doppler estimates, and thus can be considered as approximately unbiased when SNR is large. Therefore, the CRLB, which applies only to unbiased estimators, can be compared to the variance of these estimators.

In Figure 6.1, we compare $CRLB_{IQ}$ in Eqn. (6.30) to the variance of the IQ-based estimation method in Chapter 3. This figure shows that IQ-ACF-based f_m estimation algorithm does not approach the CRLB when snr is large.

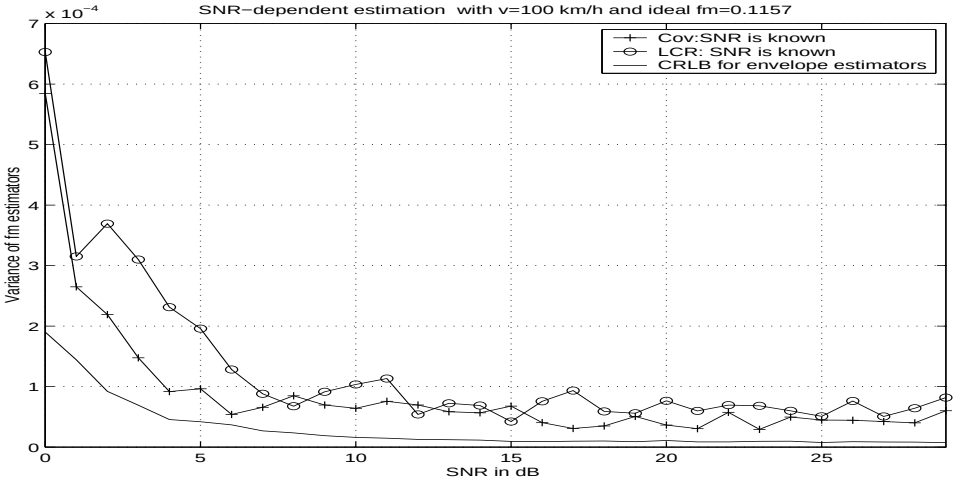

Figure 6.2: Comparison between two envelope-based ACF estimators and its CRLB; Same parameters as in Fig 6.1.

In Figure 6.2, the variance of LCR-based [6] and covariance-based [3] estimators, both of which are based on the envelope of the received signal, are compared to the CRLB in Equation (6.11) for envelope-based Doppler estimation. One hundred independent Monte-Carlo trials are used to obtain the mean value of σ_y^2 in Equation (6.11). It is observed that the variances of LCR-based and covariance-based estimators are very close, and both of them are reasonably close to the CRLB. It is known that this simulation results depend on specific realizations. Next we consider the confidence intervals for these two methods.

The LCR and covariance-based Doppler estimates are obtained over 30 independent Monte-Carlo trials, hence the Doppler estimators can be considered as approximately normal distributed according to Central Limit Theorem. From [23], the confidence interval for the variance of a normal distributed variate with coefficient

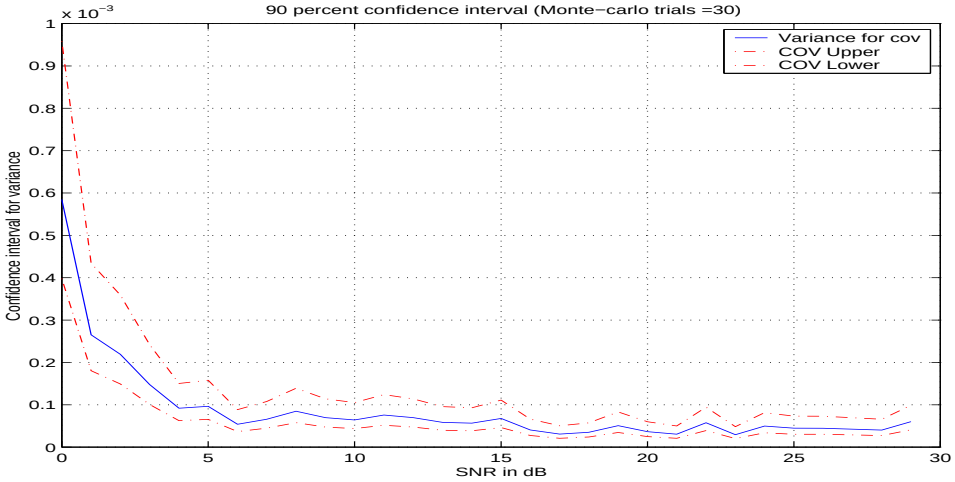

Figure 6.3: Confidence interval for Covariance-based estimators [3] for the case of velocity $100km/h$ ($f_m = 0.1157$); Same parameters as in Fig 6.2.

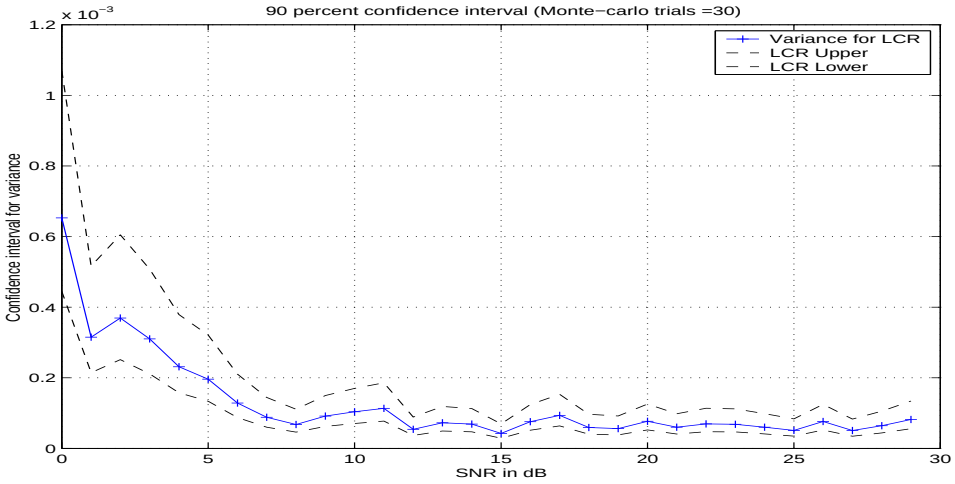

Figure 6.4: Confidence interval for LCR-based estimators [6] for the case of velocity $100km/h$ ($f_m = 0.1157$); Same parameters as in Fig 6.2.

$1-\alpha$ can be derived as

$$P\left[\frac{(n-1)s^2}{\chi^2_{1-\alpha/2}} \leq \sigma^2 \leq \frac{(n-1)s^2}{\chi^2_{\alpha/2}}\right] = 1-\alpha \tag{6.55}$$

where $P[.]$ denotes the probability, s^2 is the sample variance, n is the number of samples, $\chi^2_{1-\alpha/2}$ and $\chi^2_{\alpha/2}$ are the probability integrals of chi-square distribution for $n-1$ degrees of freedom, and σ^2 is the true variance of Doppler estimators. Hence, $1-\alpha$ confidence limits for σ^2 are,

$$\left[\frac{(n-1)s^2}{\chi^2_{1-\alpha/2}}, \frac{(n-1)s^2}{\chi^2_{\alpha/2}}\right] \tag{6.56}$$

For $\alpha = 0.1$, we have 90% confidence that σ^2 lies between above interval. Figures 6.3 and 6.4 present the 90% confidence interval of these two estimators, from which we conclude that the two methods in Figure 6.2 have equivalent performance to within 90% confidence.

Also seen from Figure 6.2, the CRLB does not approach to zero when SNR is very large as predicted and verified from the results in Section 6.5.2. We note that the curves in Figure 6.2 are not smooth due to the lack of Monte-Carlo trials.

Comparison between Figures 6.1 and 6.2 shows that IQ-based f_m estimators can achieve a lower variance bound than envelope-based estimators when the SNR is not high.

A source of discrepancy between the derived CRLBs and the simulation results in Figures 6.1 and 6.2 may be due to the fact that the fading process used in the simulations is not very closely approximated by a first-order Markov process. As

a result, we cannot attribute closeness of the simulation results to the CRLB as an accurate indication of the estimators' performance. However, since the results indicate that the estimators' variance is within the same order of magnitude as the approximate CRLBs, there is some evidence that the estimators may be reasonable.

It was found that if the SNR is very large, the CRLB of *snr* estimators will be increased greatly, and as a result, degrades the performance of *snr* estimation. Our proposed *snr* estimators are not accurate enough to be considered as approximately unbiased. Therefore, the CRLB for SNR estimators and the variance of our proposed SNR-estimators are not compared in this section.

6.6 Summary

In this chapter, approximate CRLBs for IQ and envelope-based f_m estimation for known SNR are derived. The variance of existing estimators [3], [6], and [18], are compared to the approximate CRLBs by simulation. Under the first-order Markov model assumption, we show that the variance lower bound for all unbiased estimators is infinite if SNR information is unknown.

Chapter 7

Applications to Channel Estimation

7.1 Introduction

In the previous chapters, velocity (normalized Doppler frequency) estimation algorithms and performance issues are discussed. In this chapter, we apply Doppler (f_m) information to estimate the complex gain of wireless fading channels.

We briefly survey several existing methods for channel estimation: Liu and Blostein present a decision feedback and adaptive linear prediction (DFALP) algorithm in [40]. Recently, Kalman filtering has been applied [37] [42] with some success by modeling the fading channel as an autoregressive (AR) process.

Existing Kalman-based algorithms require information about the fading process, which include the maximum Doppler frequency shift f_m and signal-to-noise ratio (SNR), as inputs. In this chapter, we will estimate the Doppler frequency f_m and

link SNR by the ACF algorithms described in Chapter 3 and 4, and then apply these estimates to track the channel gain via a minimum-mean-squared-error (MMSE) approach in the presence of flat-fading.

The remainder of this chapter is organized as follows: Section 7.2 discusses the tracking algorithms that employ training sequences, as well as a Kalman filter based on the AR(p) model. The performance analysis and simulation results of channel estimation are provided in Sections 7.3 and 7.4, respectively.

7.2 Channel Tracking Using Kalman Filter

In this section, we estimate channel state information using a training sequence via a minimum mean-square error approach.

7.2.1 The Fading Channel Based on AR(p) Model

According to [32], any linear system with a rational transfer function can be expressed in terms of an AR(p) process. Also, non-rational systems may be approximated arbitrarily closely by an AR model of high enough order. As a result, the input and output equations corresponding to frequency non-selective fading channel can be approximated by the following AR(p) process

$$h(i) = \sum_{k=1}^{p} A_k h(i-k) + u(i) \tag{7.1}$$

$$x(i) = h(i)v(i) + w(i) \tag{7.2}$$

where $x(i)$ and $h(i), i = 1, 2, ..,$ are the observed signal and channel gain at time i, respectively; $u(i)$ and $w(i), i = 1, 2, ..,$ are the driving noise with variance σ_u^2 and additive white channel noise with variance σ_w^2, respectively, and A_i, i = 1, 2, ..., p are AR(p) filter parameters. Note that (7.1) shows the dependence of the current channel state on the previous p states.

Equations (7.1) and (7.2) can also be written in the following matrix-vector form:

$$\mathbf{h}(i) = \mathbf{F}\mathbf{h}(i-1) + \mathbf{G}u(i) \tag{7.3}$$

$$x(i) = \mathbf{h}(i)^T \mathbf{v}(i) + w(i) \tag{7.4}$$

where $u(i)$, $x(i)$ and $w(i)$ have the same definitions as in (7.1) and (7.2), $\mathbf{h}(i)$, $\mathbf{h}(i-1)$, $\mathbf{v}(i)$ and $\mathbf{G}$ are the following p $\times$ 1 vectors, and $\mathbf{F}$ is the following p $\times$ p matrix:

$$\begin{aligned}
\mathbf{h}(i) &= (h(i), h(i-1), .., h(i-p+1))^T \\
\mathbf{h}(i-1) &= (h(i-1), h(i-2), .., h(i-p))^T \\
\mathbf{G} &= (1, 0, .., 0)^T \\
\mathbf{v}(i) &= (v(i), 0, .., 0)^T
\end{aligned}$$

$$\mathbf{F} = \begin{bmatrix} A_1 & A_2 & ... & A_p \\ 1 & 0 & ... & 0 \\ ... & ... & ... & ... \\ 0 & 0 & ... & 1 \end{bmatrix} \tag{7.5}$$

where $(.)^T$ denotes the transpose, $h(i-k)$ and $u(i)$ are mutually uncorrelated for any $k > 0$ and $i \geq 0$.

7.2.2 AR(p) Filter Parameters

In order to enable the AR(p) model in Equation (7.1) and (7.2) to better approximate the true channel, we calculate the parameters A_1, A_2, .., A_p and σ_u^2 according to the desired ACFs of the fading process.

In [42], higher order statistics are used to estimate the autocorrelation function of the fading process. The parameters for both flat fading and frequency-selective fading are then estimated based on the ACF estimation, in the situation that the statistics of the fading channel are unknown. In the following, we assume that the ACF of the fading channel is a Bessel function of the Doppler frequency f_m as discussed in Chapter 2. It will be shown that not only does this form of the ACF correspond to Clarke's fading model [1], but also this assumption will greatly simplify the estimation of the filter parameters. In a Rayleigh fading channel, it is known that the ACF of the fading channel at lag k can be written as

$$\phi_{hh}(k) = \sigma_h^2 J_0(2\pi f_m k) \tag{7.6}$$

where σ_h^2 is the average power of the complex fading channel.

The average power of the observed signal and signal-to-noise ratio are defined, respectively, as

$$P_x = \sigma_s^2 \sigma_h^2 + \sigma_w^2 \tag{7.7}$$

$$snr = \frac{\sigma_h^2 \sigma_s^2}{\sigma_w^2} \tag{7.8}$$

where σ_s^2 is the average power of data $v(i)$. We assume that the transmitted data

$v(i), i = 1, 2, ..,$ is a constant envelope modulated signal, therefore the average power of data $v(i)$ is invariant with time i.

Inserting Equations (7.7) and (7.8) into (7.6), we obtain

$$\phi_{hh}(k) = \frac{P_x snr}{\sigma_s^2(snr+1)} J_0(2\pi f_m k) \tag{7.9}$$

which is a function of f_m, snr and P_x.

The AR(p) parameter $A_1, A_2, .., A_p$ and σ_u^2, which are defined in (7.1), can be estimated by Levinson algorithm (see Appendix B for the derivation of AR(p) parameters) , which employs the estimated ACFs in Equation (7.9), and in turn employs f_m and SNR estimation.

It should be kept in mind that the parameters $A_1, A_2, .., A_p$ and σ_u^2 obtained above only match the desired sampled ACF up to lag p. In theory, a higher-order AR model more accurately models the true Rayleigh fading channel, and in principle, a higher-order Kalman filter can make tracking more accurate. However, only the first correlation lags can be accurately estimated. These low-order correlation lags determine most of the channel gain dynamics and may most effectively aid a tracking algorithm [37].

7.2.3 Channel Tracking Using a Training Sequence

After deriving the AR parameters, we use the following Kalman recursions involving a vector-channel-state and scalar-received-observation to calculate the channel gain

[28]

$$\hat{\mathbf{h}}(i|i-1) = \mathbf{F}\hat{\mathbf{h}}(i-1|i-1) \tag{7.10}$$

$$\mathbf{M}(i|i-1) = \mathbf{F}\mathbf{M}(i-1|i-1)\mathbf{F}^T + \sigma_u^2\mathbf{G}\mathbf{G}^T \tag{7.11}$$

$$\mathbf{K}(i) = \frac{\mathbf{M}(i|i-1)\mathbf{v}(i)}{\mathbf{v}^T(i)\mathbf{M}(i|i-1)\mathbf{v}(i) + \sigma_w^2} \tag{7.12}$$

$$\hat{\mathbf{h}}(i|i) = \hat{\mathbf{h}}(i|i-1) + \mathbf{K}(i)(x(i) - \mathbf{v}^T(i)\hat{\mathbf{h}}(i|i-1)) \tag{7.13}$$

$$\mathbf{M}(i|i) = (\mathbf{I} - \mathbf{K}(i)\mathbf{v}^T(i))\mathbf{M}(i|i-1) \tag{7.14}$$

where $\hat{\mathbf{h}}(i|k), i \geq k$ is the estimated channel gain of vector $\mathbf{h}(i)$ at time i based on all the observations up to time k; $\mathbf{K}(i)$ is the $Kalman$ gain, and $\mathbf{M}(i|k), i \geq k$ is the covariance matrix of the estimated channel gain $\mathbf{h}(i)$ based on all the previous measurements up to time k.

For simplicity, the above filter can be initialized with

$$\mathbf{h_0} = (0, 0, .., 0)^T \tag{7.15}$$

$$\mathbf{M_0} = \begin{bmatrix} \phi_{II}(0) & \phi_{II}(1) & ... & \phi_{II}(p-1) \\ \phi_{II}(1) & \phi_{II}(0) & ... & \phi_{II}(p-2) \\ ... & ... & ... & ... \\ \phi_{II}(p-1) & \phi_{II}(p-2) & ... & \phi_{II}(0) \end{bmatrix} \tag{7.16}$$

7.3 Performance Analysis for Kalman-Based Channel Tracking

Obviously, the accuracy of our proposed channel estimation method depends on the accuracy of f_m and SNR estimates. In the following, for AR(1) and AR(p) process, we first derive the steady-state MSEs for the perfect parameter match, then we will study the effect of parameter mismatch, i.e., when f_m is over- or under-estimated rather than known perfectly.

7.3.1 Steady-State Channel Estimation Error: AR(1) case

7.3.1.1 MMSE for perfect parameter match

For $p = 1$ case, the AR(1) process can be written as

$$h(i) = Ah(i-1) + u(i) \tag{7.17}$$

$$x(i) = h(i)v(i) + w(i) \tag{7.18}$$

where A is the AR(1) filter parameter.

The prediction and filtered MSEs for perfect match are given in Eqn. (7.11) and (7.14), which are also MMSEs.

In the steady-state, the filtered MMSE at time i can be considered to be same as the MMSE at time $i-1$ [28]. This observation yields the steady-state Ricatti

equation

$$M_{inf} = \frac{\sigma_w^2(A^2 M_{inf} + \sigma_u^2)}{\sigma_s^2(A^2 M_{inf} + \sigma_u^2) + \sigma_w^2} \tag{7.19}$$

The above equation is seen to be quadratic. By solving (7.19), we obtain the steady-state MMSE for perfect parameter match.

7.3.1.2 MSE for parameter mismatch

If the parameters A and σ_u^2 in Equations (7.17) and (7.18) are instead given by $A^{'}$ and $(\sigma_u^{'})^2$ due to mismatch, the model in (7.17) and (7.18) becomes

$$x(i) = h(i)v(i) + w(i) \tag{7.20}$$

$$h(i) = A^{'}h(i-1) + u^{'}(i) \tag{7.21}$$

where $u^{'}(i)$ is the driving noise with zero mean and mismatched variance $(\sigma_u^{'})^2$, and $A^{'}$ is the mismatched AR(1) parameter. For convenience, let $Q = \sigma_u^2$ and $Q^{'} = (\sigma_u^{'})^2$.

We track the channel with mismatched parameters via recursions in Equation (7.10) and (7.14),

$$\hat{h}(i+1|i) = A^{'}\hat{h}(i|i) \tag{7.22}$$

$$M^{'}(i+1|i) = (A^{'})^2 M^{'}(i|i) + Q^{'} \tag{7.23}$$

$$k^{'}(i+1) = \frac{v(i+1)M^{'}(i+1|i)}{|v(i+1)|^2 M^{'}(i+1|i) + \sigma_w^2} \tag{7.24}$$

$$\hat{h}(i+1|i+1) = \hat{h}(i+1|i) + k^{'}(i+1)\Big(x(i+1) - v(i+1)\hat{h}(i+1|i)\Big) \tag{7.25}$$

$$M^{'}(i+1|i+1) = M^{'}(i+1|i) - k^{'}(i+1)v(i+1)M^{'}(i+1|i) \tag{7.26}$$

We should note that the above $M^{'}(i+1|i)$ and $M^{'}(i+1|i+1)$ differ from the true prediction MSE and filtered MSE due to the mismatch. The true prediction MSE is given by

$$\begin{aligned} M(i+1|i) &= E[|\hat{h}(i+1|i) - h(i+1)|^2] \\ &= E[|A^{'}\hat{h}(i|i) - A^{'}h(i) + A^{'}h(i) - Ah(i) - u(i+1)|^2] \\ &= E[|A^{'}|^2 M(i|i) + |A^{'} - A|^2 |h(i)|^2 + |u(i+1)|^2] \\ &\quad + E[A^{'}(\hat{h}(i|i) - h(i))h^*(i)(A^{'} - A)^*] \\ &\quad + E[(A^{'} - A)h(i)(\hat{h}(i|i) - h(i))^*(A^{'})^*] \\ &= [A^{'}A^* + A(A^{'})^* - |A^{'}|^2]M(i|i) + |A^{'} - A|^2 E[|h(i)|^2] + Q + D \end{aligned} \tag{7.27}$$

where

$$D = -(A^{'})^*(A^{'} - A)E[\hat{h}(i|i)(h(i) - \hat{h}(i|i))^*] - A^{'}(A^{'} - A)^* E[(h(i) - \hat{h}(i|i))\hat{h}(i|i)^*] \tag{7.28}$$

The above assumes that $u(i+1)$ is independent of $h(i), h(i-1), .., h_0$, and $x(i), x(i-1), .., x(0)$. We mention that D is not zero, since $\hat{h}(i|i)$ is the mismatched estimator instead of the true MMSE estimator, and the orthogonality principle cannot be employed.

By defining $\epsilon_i = \hat{h}_i - \hat{h}(i|i)$, where $\hat{h}_i$ is the channel gain estimate for a perfect

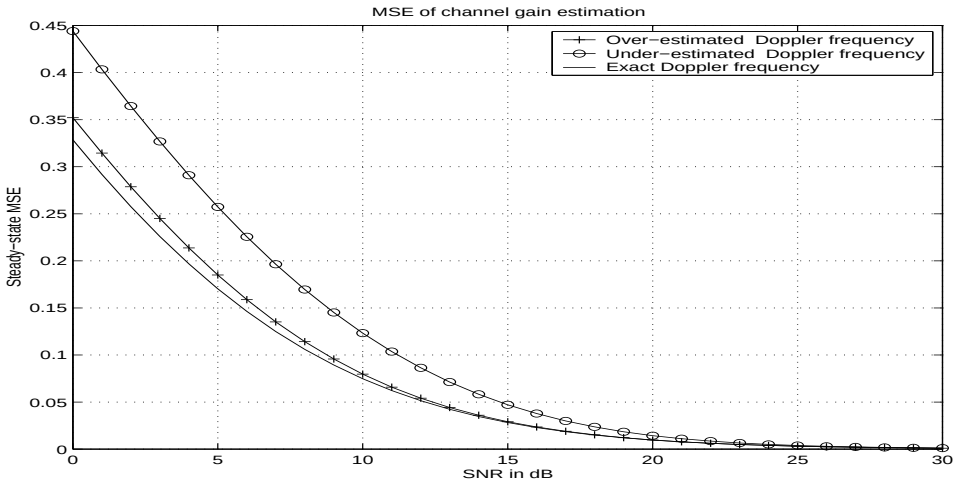

Figure 7.1: Steady-state MSE for the case of AR(1) generator, first-order Kalman-based tracking and exact velocity of $100km/h$.

channel match, and ϵ_i is independent of $\hat{h}_i$, D can be expressed as

$$D = -2(A^{'})(A^{'} - A)E[\hat{h}(i|i)(h(i) - \hat{h}(i|i))^*] \tag{7.29}$$

$$\begin{aligned} &= -2(A^{'})(A^{'} - A)E[(\hat{h}_i - \epsilon_i)(h(i) - \hat{h}_i + \epsilon_i)^*] \\ &= -2(A^{'})(A^{'} - A)E[\hat{h}_i(h(i) - \hat{h}_i) + \hat{h}_i\epsilon_i - \epsilon_i(h(i) - \hat{h}_i)^* - |\epsilon_i|^2] \\ &= 2(A^{'})(A^{'} - A)E[|\epsilon_i|^2] \end{aligned} \tag{7.30}$$

The above equation assumes that A and $A^{'}$ are both real-valued, and the mean of the fading channel is zero.

Therefore, the prediction MSE can be derived as

$$M(i+1|i) \tag{7.31}$$

$$= [2A^{'}A - (A^{'})^2]M(i|i) + (A^{'} - A)^2E[|h(i)|^2] + Q + 2(A^{'})(A^{'} - A)E[|\epsilon_i|^2] \tag{7.32}$$

Next, the true filtered MSE is obtained

$$M(i+1|i+1) = E[(\hat{h}(i+1|i+1) - h(i+1))^2] \tag{7.33}$$

$$= M(i+1|i) + [k^{'}(i+1)]^2[v^2(i+1)M(i+1|i) + \sigma_w^2] - 2k^{'}(i+1)v(i+1)M(i+1|i) \tag{7.34}$$

In the steady-state, let $M(i|i) = M(i-1|i-1)$ in Equation (7.34). The mismatched steady-state MSE for the AR(1) model is given as

$$M_{inf-mis} = \frac{[1 + (k_{inf}^{'})^2\sigma_s^2 - 2k_{inf}^{'}\sigma_s][(A^{'} - A)^2E[|h(i)|^2] + Q + 2(A^{'})(A^{'} - A)E[|\epsilon_i|^2]] + (k_{inf}^{'})^2\sigma_w^2}{1 - [1 + (k_{inf}^{'})^2\sigma_s^2 - 2k_{inf}^{'}\sigma_s](2A^{'}A - (A^{'})^2)} \tag{7.35}$$

where the steady-state (mismatch) Kalman gain $k_{inf}^{'}$ can be obtained from steady-state mismatch MSE $M_{inf}^{'}$ by (7.24),

$$k_{inf}^{'} = \frac{\sigma_s((A^{'})^2M_{inf}^{'} + Q^{'})}{\sigma_s^2((A^{'})^2M_{inf}^{'} + Q^{'}) + \sigma_w^2} \tag{7.36}$$

and $M_{inf}^{'}$ is the solution to (7.19) with A and σ_u^2 replaced by $A^{'}$ and $Q^{'}$.

Figure 7.1 shows the steady-state MSEs in Equation (7.35) versus SNR for perfect and mismatched parameters. Figures 7.2 and 7.3 plot the MSEs versus the mismatched Doppler ratio, which is defined as $\frac{\hat{f_m}}{f_m}$, where $\hat{f}_m$ and f_m are the estimated and exact Doppler frequency, respectively. These figures quantify the degree to which parameter mismatch affects the channel tracking for SNR=5 dB and SNR=15 dB. The true velocity is 100 km/h. The term $E[|\epsilon_i|^2]$ in Eqn. (7.35) can be obtained by Monte-Carlo techniques.

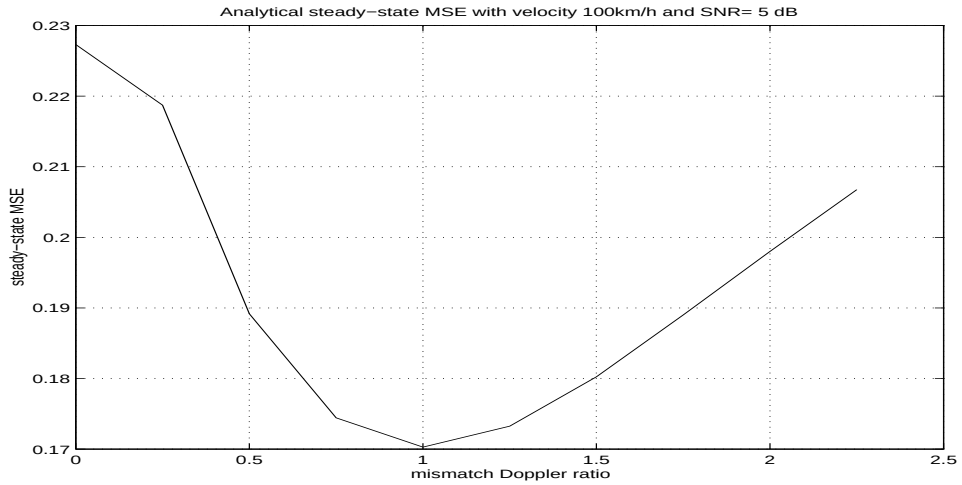

Figure 7.2: Steady-state MSE versus deviation of the estimated f_m with velocity $100km/h$ and SNR 5 dB.

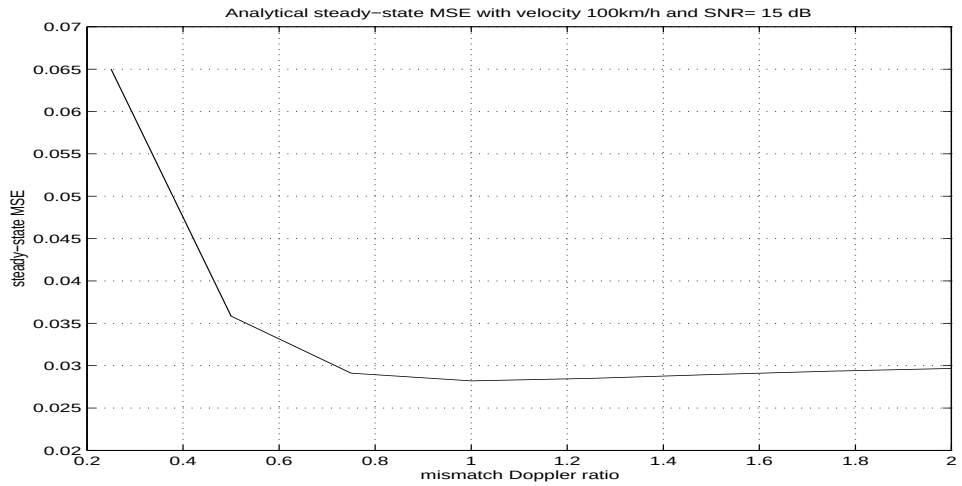

Figure 7.3: Steady-state MSE versus deviation of the estimated f_m with velocity $100km/h$ and SNR 15 dB.

From Figures 7.1 to 7.3, it is observed that an under-estimated f_m will significantly degrade the performance, while over-estimated f_m only affects the performance moderately, especially at high SNRs.

Also can be seen from Figures 7.2 and 7.3, as the SNR increases, the MSE becomes more insensitive to parameter mismatch. This can be explained by the fact that if the *snr* is very high, the channel gain in Equation (7.2) will approach $\frac{x(i)}{v(i)}$, thus the channel gain estimates are hardly affected by state Equation (7.1). In the limiting case, when the *snr* is infinite, the channel gain becomes $\frac{x(i)}{v(i)}$, which is independent of the state equation, and thus independent of parameters $A_1, A_2, .., A_p$ and σ_u^2 in (7.1).

7.3.2 Steady-State Channel Estimation Error: AR(p) case

For p^{th} order AR(p) model with perfect parameter match, by letting $\mathbf{M}(i|i)$ equal to $\mathbf{M}(i-1|i-1)$ in (7.14) and (7.11), the steady-state MMSE can be written as

$$\mathbf{M_{inf}} = (\mathbf{I} - \mathbf{K}(i)\mathbf{v}(i)^T)(\mathbf{F}\mathbf{M_{inf}}\mathbf{F}^T + \mathbf{G}\mathbf{G}^T\sigma_u^2) \tag{7.37}$$

where $\mathbf{M_{inf}}$ is the steady-state covariance matrix, $\mathbf{I}$ is the identity matrix, and Kalman gain

$$\mathbf{K}(i) = \frac{(\mathbf{F}\mathbf{M_{inf}}\mathbf{F}^T + \sigma_u^2\mathbf{G}\mathbf{G}^T)\mathbf{v}(i)}{\sigma_w^2 + \mathbf{v}(i)^T(\mathbf{F}\mathbf{M_{inf}}\mathbf{F}^T + \sigma_u^2\mathbf{G}\mathbf{G}^T)\mathbf{v}(i)} \tag{7.38}$$

The steady-state covariance matrix $\mathbf{M_{inf}}$ can be obtained by solving matrix Equation (7.37).

If the true $p-th$ order AR model is mismatched by the following model

$$\mathbf{h}(i) = \mathbf{F}^{'}\mathbf{h}(i-1) + \mathbf{G}u^{'}(i) \tag{7.39}$$

$$x(i) = \mathbf{h}(i)^T\mathbf{v}(i) + w(i) \tag{7.40}$$

where $u^{'}(i)$ is an i.i.d. sequence with zero-mean and mismatched variance $Q^{'}$.

We track the channel when $\mathbf{F}$ and Q are replaced by the mismatched $\mathbf{F}^{'}$ and $Q^{'}$, respectively. The recursions are given by

$$\hat{\mathbf{h}}(i+1|i) = \mathbf{F}^{'}\hat{\mathbf{h}}(i|i) \tag{7.41}$$

$$\mathbf{M}^{'}(i+1|i) = \mathbf{F}^{'}\mathbf{M}^{'}(i|i)(\mathbf{F}^{'})^T + \mathbf{G}\mathbf{G}^TQ^{'} \tag{7.42}$$

$$\mathbf{K}^{'}(i+1) = \frac{\mathbf{M}^{'}(i+1|i)\mathbf{v}(i+1)}{\mathbf{v}(i+1)^T\mathbf{M}^{'}(i+1|i)\mathbf{v}(i+1)+\sigma_w^2} \tag{7.43}$$

$$\hat{\mathbf{h}}(i+1|i+1) = \hat{\mathbf{h}}(i+1|i) + \mathbf{K}(i+1)\left(x(i+1) - \mathbf{v}^T(i+1)\hat{\mathbf{h}}(i+1|i)\right)$$

$$\mathbf{M}^{'}(\mathbf{i+1|i+1}) = \mathbf{M}^{'}(\mathbf{i+1|i}) - \mathbf{K}^{'}(\mathbf{i+1})\mathbf{v}^{\mathbf{T}}(\mathbf{i+1})\mathbf{M}^{'}(\mathbf{i+1|i}) \tag{7.44}$$

The true prediction MSE (which is no longer the MMSE prediction except for when $\mathbf{F}=\mathbf{F}^{'}$) is given by

$$\begin{aligned}\mathbf{M}(i+1|i) &= E[(\hat{\mathbf{h}}(i+1|i)-\mathbf{h}(i+1))^2] \\ &= \mathbf{F}^{'}\mathbf{M}(i|i)(\mathbf{F}^{'})^H - (\mathbf{F}^{'}-\mathbf{F})\mathbf{M}(i|i)(\mathbf{F}^{'})^H \\ &\quad -\mathbf{F}^{'}\mathbf{M}(i|i)(\mathbf{F}^{'}-\mathbf{F})^H + (\mathbf{F}^{'}-\mathbf{F})E[|\mathbf{h}(i)\mathbf{h}^H(i)|](\mathbf{F}^{'}-\mathbf{F})^H \\ &\quad +\mathbf{D} + \mathbf{G}\mathbf{G}^{\mathbf{H}}Q\end{aligned} \tag{7.45}$$

where $(.)^H$ denotes the Hermitian operator, and

$$\begin{aligned}\mathbf{D} &= \mathbf{F}^{'}E[\hat{\mathbf{h}}(i|i)-\mathbf{h}(i)](\hat{\mathbf{h}}(i|i))^H(\mathbf{F}^{'}-\mathbf{F})^H \\ &\quad +(\mathbf{F}^{'}-\mathbf{F})\hat{\mathbf{h}}(i|i)(\hat{\mathbf{h}}(i|i)-\mathbf{h}(i))^H(\mathbf{F}^{'})^H\end{aligned} \tag{7.46}$$

The true filtered MSE will be

$$\begin{aligned}\mathbf{M}(i+1|i+1) &= E[|\hat{\mathbf{h}}(i+1|i+1) - \mathbf{h}(i+1)|^2] \\ &= \mathbf{M}(i+1|i) - \mathbf{M}(i+1|i)\mathbf{v}(i+1)^*(\mathbf{K}'(i+1))^H \\ &\quad -\mathbf{K}'(i+1)\mathbf{v}^T(i+1)\mathbf{M}(i+1|i) \\ &\quad +\mathbf{K}'(n+1)[\mathbf{v}^T(i+1)\mathbf{M}(i+1|i)\mathbf{v}^*(i+1) + \sigma_w^2](\mathbf{K}'(i+1))^H\end{aligned} \tag{7.47}$$

The above equation uses the assumption that $u(i+1)$ is independent of $\mathbf{h}(i)$ and $\mathbf{h}(i|i)$.

7.3.3 Channel model order mismatch

Here, we briefly consider the case where the true model order is p, while the estimated model order is q, where q can be lower or higher than p.

Assume that the AR(p) model

$$h_p(k) = \sum_{i=1}^{p} A_i h_p(k-i) + u(i) \tag{7.48}$$

is mismatched by AR(q) model

$$h_q(k) = \sum_{i=1}^{q} A_i' h_q(k-i) + u'(i) \tag{7.49}$$

If $p \geq q$, the mismatched model in (7.49) is equivalent to the following p^{th} order

model

$$\begin{aligned} h_q(k) &= \sum_{i=1}^{q} A_i' h_q(k-i) + \sum_{i=q+1}^{p} 0 \times h_q(k-i) + u'(i) \\ &= \sum_{i=1}^{p} A_i' h_q(k-i) + u'(i) \end{aligned} \tag{7.50}$$

with mismatched parameter $A_1', .., A_p'$. Therefore, the model (order) mismatch can be shown to be equivalent to parameter mismatch, which has been discussed in previous section.

Similarly, if $p < q$, the model in (7.48) can be written as the equivalent q^{th} order model

$$\begin{aligned} h_p(k) &= \sum_{i=1}^{p} A_i h_p(k-i) + \sum_{i=p+1}^{q} 0 \times h_p(k-i) + u(i) \\ &= \sum_{i=1}^{q} A_i h_p(k-i) + u(i) \end{aligned} \tag{7.51}$$

with true parameter $A_1, .., A_q$. Again the model order mismatch can be considered as a type of parameter mismatch.

Summing above, we have shown that we can express true channel model and mismatched model with same order g, where $g = max(p, q)$. The MSE for mismatched model parameters of the same order derived in previous section can be employed.

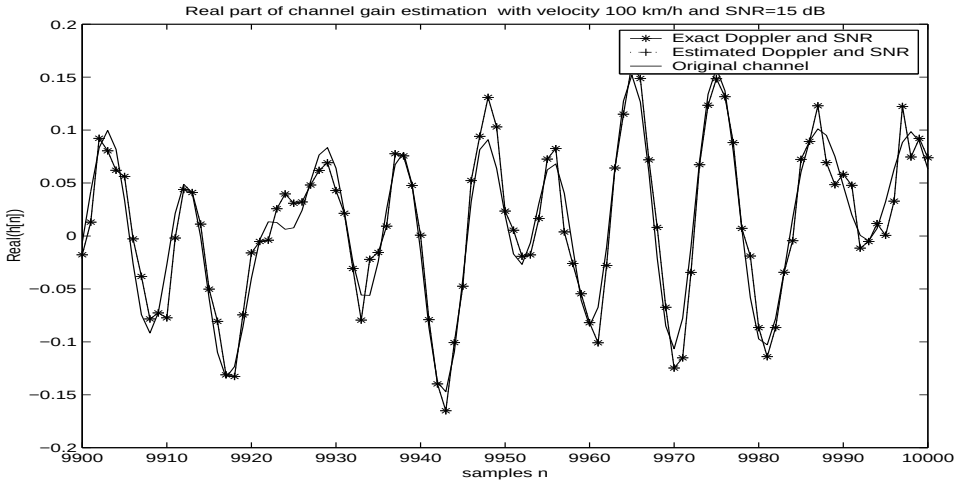

Figure 7.4: Channel gain tracking for the case of IDFT generator, first-order Kalman filter tracking and SNR=15 dB.

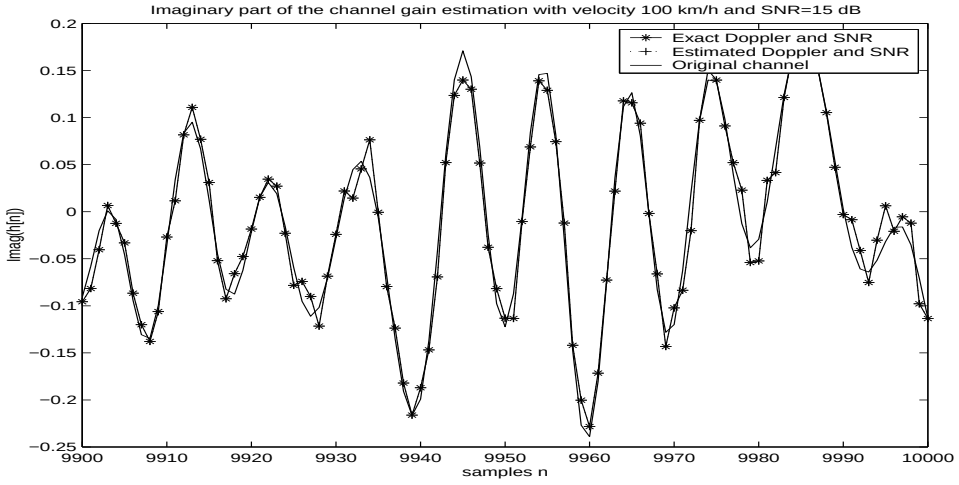

Figure 7.5: Channel gain tracking for the case of IDFT generator, first-order Kalman filter tracking and SNR=15 dB.

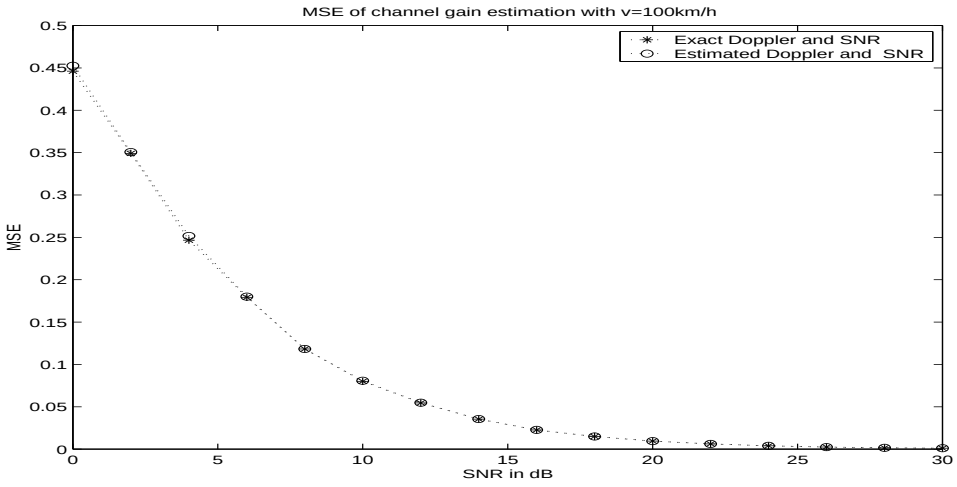

Figure 7.6: MSE for channel estimation for the case of IDFT generator, first-order Kalman filter tracking, and velocity 100 km/h.

7.4 Simulation Results

With the increase of the AR filter order, the AR(p) process is close to the real Rayleigh fading process, which can be generated accurately by IDFT algorithm [17]. This section shows some Monte-Carlo simulation results for fading channel gain estimation when the flat fading channel is generated by IDFT algorithm, and tracked by first-order Kalman-filtering. These examples illustrate the performance when the order of the tracking model is much lower than the order of the generated channel model. During the simulations, the IQ-ACF-based algorithm is employed to estimate parameters f_m and SNR, and fifty Monte-Carlo trials are used to track the fading channel gain.

Sample channel tracking results using the very accurate IDFT simulator are presented in Figures 7.4 and 7.5, which show that, under not very low SNR, first-order Kalman-filtering can capture most of the channel's dynamics even if the channel is generated by very high order AR model or IDFT simulator. Figure 7.6 plots the MSE of channel estimation using first-order Kalman filter tracking when either exact or estimated Doppler frequencies are used. It is observed that the IQ-ACF-based SNR and Doppler estimators can result in very accurate channel estimation, and only slightly inferior to that for exact parameters. As the SNR increases, the performance using estimated f_m and SNR improves.

7.5 Summary

In this chapter, Doppler frequency and SNR information are employed as input to estimate the channel gain using a Kalman filter. From performance analysis, we conclude that Kalman-based channel estimation is more robust to over-estimated f_m. Simulation results show that by using our proposed IQ-based f_m and SNR estimates, the first-order Kalman filtering can capture most of the channel's characters even if the channel is generated by very high-order AR process.

Chapter 8

Summary and Conclusions

8.1 Summary

In a Rayleigh fading channel, the statistics of the received random process are related to the normalized Doppler frequency since the fading depends on the mobile velocity. In this thesis, we reviewed Clarke's fading model and the generation of Rayleigh fading signals using the IDFT algorithm proposed by Smith [17]. Then several existing Doppler f_m estimation algorithms were reviewed that required SNR as side information. The main contribution of this thesis is a new class of Doppler frequency estimators which do not depend on SNR. The principle is to estimate several ACF lags to replace the missing SNR information. Chapter 3 discusses an IQ-based method that assumes coherent demodulation at the receiver. Chapter 4 presents envelope-based methods assuming non-coherent demodulation. The performance of the proposed methods is investigated by Monte-Carlo simulation, and these methods

are compared against several existing methods in Chapter 5.

The performance analysis of the algorithm-independent f_m estimation is discussed in Chapter 6. Approximate Cramer-Rao lower bounds for IQ-based and envelope-based estimators are derived.

In Chapter 7, we applied the estimates of velocity to the problem of channel tracking. A simple Kalman filter tracking method is proposed, taking into account channel estimation and velocity measurement. An analysis of the Kalman-based channel tracking is performed for a simple first-order case.

8.2 Conclusions

Both IQ-ACF-based and squared-envelope-ACF-based estimation methods can be extended to be SNR-independent, and still maintain high accuracy at SNRs higher than 10 dB. Monte-Carlo simulations show that the performance of the SNR-independent method is not as accurate as that of the SNR-dependent method, especially for SNRs lower than 10 dB.

IQ-based SNR estimates can also be obtained together with velocity estimates and have been shown to be very accurate at SNRs lower than 20 dB. Velocity and SNR estimates based on IQ ACFs can always achieve lower bias and variance than squared-envelope-based estimators, but require coherent demodulation.

The approximate Cramer-Rao lower bounds for IQ-based and envelope-based

methods are derived under a first-order Markov process assumption. It has been shown that the IQ-based method can attain a smaller CRLB than the envelope-based method at low SNRs. Under the same assumption, we also show that unbiased SNR-independent velocity estimators will have very poor performance. Therefore, a reasonable velocity estimator should be biased if the SNR is unknown.

Velocity and SNR estimators can also be applied to track the fading channel gain. From the steady-state performance analysis, it is observed that channel estimation is more insensitive to over-estimated velocities than under-estimated ones.

8.3 Suggestions for future work

In this thesis, we proposed some Doppler estimators based on a flat Rayleigh fading channel. However, this model should be further refined in order to be used in practical mobile channels. For example, we assume that line-of-sight (LoS) is not present, and isotropic scattering environment is present. One should investigate with extending the SNR-independent Doppler estimation method to non-isotropic scattering, LoS, and frequency-selective fading.

The CRLBs for velocity estimators are derived under a first-order Markov process assumption. However, this assumption may not always hold in practical systems. An exact CRLB for envelope-based estimators should be investigated.

We also observe that when we employ a Kalman filter to estimate the channel gain, the performance seems to be insensitive to over-estimation of velocity. This

observation should be investigated in greater detail.

Appendix A

Determination of R_{upp}

Before discussing the determination of R_{upp}, we note that Equation (3.6) has two Bessel functions, which are plotted in Figure A.1. It is observed that if $0 \leq f_m \leq 0.3$, both $J_0(2\pi f_m)$ and $J_0(4\pi f_m)$ have a one-to-one mapping to f_m. If $f_m \geq 0.3$, inconsistent solutions may occur. Therefore, R_{upp} should be smaller than 0.3.

Equation (3.12) is a non-linear equation which contains more than one Bessel function and sinc function. As a result, it is not easy to determine the range of possible roots analytically. In this thesis, the following numerical interval-finding method is used:

1. Assume that $B_n T_s$ is known.

2. Let $f_m = 0.01$. For smaller f_m, a unique solution can always be approximated via a series approximation to the Bessel function. The SNR can be chosen arbitrarily, since it is shown in Section 3.2 that the zero of $g(x)$ is independent

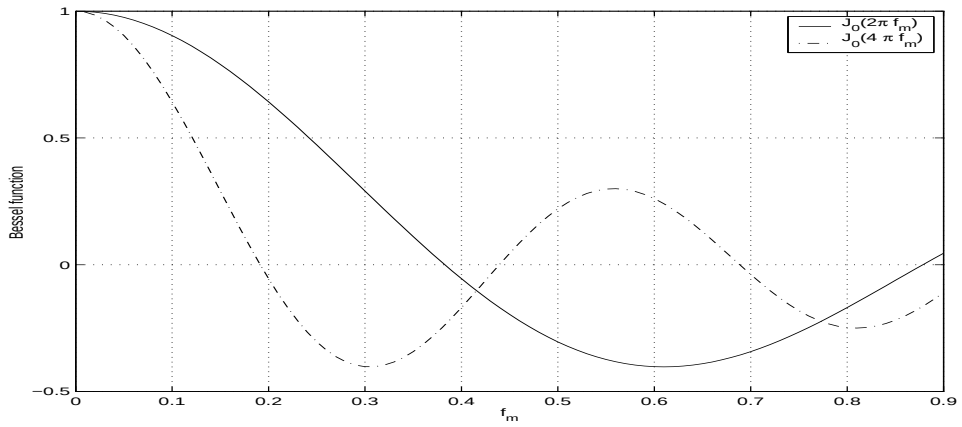

Figure A.1: Bessel function plots

of SNR for a large number of samples.

3. Plot $g(x)$ in (3.12) for $0 \leq x \leq 0.3$.

4. Find a range [0, R_{upp1}], in which only one zero of $g(x)$ exists.

5. Increase f_m to $f_m = f_m + \triangle f$, plot $g(x)$ versus x again, find another range [0, R_{upp2}].

6. Repeat above step by incrementing f_m until $f_m = 0.3$. We obtain a sequence of $R_{uppi}, i = 1, 2, ...$

7. Find the minimum value among R_{uppi}, i.e., $R_{upp} = min\{R_{uppi}\}$

Therefore, [0, R_{upp}] is the range in which a unique solution exists. We note that the above range is only a sufficient condition for uniqueness, not a necessary one. That is, the interval in which a unique solution exists may be larger than $[0, R_{upp}]$.

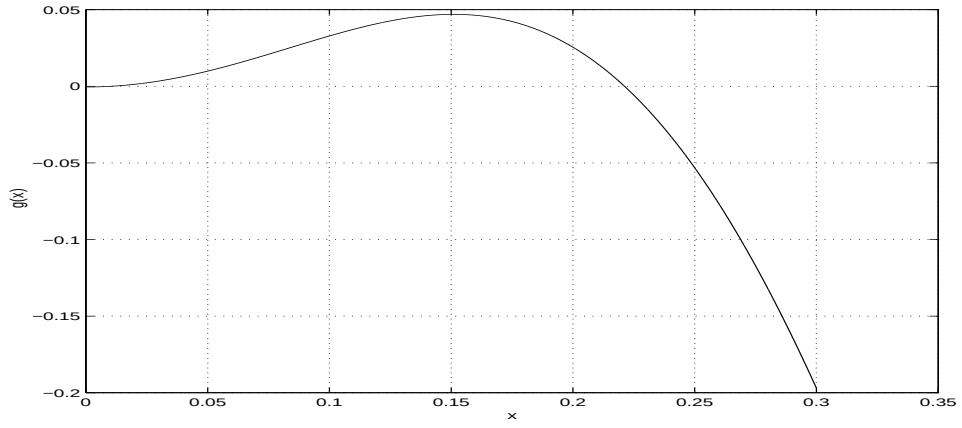

Figure A.2: Plot of $g(x)$ for $f_m = 0.01$

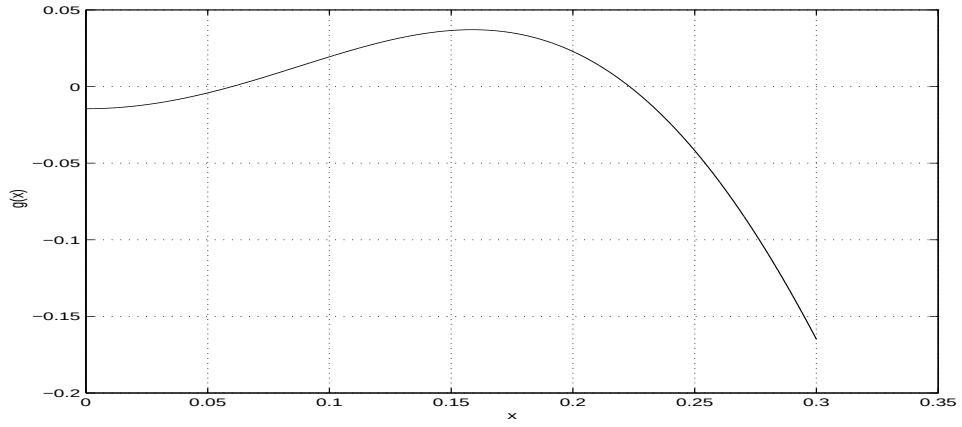

Figure A.3: Plot of $g(x)$ for $f_m = 0.06$

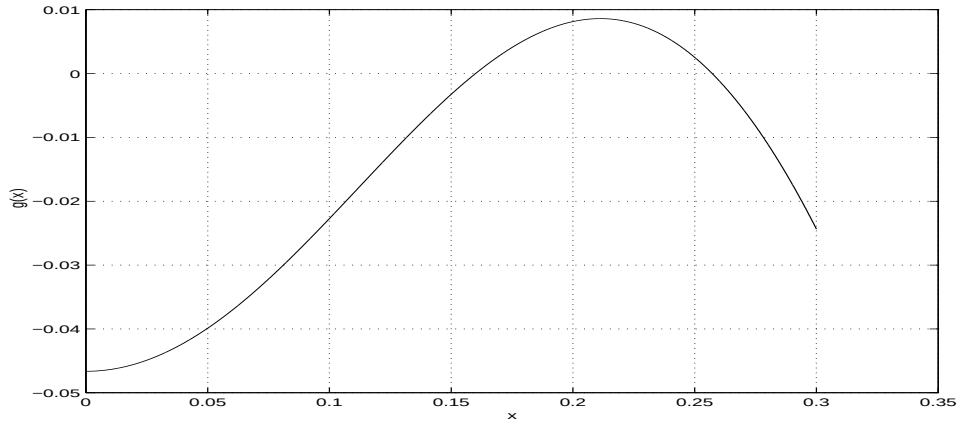

Figure A.4: Plot of $g(x)$ for $f_m = 0.16$

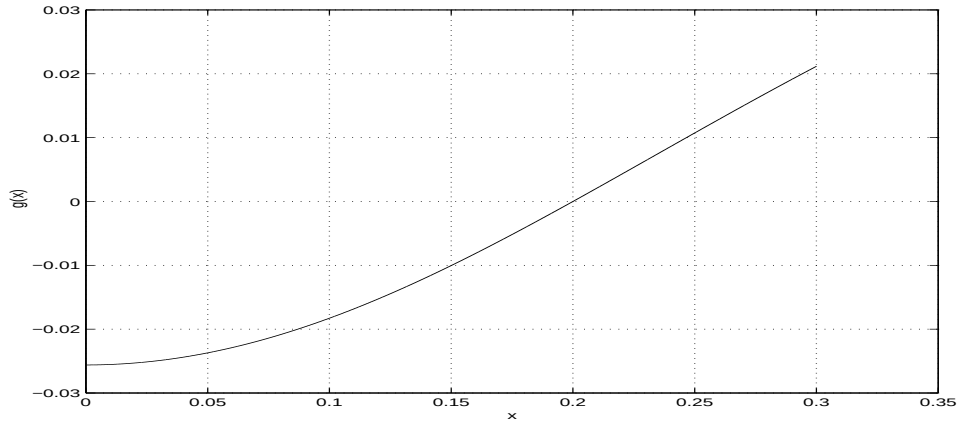

Figure A.5: Plot of $g(x)$ for $f_m = 0.2$

For example, in the signals used in the simulations in Chapter 3-5, we set $\triangle f = 0.01$, $B_n T_s = \frac{1}{2}$ (which is same as in [6] and [7]), and following above steps, we conclude that $0 \leq f_m \leq R_{upp}$, where $R_{upp} = 0.214$, is a sufficient condition for unique zero of $g(x)$. Figures A.2 to A.5 present some of these plots from the above procedure.

We remark that a similar f_m interval-finding method can also be applied to envelope-based and squared-envelope-based methods to ensure a unique root.

Appendix B

Generation of Fading Process Using AR(p) Filter

For AR(p) algorithm, we generate the fading process via the time domain recursion

$$h(n) = \sum_{i=1}^{p} A_i h(n-i) + u(n) \tag{B.1}$$

where p is the order of AR model, driving noise $u(n)$ is an i.i.d. Normal process with zero mean and variance σ_u^2. We decide the AR model parameters $A_1, ..., A_p$ and σ_u^2 by matching the autocorrelation function of the desired statistics of correlated Rayleigh fading channel with that for an AR(p) process.

The ACF of the fading channel can be written as the following recursive form

$$\phi_{hh}(k) = \sum_{l=1}^{p} A_l \phi_{hh}(k-l) + \sigma_u^2 \delta(k) \tag{B.2}$$

where $\phi_{hh}(k)$ is the ACF of fading channel $h(i)$ at lag k. By letting $k = 1, 2, .., p$, we

obtain the following matrix form

$$\mathbf{r} = \mathbf{R_h A} \tag{B.3}$$

where $\mathbf{r}$, $\mathbf{R_h}$, and $\mathbf{A}$ are defined as

$$\mathbf{r} = (\phi_{hh}(1), \phi_{hh}(2), ..., \phi_{hh}(p))^T \tag{B.4}$$

$$\mathbf{R_h} = \begin{vmatrix} \phi_{hh}(0) & \phi_{hh}(1) & ... & \phi_{hh}(p-1) \\ \phi_{hh}(1) & \phi_{hh}(2) & ... & \phi_{hh}(p) \\ ... & ... & ... & ... \\ \phi_{hh}(p-1) & \phi_{hh}(p-2) & ... & \phi_{hh}(0) \end{vmatrix} \tag{B.5}$$

and

$$\mathbf{A} = (A_1, A_2, ..., A_p)^T \tag{B.6}$$

where

$$\begin{aligned} \phi_{hh}(k) &= E[h(i)h^*(i-k)] \\ &= \sigma_h^2 J_0(2\pi f_m k) \end{aligned} \tag{B.7}$$

in which σ_h^2 is the variance of the fading complex channel $h(i)$.

By solving Equation (B.3) using the Levinson algorithm [32], parameters $A_1, A_2, .., A_p$ can be obtained.

After obtaining $A_1, A_2, .., A_p$, we then determine the variance of the driving noise, which can be derived as

$$\sigma_u^2 = \phi_{hh}(0) - \sum_{i=1}^{p} A_i \phi_{hh}(i) \tag{B.8}$$

by setting $k = 0$ in (B.2).

Obtaining all the parameters of AR(p) process, we use the model in (B.1) to generate the fading process recursively. The initial p samples of $h(n)$ can be set according to Baddour and Beaulieu's start-up procedure [38].

It was found that lower order AR models have significantly lower accuracy, but if p is large ($p > 8$), ill-conditioning occurs due to the near-singularity of autocorrelation matrix $\mathbf{R_h}$. For this case, if we still use Levinson method to determine AR parameters, significant errors will occur in the computed parameters, since higher order models will yield filters with poles outside the unit circle [39]. In order to avoid this problem and improve the conditioning of the autocorrelation matrix, a simple heuristic approach can be used to resolve this problem by increasing the values along the principal diagonal of $\mathbf{R_h}$ by a very small positive amount ϵ_{AR}. This is equivalent to adding white noise of variance ϵ_{AR} to the original process. The choice of ϵ_{AR} represents a tradeoff between the improved condition of $\mathbf{R_h}$ and bias introduced in the model [37]. Though biased, we are able to obtain generally high accuracy of the AR(p) model and avoid the ill-conditioning problem.

Appendix C

Derivation of Approximate CRLB for Envelope-Based Doppler Estimators

The CRLB for envelope-based Doppler $\hat{f_m}$ estimators assuming that SNR information is available can be written as [28]

$$CRLB_{env}(\hat{f_m}) = \frac{1}{-E(\frac{\partial^2 \Psi_{env}}{\partial f_m^2})} \tag{C.1}$$

where Ψ_{env} is the log-likelihood function of joint PDF $p_n(z(1), ..., z(n))$, which is given in Equation (6.1).

According to the chain rule, the expectation term in (C.1) will be

$$E[\frac{\partial^2 \Psi_{env}}{\partial f_m^2}] = (\frac{\partial \phi_{II}(1)}{\partial f_m})^2 E(\frac{\partial^2 \Psi_{env}}{\partial \phi_{II}^2(1)}) + \frac{\partial^2 \phi_{II}(1)}{\partial f_m^2} E(\frac{\partial \Psi_{env}}{\partial \phi_{II}(1)}) \tag{C.2}$$

Substituting (C.2) into (C.1),

$$CRLB_{env}(\hat{f_m}) = \frac{-1}{(\frac{\partial \phi_{II}(1)}{\partial f_m})^2 E(\frac{\partial^2 \Psi_{env}}{\partial \phi_{II}^2(1)}) + \frac{\partial^2 \phi_{II}(1)}{\partial f_m^2} E(\frac{\partial \Psi_{env}}{\partial \phi_{II}(1)})} \tag{C.3}$$

Under the first-order Markov process assumption, the log-likelihood function can be approximated by

$$\Psi_{env} = \ln p\,(z(1)) + \sum_{i=1}^{n-1} \ln p\,(z(i), z(i+1)) - \sum_{i=1}^{n-1} \ln p(z(i)) \tag{C.4}$$

where $\ln p(z(k)), k = 1, 2, .., n-1$ is not a function of $\phi_{II}(1)$, so the expectation term in (C.3) can be written as

$$E[\frac{\partial \Psi_{env}}{\partial \phi_{II}(1)}] = (n-1)E[\frac{\partial \ln p(z(i), z(i+1))}{\partial \phi_{II}(1)}] \tag{C.5}$$

$$E[\frac{\partial^2 \Psi_{env}}{\partial \phi_{II}^2(1)}] = (n-1)E[\frac{\partial^2 \ln p(z(i), z(i+1))}{\partial \phi_{II}^2(1)}] \tag{C.6}$$

Substituting Equation (2.21) into (C.5) and (C.6), we obtain

$$\begin{aligned} E[\frac{\partial \ln p(z(i), z(i+1))}{\partial \phi_{II}(1)}] &= E[-\frac{\phi_{II}(0)\phi_{II}(1)}{(\phi_{II}^2(0) - \phi_{II}^2(1))^2}(z^2(i) + z^2(i+1))] \\ &\quad + \frac{2\phi_{II}(1)}{\phi_{II}^2(0) - \phi_{II}^2(1)} + E[\frac{I_1}{I_0} z(i)z(i+1) \frac{\phi_{II}^2(0) + \phi_{II}^2(1)}{(\phi_{II}^2(0) - \phi_{II}^2(1))^2}] \\ &= -\frac{\phi_{II}(0)\phi_{II}(1)4\phi_{II}(0)}{(\phi_{II}^2(0) - \phi_{II}^2(1))^2} + \frac{2\phi_{II}(1)}{\phi_{II}^2(0) - \phi_{II}^2(1)} \\ &\quad + E[\frac{I_1}{I_0} z(i)z(i+1)] \frac{\phi_{II}^2(0) + \phi_{II}^2(1)}{(\phi_{II}^2(0) - \phi_{II}^2(1))^2}] \end{aligned} \tag{C.7}$$

$$\begin{aligned} E[\frac{\partial^2 \ln p(z(i), z(i+1))}{\partial \phi_{II}^2(1)}] &= E[-\frac{\phi_{II}(0)(\phi_{II}^2(0) + 3\phi_{II}^2(1))}{(\phi_{II}^2(0) - \phi_{II}^2(1))^3}(z^2(i) + z^2(i+1))] \\ &\quad + E[\frac{z^2(i)z^2(i+1)(\phi_{II}^2(0) + \phi_{II}^2(1))^2}{(\phi_{II}^2(0) - \phi_{II}^2(1))^4} - \frac{z(k)z(k+1)I_1(\phi_{II}^2(0) + \phi_{II}^2(1))^2}{I_0\phi_{II}(1)(\phi_{II}^2(0) - \phi_{II}^2(1))^3}] \\ &\quad + E[\frac{2I_1\phi_{II}(1)z(i)z(i+1)}{I_0(i, i+1)(\phi_{II}^2(0) - \phi_{II}^2(1))^2} - \frac{z^2(i)z^2(i+1)I_1^2(\phi_{II}^2(0) + \phi_{II}^2(1))^2}{I_0^2(\phi_{II}^2(0) - \phi_{II}^2(1))^4}] \\ &\quad + E[\frac{4z(i)z(i+1)I_1\phi_{II}(1)(\phi_{II}^2(0) + \phi_{II}^2(1))}{I_0(\phi_{II}^2(0) - \phi_{II}^2(1))^3}] + \frac{2(\phi_{II}^2(0) + \phi_{II}^2(1))}{(\phi_{II}^2(0) - \phi_{II}^2(1))^2} \end{aligned} \tag{C.8}$$

where $I_0(i,i+1)$ and $I_1(i,i+1)$, which are defined as previously, are also written as I_0 and I_1, respectively, for convenience.

It is known that

$$\begin{aligned} E[z^2(i)] &= E[z^2(i+1)] \\ &= 2\phi_{II}(0) \end{aligned} \tag{C.9}$$

and

$$E[z^2(i)z^2(i+1)] = 4\phi_{II}^2(0) + 4\phi_{II}^2(1) \tag{C.10}$$

Therefore, the calculation of (C.7) and (C.8) depends on the derivation of the following terms

$$E[\frac{I_1}{I_0}z(i)z(i+1)] \tag{C.11}$$

$$E[\frac{I_1^2}{I_0^2}z^2(i)z^2(i+1)] \tag{C.12}$$

(C.11) can be written as

$$\begin{aligned} E[\frac{I_1}{I_0}z(i)z(i+1)] &= \frac{1}{(\phi_{II}^2(0)-\phi_{II}^2(1))}\int_0^\infty\int_0^\infty z(i)z(i+1)\frac{z(i)z(i+1)}{\phi_{II}^2(0)-\phi_{II}^2(1)} \\ &\quad I_1\exp\left(-\frac{\phi_{II}(0)(z^2(i)+z^2(i+1))}{2(\phi_{II}^2(0)-\phi_{II}^2(1))}\right)dz(i)dz(i+1) \\ &= \int_0^{+\infty} z^2(i+1)\exp(-bz^2(i+1))dz(i+1)\frac{1}{\phi_{II}^2(0)-\phi_{II}^2(1)} \\ &\quad \int_0^\infty z^2(i)\exp\left(-bz^2(i)\right)I_1dz(i) \end{aligned} \tag{C.13}$$

where

$$a = \frac{z(i+1)\phi_{II}(1)}{\phi_{II}^2(0)-\phi_{II}^2(1)} \tag{C.14}$$

$$b = \frac{\phi_{II}(0)}{2(\phi_{II}^2(0)-\phi_{II}^2(1))} \tag{C.15}$$

The last term of Equation (C.13) can be derived as

$$\int_0^\infty z^2(i)\exp\left(-bz^2(i)\right) I_1 dz(i) = \frac{a}{4b^2}\exp(\frac{a^2}{4b}) \tag{C.16}$$

Therefore, (C.11) will be

$$\begin{aligned} E[\frac{I_1}{I_0}z(i)z(i+1)] &= \int_0^\infty \frac{a}{4b^2}\exp\left(\frac{a^2}{4b}\right)\frac{z^2(i+1)}{\phi_{II}^2(0)-\phi_{II}^2(1)}\exp\left(-bz^2(i+1)\right)dz(i+1) \\ &= 2\phi_{II}(1) \end{aligned} \tag{C.17}$$

By defining $y_i = \frac{I_1}{I_0}z(i)z(i+1)$, (C.12) can be obtained as

$$\begin{aligned} E[\frac{I_1^2}{I_0^2}z^2(i)z^2(i+1)] &= E^2[\frac{I_1}{I_0}z(i)z(i+1)] + variance(\frac{I_1}{I_0}z(i)z(i+1)) \\ &= 4\phi_{II}^2(1) + \sigma_y^2 \end{aligned} \tag{C.18}$$

Inserting (C.7), (C.8), (C.17) and (C.18) into (C.5) and (C.6), we obtain

$$\begin{aligned} &E[\frac{\partial\Psi_{env}}{\partial\phi_{II}(1)}] = 0 \\ &E[\frac{\partial^2\Psi_{env}}{\partial\phi_{II}^2(1)}] = \\ &\quad (n-1)\frac{\left(\phi_{II}^2(0)+\phi_{II}^2(1)\right)\left(8\phi_{II}^2(0)\phi_{II}^2(1)-\sigma_y^2\left(\phi_{II}^2(0)+\phi_{II}^2(1)\right)\right)}{\left(\phi_{II}^2(0)-\phi_{II}^2(1)\right)^4} \end{aligned} \tag{C.19}$$

By substituting above equations into (C.3), and using the fact that

$$\frac{\partial\phi_{II}(1)}{\partial f_m} = -\frac{2\pi\phi_{II}(0)J_1(2\pi f_m)snr}{1+snr} \tag{C.20}$$

the approximate CRLB for envelope-based Doppler estimators can be derived as

follows,

$$CRLB_{env}(\hat{f_m}) =$$

$$\frac{(1+snr)^2(\phi_{II}^2(0)-\phi_{II}^2(1))^4}{(1-n)4\pi^2\phi_{II}^2(0)J_1^2(2\pi f_m)snr^2(\phi_{II}^2(0)+\phi_{II}^2(1))[8\phi_{II}^2(0)\phi_{II}^2(1)-\sigma_y^2(\phi_{II}^2(0)+\phi_{II}^2(1))]} \tag{C.21}$$

where σ_y^2 is the variance of y_i, which can be obtained numerically or by Monte-Carlo methods.

Bibliography

[1] R.H. Clarke, " A statistical theory of mobile radio reception, " *Bell Syst. Tech. J.,* Vol. 47, No. 6, pp. 957-1000, 1968.

[2] T.S. Rappaport, *Wireless Communications: Principles and Practice,* Prentice Hall, 1999.

[3] A. Sampath and J.M. Holtzman, "Estimation of maximum Doppler frequency for hand-off decisions," *IEEE Proceeding on VTC,* pp. 859–862, May 1993.

[4] H. S. Wang and P. Chang, "On verifying the first-order Markovian assumption for a Rayleigh fading channel model," *IEEE Transactions on Vehicular Technology,* Vol. 45, pp. 353–357, May 1996.

[5] J.I. Smith "A computer generated multipath fading simulation for mobile radio," *IEEE Transactions on Vehicular Technology,* Vol. VT-24, No. 3, pp. 39–40, August 1975.

[6] B. Zhou and S. D. Blostein, "Doppler frequency estimation in multi-path fading channels," *Sixth Can. Workshop on Info. Theory,* pp. 111–114, June 1999.

[7] L. Zhao and S. D. Blostein, "Recursive maximum likelihood estimation of maximum Doppler frequency of a sampled fading signal," *Biennial Sym. on Communications,* pp. 361–365, June 2000.

[8] M. Turkboylari and G.L.Stuber, "Eigen-matrix pencil method-based velocity estimation for mobile cellular Radio systems" *Proceeding on ICC,* 2000.

[9] G.L. Stuber, *Principles of Mobile Communication,* Kluwer Academic Publishers, 2000.

[10] G.L.R. Povey, P.M. Grant, and R.D. Pringle, "A decision-directed spread-spectrum Rake receiver for fast-fading mobile channels," *IEEE Trans. on Vehicular Technology,* Vol. 45, pp. 491-502, August 1996.

[11] S. Min and K.B. Lee, "Channel estimation based on pilot and data traffic channels for DS/CDMA systems," *Proceeding on GLOBECOM,* pp. 1384-1388, November 1998.

[12] G. Azemi, B. Senadji and B. Boashash, "Estimation of the velocity of mobile units in micro-cellular systems using the instantaneous frequency of the received signals," *Proceeding on International Conference on Acoustic Speech and Signal Processing*, May 2001.

[13] E. Biglieri, F. Abrishamkar and Y. Jou, "Doppler frequency shift estimation for differentially coherent CPM," *IEEE Trans. on Communications,* Vol. 38, No. 10, October 1990.

[14] M.D. Austin, and G.L. Stuber, "Eigen-based Doppler estimation for differentially coherent CPM," *IEEE Trans on Vehicular Technology,* Vol. 43, No. 3, pp. 781-785, August 1994.

[15] M.D. Austin, and G.L. Stuber, "Velocity adaptive hand-off algorithms for micro-cellular systems," *IEEE Trans on Vehicular Technology,* Vol. 43, No. 3, pp. 549-561, August 1994.

[16] K.D. Anim-Appiah, "On generalized covariance-based velocity estimation," *IEEE Trans on Vehicular Technology,* Vol. 48, No. 5, pp. 1546-1557, 1999.

[17] D.J. Young and N.C. Beaulieu, "The generation of correlated Rayleigh random variates by inverse discrete Fourier transform," *IEEE Trans on Communications*, Vol. 48, No. 7, pp. 1114-1127, July 2000.

[18] W. Sheng and S. D. Blostein, " SNR-Independent velocity estimation for mobile cellular communication systems," *Proceeding on International Conference on Acoustics, Speech and Signal Processing,* May 2002.

[19] C. Tepedelenlioglu and G.B. Giannakis, "On velocity estimation and correlation properties of narrow-band mobile communication channels," *IEEE Trans. on Vehicular Technology*, Vol. 50, No. 4, pp. 1039-1052, July 2001.

[20] C. Tepedelenlioglu, "Performance analysis of velocity (Doppler) estimators in mobile communications," *Proceeding on International Conference on Acoustic Speech and Signal Processing*, May 2002.

[21] A. Zeira and A. Nehorai, "Frequency domain Cramer-Rao bound for Gaussian processes," *IEEE Trans. on ASSP,* Vol. 38, No. 6, pp. 1063-1066, June 1990.

[22] E.J. Dudewicz and S.N. Mishra, *Modern Mathematical Statistics,* John Wiley & Sons, Inc., 1988.

[23] I.W. Burr, *Applied Statistical Methods,* Academic Press, Inc., 1974.

[24] J.G. Proakis, *Digital Communications,* Third Edition, McGraw-Hill, Inc., 1995.

[25] H.R. Schwarz, *Numerical Analysis,* John Wiley & Sons, Inc., 1989.

[26] W.C. Y. Lee, *Mobile Communications Engineering,* McGraw-Hill, Inc., 1982.

[27] W. C. Jakes, *Microwave Mobile Communications,* John Wiley & Sons, Inc., 1974.

[28] S.M. Kay, *Fundamentals of Statistical Signal Processing Volume 2 - Estimation Theory,* Prentice Hall PTR, 1998.

[29] H.V. Poor, *An Introduction to Signal Detection and Estimation,* Springer-Verlag, Second Edition, 1994.

[30] C.C. Tan and N.C. Beaulieu, " On first-order Markov modeling for the Rayleigh fading channel, " *IEEE Trans. on Communications,* Vol. 48, No. 12, December 2000.

[31] A. Papoulis, *Probability, Random Variables, and Stochastic Process,* McGraw-Hill, Inc., Third Edition, 1991.

[32] J.G. Proakis and D.G. Manolakis, *Digital Signal Processing: Principles, Algorithms, and Applications,* Prentice Hall, 1996.

[33] F.Swarts and H.C.Ferreira, " Markov characterization of channels with soft decision outputs," *IEEE Trans. on Communications,* Vol. 41, pp. 678-682, May 1993.

[34] H.S.Wang and N.Moayeri, "Finite-state Markov channel- A useful model for radio communication channels, " *IEEE Trans. on Vehicular Technology,* Vol. 44, February 1995.

[35] B.D. Fritchman, "A binary channel characterization using partitioned Markov chains," *IEEE Trans. Inform. Theory,* Vol. IT-13, April 1967.

[36] G. T. Irvine and P. J. McLane, "Symbol-aided plus decision-directed reception for PSK/TCM modulation on shadowed mobile satellite fading channels," *IEEE Journal on Selected Areas in Communications,* Vol. 10(8), pp. 1289-1299, 1992.

[37] C. Komninakis, C. Fragouli, A.H. Sayed, and R.D.Wesel, "Channel estimation and equalization in fading," *IEEE Trans. on Signal Processing,* Vol. 50, No. 5, pp. 1065-1076, May 2002.

[38] K.E. Baddour and N. C. Beaulieu, "Autoregressive models for fading channel simulation," *Proceeding on GLOBECOM*, 2001.

[39] G.W. K. Colman, *An investigation into the capacity of cellular CDMA communication systems with beam-forming in environments with scatter,* Master thesis, Department of Electrical and Computer engineering, Queen's university, 1998.

[40] Y.Liu and S.D. Blostein, "Identification of frequency non-selective fading channels using decision feedback and adaptive linear prediction," *IEEE Trans. on Communications,* Vol. 43(2/3/4), pp. 1484-1492, 1995.

[41] Z. Liu, X. Ma and G. B. Giannakis, "Space-time coding and Kalman filtering for diversity transmissions through time-selective fading channels," *IEEE Trans. on Communications*, Feb. 2002 (to appear).

[42] M.K. Tsatsanis, G.B. Giannakis, and G.Zhou, "Estimation and equalization of fading channels with random coefficients," *Signal Processing*, Vol. 53, No.2/3, pp. 211–228, 1996.

[43] R. Haeb and H. Meyr, "A systematic approach to carrier recovery and detection of digitally phase modulated signals on fading channels," *IEEE Trans. on Communications*, Vol. 37, No. 7, pp. 748–754, 1989.

[44] H. Wu and A. Duel-Hallen, "On the performance of coherent and non-coherent multiuser detectors for mobile radio CDMA channels," *In 5th IEEE international conference on universal personal communications,* pp. 76-80, 1996.

[45] M. Niedzwiecki, *Identification of Time-Varying Processes,* John Wiley & Sons, Ltd, 2000.

vita

Wei Sheng

EDUCATION

Queen's University	M.Sc.	2000–2002
Beijing University of Posts and Telecom.	Bachelor of Engineering	1990–1994

EXPERIENCE

Research Assistant (2000–2002),

Electrical and Computer Engineering, Queen's University

Teaching Assistant (2001–2002),

Electrical and Computer Engineering, Queen's University

Telecommunication Engineer (1994-2000),

Telecommunication Standard Research Institute, Ministry of Information Industry, Beijing, China

Awards

Ontario Graduate Scholarship (2001, 2002)

Queen's Graduate Award (2000-2002)

Publications

W. Sheng and S. D. Blostein, " SNR-Independent velocity estimation for mobile cellular communication systems," *Proceeding on International Conference on Acoustics, Speech and Signal Processing,* May 2002.